

# **Novel Processing Technologies for Recombinant Spider Silk Proteins**

Von der Fakultät für Ingenieurwissenschaften  
der Universität Bayreuth  
zur Erlangung der Würde eines  
Doktor-Ingenieur (Dr.-Ing.)  
genehmigte Dissertation

**vorgelegt von  
Stephan Jokisch (M. Sc.)  
aus  
Hoyerswerda**

|                             |                                     |
|-----------------------------|-------------------------------------|
| Erstgutachter:              | Prof. Dr. rer. nat. Thomas Scheibel |
| Zweitgutachter:             | Prof. Dr.-Ing. Volker Altstädt      |
| Tag der mündlichen Prüfung: | 14.10.2019                          |

**Lehrstuhl Biomaterialien  
Universität Bayreuth**

**2019**



*„Phantasie ist wichtiger als Wissen, denn  
Wissen ist begrenzt.“*

- Albert Einstein -



# Contents

|  |            |
|--|------------|
| <b>Contents</b> .....  | <b>iv</b>  |
| <b>List of Figures</b> .....   | <b>vii</b> |
| <b>List of Tables</b> .....  | <b>xiv</b> |
| <b>List of Abbreviations and Symbols</b> .....   | <b>xvi</b> |
| <b>1 Introduction</b> .....  | <b>1</b>   |
| 1.1 Polymers in modern production processes and the need of surface modification ..... | 1          |
| 1.2 Filtration .....   | 3          |
| 1.3 Synthetic polymers .....   | 4          |
| 1.3.1 Poly(ethylene terephthalate).....  | 5          |
| 1.3.2 Poly(acrylonitrile) .....  | 6          |
| 1.3.3 Poly(ethylene oxide) .....   | 7          |
| 1.4 Biopolymers .....  | 8          |
| 1.4.1 Natural Polymers .....   | 10         |
| 1.5 Properties of synthetic and natural polymers .....                                 | 15         |
| 1.6 Fiber production methods .....   | 18         |
| 1.6.1 Melt spinning.....   | 20         |
| 1.6.2 Solution spinning methods.....   | 22         |
| 1.6.3 Centrifugal spinning methods .....   | 26         |
| 1.6.4 Electrospinning methods .....  | 27         |
| 1.7 Mechanical textile processing.....   | 34         |
| 1.7.1 Compacting.....  | 34         |
| 1.7.2 Calendering.....   | 34         |
| 1.7.3 Raising or napping.....  | 35         |
| 1.7.4 Sueding.....   | 35         |
| 1.8 Coating methods.....   | 36         |
| 1.8.1 Protective planar coatings in form of closed layers .....                        | 36         |
| 1.8.2 Special coatings in form of nonwoven meshes .....                                | 38         |
| 1.9 Motivation and aim of the thesis .....   | 40         |

|          |   |           |
|----------|---|-----------|
| <b>2</b> | <b>Materials and Methods .....</b>  | <b>43</b> |
| 2.1      | Materials and instruments .....   | 43        |
| 2.1.1    | Chemicals and Consumables .....   | 43        |
| 2.1.2    | Textiles and yarns .....  | 44        |
| 2.1.3    | Instruments and devices .....   | 45        |
| 2.1.4    | Software .....  | 47        |
| 2.2      | Recombinant production of ChryC1 lacewing and eADF4(C16) spider silk proteins .....             | 48        |
| 2.3      | Foam processing from spider silk solutions .....  | 48        |
| 2.4      | Foam coating of fibers and fabrics .....  | 49        |
| 2.5      | Processing of spider silk protein and polymer solutions for production of nonwoven meshes ..... | 50        |
| 2.5.1    | Electrospinning .....   | 50        |
| 2.5.2    | Centrifuge electrospinning .....  | 50        |
| 2.6      | Processing of nonwoven meshes for filter production .....                                       | 51        |
| 2.7      | Analytical methods .....  | 52        |
| 2.7.1    | Spectroscopic methods .....   | 52        |
| 2.7.2    | Microscopy .....  | 53        |
| 2.7.3    | Rheological characterization of foaming and spinning dopes .....                                | 54        |
| 2.7.4    | Analysis of coating stability and efficiency .....  | 55        |
| 2.7.5    | Mechanical analytical methods for foam coated yarns and textiles .....                          | 55        |
| 2.7.6    | Filtration efficiency tests .....   | 57        |
| <b>3</b> | <b>Results .....</b>  | <b>59</b> |
| 3.1      | Protective effects of spider silk foam coatings on furniture textiles .....                     | 59        |
| 3.1.1    | Textiles and yarns for coating .....  | 59        |
| 3.1.2    | Rheological analysis of spider silk foaming dopes .....   | 60        |
| 3.1.3    | Analysis of foam coating parameters .....   | 62        |
| 3.1.4    | Distribution of spider silk foams on furniture textiles .....                                   | 63        |
| 3.1.5    | Coating stability and protective effects of spider silk on single yarns .....                   | 64        |
| 3.1.6    | Abrasion tests of spider silk coated fabrics .....  | 66        |
| 3.2      | Electrospun nonwoven mesh for the improvement of a filtration surface .....                     | 68        |
| 3.2.1    | Preliminary analyzes .....  | 68        |
| 3.2.2    | Electrospun nonwoven fiber meshes for filtration purposes .....                                 | 71        |
| 3.2.3    | Centrifuge electrospinning parameter analysis for large scale nonwoven mesh production .....    | 88        |

|          |  |            |
|----------|--|------------|
| 3.3      | Influences of E- and CE-spinning on the resulting fiber mesh quality .....                     | 94         |
| 3.3.1    | Comparison of resulting fiber diameter in classical and centrifuge electrospinning.....        | 95         |
| 3.3.2    | Influence of ES and CES on the secondary structure of spider silk fibers .....                 | 98         |
| <b>4</b> | <b>Discussion.....</b>   | <b>101</b> |
| 4.1      | Coating of industrially produced fibers using spider silk proteins.....                        | 101        |
| 4.1.1    | Influence of shear forces and surfactant deployment on foam production.....                    | 102        |
| 4.1.2    | Adhesion behavior of spider silk proteins on different yarn fiber materials .....              | 105        |
| 4.1.3    | Stabilizing and protective effects of spider silk protein foam coatings .....                  | 106        |
| 4.2      | Fiber production based on spider silk proteins .....   | 110        |
| 4.2.1    | Differences in the dope materials and their rheological effects and concentration ranges ..... | 110        |
| 4.2.2    | The field strength as guiding spinning parameter for upscaling purposes .....                  | 112        |
| 4.2.3    | Effects of silk protein nanofiber nonwovens on particle deposition .....                       | 114        |
| 4.3      | Upscaling potential of nonwoven coatings by centrifugal electrospinning .....                  | 117        |
| <b>5</b> | <b>Summary.....</b>  | <b>119</b> |
| <b>6</b> | <b>Zusammenfassung .....</b>   | <b>121</b> |
| <b>7</b> | <b>Appendix.....</b>   | <b>125</b> |
|          | <b>Supportive Information.....</b>   | <b>125</b> |
|          | <b>References .....</b>  | <b>127</b> |
|          | <b>Danksagung.....</b>   | <b>143</b> |
|          | <b>Lebenslauf .....</b>  | <b>145</b> |
|          | <b>Erklärung.....</b>  | <b>147</b> |

## List of Figures

|                     |  |    |
|---------------------|--|----|
| <b>Figure 1.1:</b>  | Characteristic ester group (monomer) in polyester molecules, derived from poly-condensation reactions between acids and alcohols or phenols.....   | 5  |
| <b>Figure 1.2:</b>  | Monomer of PET, derived from poly-condensation reaction between ethylene glycol and dimethyl terephthalate or terephthalic acid. ....  | 6  |
| <b>Figure 1.3:</b>  | Characteristic acrylonitrile monomer in PAN molecules. ....  | 7  |
| <b>Figure 1.4:</b>  | Monomeric unit (ethylene oxide) of PEO. <sup>[47]</sup> .....  | 7  |
| <b>Figure 1.5:</b>  | Definition of biopolymers modified after CEN/TR 15932. <sup>[65]</sup> .....   | 9  |
| <b>Figure 1.6:</b>  | Monomeric unit (lactic acid) of PLA. <sup>[73]</sup> .....   | 10 |
| <b>Figure 1.7:</b>  | European garden cross spider ( <i>A. diadematus</i> ) while rappelling using its dragline with highlighted spinneret.....  | 11 |
| <b>Figure 1.8:</b>  | Web construction of orb-weaving spiders from different silk types with outer and inner shell of their cocoon (white, 1/2), the framework of the web (bold black, 3.1), the spiders dragline (bold black/red, 3.2), the supporting spiral (light grey, 4) which is used by the spider to build up the catching spiral (black, 5) covered with sticky silk droplets (brown, 6); the whole web constructions are fixed on surfaces via the frame construction using cement silk dots (grey, 7).....   | 12 |
| <b>Figure 1.9:</b>  | Overview of the mainly industrially employed spinning methods and the respective fiber diameter range. <sup>[128-143]</sup> .....  | 19 |
| <b>Figure 1.10:</b> | Basic scheme of melt spinning method; a polymer is led into a heated extruder screw where the material is molten and then extruded with a constant flow through a multifilament spinneret with the help of a metering pump (A). In classical melt spinning, the fibers are cooled and hardened by quenching air and let into a stretching pipe. Subsequently, the filament bundles are either collected to be post-stretched with altering rotational velocities, followed by a yarn take-up (B) or deflected to be randomly deposited on receiver mat using suction-air via a spunbonded process (C). For melt blow processes the polymer melt is directly pumped into a blowing nozzle, here hot air is used to accelerate multiple fiber jets. These fly towards a collection unit and solidify due to cooling by the quenching air (D). <sup>[133-135]</sup> ..... | 21 |



- Figure 1.11:** Basic scheme of solution spinning methods; a polymer is dissolved in a proper solvent; either a low viscous polymer solution is pumped, using a liquid pump (A), or a highly viscous high molecular weight polymer solution is extruded, using a rotating extruder (B), into multi-hole spinnerets. Hot drying air is directly streamed at the emerging filaments, which solidify and are subsequently collected, using godets regarding dry spinning (C). Emerging fibers might be led into a coagulation bath, either sub-liquid level (C1, classical wet spinning), or using an air gap (C2) and collected upon solidification. The fiber bundles from dry or wet spinning may be poststretched, using godets with slightly increasing rotational velocities, if desired (E). Regarding ultra-high molecular polyethylene poststretching is performed in a heated drying chamber with fibers in a gel state to create high modulus polyethylene filaments (F).<sup>[133,136-138,140-147]</sup>..... 23
- Figure 1.12:** Schematic of a standard electrospinning device; a high electric potential is applied to a capillary tip acting as an electrode and a collector plate acting as a counter electrode. The latter is placed in a distance of 1 - 40 cm, using high electric voltage (0-45 kV) which leads to a strong electrostatic field. Dope solution is extruded through the capillary tip. The electrostatic field induces repulsive forces inside of the emerging droplet forming a Taylor cone. If the attractive forces of the electrostatic field overcome the surface tension of the solvent, then a thin jet erupts from the cone, which is affected by bending instabilities causing loops and turbulences, and therefore stretching the fiber while traveling to the collector plate and solidifying them. Multiple chaotically deposited fibers form a nonwoven mesh..... 28
- Figure 1.13:** Schematic of a Taylor cone in proper form (A), an overflowing Taylor cone with emerging droplet (B), and the cannula electrode with retracted and dried out Taylor cone (C). ..... 31
- Figure 1.14:** Schematic of a centrifugal electrospinning device where a high electric voltage (0-90 kV) is applied to a rotating center bell, a syringe filled with a spinning dope solution, and a grounded collector plate electrode is placed in a distance (spinning height  $d_x$ ) of 20-100 cm. This setup leads to a strong electrostatic field, inducing attractive and repulsive forces to the dope solution, which forms a torus that emerges at the inner wall edge of the center bell. If the surface tension is exceeded, thin jets erupt from the highest points of the torus which are affected by rotational forces and

|                     |   |    |
|---------------------|---|----|
|                     | bending instabilities, causing further stretching as the solvent evaporates. Numerous solid fibers are formed, which are finally randomly deposited on the counter electrode in the form of a nonwoven mesh. ....   | 33 |
| <b>Figure 1.15:</b> | Flowchart of the outline of the work of this thesis. ....   | 42 |
| <b>Figure 2.1:</b>  | Foam production; A: aeration of coating solution, B: shearing of silk solution with mixing rotor, C: combination leads to foam creation with air flow rate $\dot{v}$ [L/h], air pressure $p_{air}$ [bar(g)] and number of revolutions $\omega$ [rpm].....   | 49 |
| <b>Figure 2.2:</b>  | Schematic procedure of post-treatment of electro-spun eADF4(C16) and ChryC1 nonwoven meshes. Regarding eADF4(C16), the chamber was preliminary filled with ethanol and the sample was steamed at 60°C for 120 min. In order to soften the nonwoven meshes for subsequent handling, ethanol was removed in a second step, and the fibers were treated with water vapor according to step 1. For ChryC1, the post-processing is carried out with water vapor (Step 2) only, modified from. <sup>[202]</sup> ..... | 51 |
| <b>Figure 2.3:</b>  | Schematic illustration of the cone-plate system implemented in the rheological characterization set-up with a truncation gap between cone and heating plate, a sample placed between both components with a sample volume of $V=180\mu\text{L}$ , a cone diameter of $d=40\text{mm}$ and a cone angle of $0.5^\circ$ .....  | 54 |
| <b>Figure 2.4:</b>  | Schematic illustration of yarn to fabric characterization modified after Capstan test with a standard cotton textile SM25 attached to a cylinder, the fiber is connected to a weight on one end and to a force sensor on the other; a vertically reciprocating movement of the construction caused a scrubbing and the induction of nodules on the yarn indicating its destruction; modified after <sup>[219,220]</sup> .....   | 56 |
| <b>Figure 2.5:</b>  | Schematic abrasion resistance (pilling) test module after Martindale in accordance with EN ISO 12945-2 with a SM25 cotton standard textile attached to a stamp-like mounting which is pressed onto the textile sample and rotated; the suspension is moving in x and y direction to cover the whole surface; the rotational movement destroys the textile surface integrity by the build-up of pills and nodules. ....  | 57 |
| <b>Figure 3.1:</b>  | Dynamic rheology of foaming dopes with different silk protein concentrations, 10g/L (A), 2g/L (B), 0.1g/L (C), each solution contains the foaming agent Ultravon Jun (3g/L).....  | 61 |

---

|                     |   |    |
|---------------------|---|----|
| <b>Figure 3.2:</b>  | Foamed spider silk media (10 g/L) amount and the blow ratio at 800 rpm (A); and at 1 bar (g) (B). .....   | 62 |
| <b>Figure 3.3:</b>  | Overview of fluorescence and scanning electron microscopy images of coated natural (N, A1-A3), rough polymeric (P1, B1-B3) and smooth polymeric (P2, C1-C3) yarns after single and double coating. Fluorescence images indicating homogeneous coverage of all tested textiles (A1, B1 and C1) not providing inherent fluorescence. Film-like coatings cover single fibers of the yarn (A2, C3) and fiber-interconnecting bridges (A3, C2) are depicted. Increasing film thickness is reached upon a second coating step (B2, B3), modified from. <sup>[216]</sup> ..... | 63 |
| <b>Figure 3.4:</b>  | Analysis of the protein amount in the used foam vs. the adsorbed protein amount on the fabric for single-coated and double-coated (repeated first coating step) textiles. ....  | 64 |
| <b>Figure 3.5:</b>  | Fraying test of a LI fiber yarn, Art. 927 (textile N), uncoated yarn after fraying test (A), spider silk coated yarn after fraying test (B); Examples of yarn fraying test analysis using black/white pixel ratio analysis of uncoated yarn volume after fraying (C), silk coated yarn volume after fraying (D) and overlay of C and D for direct comparison (E), modified from. <sup>[216]</sup> .....   | 65 |
| <b>Figure 3.6:</b>  | Pilling abrasion test; A: rough partially natural fiber textile (N); B: rough polymeric textile (P1); C: smooth polymeric textile (P2). Three independent samples were tested for each material and level of strain/number of revolutions (n = 3), modified from. <sup>[216]</sup> .....  | 67 |
| <b>Figure 3.7:</b>  | Mean viscosity of spinning dopes under increasing shear forces from 0 to 286 1/s .....  | 68 |
| <b>Figure 3.8:</b>  | Overview of resulting dynamic viscosities after rheological characterization of the used synthetic polymer (PEO, 400 kg/mol and PLA, 39 kg/mol) and the recombinant proteins (eADF4(C16), 48 kg/mol and ChryC1, 82 kg/mol) at different dope concentrations.....  | 70 |
| <b>Figure 3.9:</b>  | Overview of resulting fiber diameters after electrospinning of the synthetic polymer (PEO, 400 kg/mol and PLA, 39 kg/mol) and the recombinant proteins (eADF4(C16), 48 kg/mol and ChryC1, 82 kg/mol).....   | 70 |
| <b>Figure 3.10:</b> | Electrode distance comparison for electrospinning of different polymer solutions; eADF4(C16) 100 g/L (A), ChryC1 70 g/L (B), PLA 60 g/L (C),  |    |

|                     |   |    |
|---------------------|---|----|
|                     | PEO 35 g/L (D) at voltages 15 kV (A), 12.5 kV (B), 12.5 kV (C) and 27.5 kV (D). .....   | 72 |
| <b>Figure 3.11:</b> | Spider silk protein fiber mesh fine particle layer and complete dust bag production process with A: polyamide support material with 90 $\mu\text{m}$ gap width, B: deposited nonwoven mesh on the support layer and C: exemplary particle deposition filtration test of fine particle filter layer as well as D: scheme of the complete spider silk protein based filter setup and E: scheme of a complete dust bag (double mirrored stack of D) and F: photograph of E, modified from. <sup>[11]</sup> ..... | 75 |
| <b>Figure 3.12:</b> | Deposition rates of poly(lactic acid) (PLA) and poly(ethylene oxide) (PEO) meshes with different grammage each on PA supports and of standard dust bag respectively using a A2 - Arizona fine test dust. ....   | 79 |
| <b>Figure 3.13:</b> | Deposition rates of lacewing silk protein (ChryC1) meshes (different grammage, as well as, dope concentrations) on PA supports in comparison to standard dust bags using A2 - Arizona fine test dust. ....  | 80 |
| <b>Figure 3.14:</b> | Deposition rates of spider silk protein eADF4(C16) meshes with different grammage, as well as, dope concentrations each on PA supports and of standard dust bag respectively using A2 - Arizona fine test dust. ....  | 82 |
| <b>Figure 3.15:</b> | Deposition rates of spider silk protein of spider silk (eADF4(C16)) fiber meshes on PA support implemented in a prototype dust bag in comparison of a prototype dust bag with PA support and without silk protein mesh fine dust filtration layer, as well as, a standard dust bag respectively using an A2 - Arizona fine test dust. ....  | 84 |
| <b>Figure 3.16:</b> | Quality factor of a spider silk-containing filter set-up in comparison to that of a conventional one at different particle size and the pressure drop, modified from. <sup>[11]</sup> .....   | 87 |
| <b>Figure 3.17:</b> | Explanation and exemplary images of evaluation (quality) classes of centrifuge electro-spun fiber mats. ....  | 89 |
| <b>Figure 3.18:</b> | Three dimensional quality plots of centrifuge electro-spun nonwoven meshes using the materials PEO, PLA and eADF4(C16) at a voltage difference $\Delta U$ [kV] and rotational speed $\omega$ [krpm]; quality is rated from 1 (red, worst result, no fibers) to 7 (bright green, best result, dense and closed homogeneous fiber mesh). ....   | 90 |
| <b>Figure 3.19:</b> | Schematic collection of centrifugal electrospinning samples for disk extrapolation and electrode distance evaluation, three samples were  |    |

|                     |   |     |
|---------------------|---|-----|
|                     | placed into vertical, as well as, horizontal direction starting from the center of the deposition area. ....  | 91  |
| <b>Figure 3.20:</b> | Colored disk stack height comparison of centrifuge electrospun PLA (A) and PEO (B) at optimal spinning parameters, as well as, of eADF4(C16) (60g/L) at voltage differences 50 kV (C), 70 kV (D) and 90 kV (C) and resulting electric field strengths at constant rotating velocities of 20 krpm. ....  | 94  |
| <b>Figure 3.21:</b> | Fiber diameter comparison for classical and centrifuge electrospinning of all materials at all tested different dope concentrations, spun at best obtained conditions for ES (see Table 3.5) and CES (see Figure 3.20). ....  | 96  |
| <b>Figure 3.22:</b> | SEM pictures of fiber meshes of all tested raw materials and dope concentrations yielding comparable nonwoven fiber meshes with same diameters for each material processed with ES and CES. ....  | 97  |
| <b>Figure 3.23:</b> | Fourier self-deconvoluted amide I band of an untreated (A) and a post-treated (B) spider silk nonwoven mesh. The solid line displays the absorbance band resulting from the single contribution peaks (dotted lines) as derived after deconvolution. The assignment of the respective curves was based on the published values from Hu et al. <sup>[218]</sup> .... | 98  |
| <b>Figure 3.24:</b> | Secondary structure content of classical and centrifuge electrospun eADF4(C16) fiber meshes as spun and after ethanol vapor treatment, n = 3. ....  | 99  |
| <b>Figure 3.25:</b> | Optical images of ES and CES-spun eADF4(C16) fiber meshes as-spun and after ethanol vapor treatment with bright field (left) and polarized light microscopy (right). ....   | 100 |
| <b>Figure 4.1:</b>  | Schematic illustration of laboratory scale foaming process with an air flow rate, yielding no foam (A), exceeding air flow, air bubble aggregation and collapsing foam (B) and ideal air flow rate and accumulating foam (C). ....  | 103 |
| <b>Figure 4.2:</b>  | Ultravon Jun surfactant main ingredient, Iso-tridecyl-alcohol. ....   | 104 |
| <b>Figure 4.3:</b>  | Schematic illustration of a water (6) molecule cluster (A), a foam bubble with water cluster-surfactant (iso-tridecyl-alcohol) conjugations (B), and an ideal bubble (C) carrying a membrane of surfactant enveloped silk protein - water conjugations on its surface. ....   | 105 |
| <b>Figure 4.4:</b>  | Schematic illustration of possible molecular particle deposition effects in air filtration processes: interception (A), impaction (B), diffusion (C), extended by electrostatic interaction (D), with the illustrated air stream  |     |

(blue arrow) carrying dust particles (gray), that are caught on the fiber surface (red), modified from stated sources <sup>[232]</sup> and <sup>[254]</sup>. ..... 114

**Figure 4.5:** Schematic overview of molecular particle filtration effects in nonwoven meshes in dependence of airflow velocity,  $V$  and particle diameter,  $d$  featuring diffusive motions, interception, impaction and gravity effects, modified from sources <sup>[232]</sup> and <sup>[254]</sup>. ..... 115

## List of Tables

|                   |  |    |
|-------------------|--|----|
| <b>Table 1.1:</b> | Overview of a selection of the most common and best known synthetic polymers used for industrial scale applications. ....  | 16 |
| <b>Table 1.2:</b> | Overview of the renewable polymers under research and their properties as well as possible applications. ....  | 18 |
| <b>Table 2.1:</b> | Overview of all used chemicals and consumables. ....   | 43 |
| <b>Table 2.2:</b> | Overview of used devices for analytics and material processing. ....   | 45 |
| <b>Table 2.3:</b> | Overview of used software for device operation, analysis, and graphic processing. ....   | 47 |
| <b>Table 3.1:</b> | Overview of used fabrics; fabric (N) containing 2/3 of natural material based LI and CV as well as 1/3 PET yarn with intermediate surface roughness, polymeric material fabrics based on PAN and PET yarns with high (P1) and low (P2) surface roughness, modified from. <sup>[216]</sup> .... | 60 |
| <b>Table 3.2:</b> | Single fiber fraying test and reduced single fiber fraying upon coating, modified from. <sup>[216]</sup> ....  | 65 |
| <b>Table 3.3:</b> | Coating stability, tested by washing with water and ethanol; ten independent samples were tested ( $n_s = 10$ ), modified from. <sup>[216]</sup> ....  | 66 |
| <b>Table 3.4:</b> | Asymptotic approximation values of rheological analysis of electrospinning dopes with dynamic viscosities of all used spinning dopes at highest tested shear rate. ....  | 69 |
| <b>Table 3.5:</b> | Comparison of required electric field strengths for electrospinning of the tested materials, highlighted values depict dope concentrations, voltage differences, collector distances and resulting electric field strengths to obtain best results and similar fiber diameters. ....           | 74 |
| <b>Table 3.6:</b> | Basic information of electro-spun nonwoven mats including materials, molecular weight, main fiber diameter, average pore size, surface charge at neutral pH and exemplary SEM images, modified from. <sup>[11]</sup> ....  | 77 |
| <b>Table 3.7:</b> | Filter parameters and deposition rates of poly(lactic acid) (PLA) and poly(ethylene oxide) (PEO) meshes on PA supports using a A2-Arizona fine test dust. Pressure drop differences $\Delta p$ were determined between that of clean and dust filled filter layers. ....                       | 79 |

**Table 3.8:** Filter parameters and deposition rates of lacewing silk (ChryC1) meshes on PA supports using A2 - Arizona fine test dust. Pressure drop differences  $\Delta p$  were determined between that of clean and dust filled filter layers, modified from.<sup>[11]</sup> ..... 81

**Table 3.9:** Filter parameters and deposition rates of spider silk (eADF4(C16)) fiber meshes on PA supports using a A2 - Arizona fine test dust. Pressure drop differences  $\Delta p$  were determined between that of clean and dust filled filter layers, modified from <sup>[11]</sup>. ..... 83

**Table 3.10:** Filter parameters and deposition rates of spider silk (eADF4(C16)) fiber meshes on PA support implemented in a test dust bag (Figure 3 A) compared to that of the conventional filter using a A2 - Arizona fine dust test. Pressure drop differences  $\Delta p$  were determined between that of clean and dust filled filter layers. .... 85

**Table 3.11:** Air permeability of different dust filter systems on PA mesh support, modified from.<sup>[11]</sup> ..... 86

**Table 4.1:** Electrostatic field strength of all tested dope materials at best spinning results for classical and centrifuge electrospinning and their factor after transfer. .... 112



## List of Abbreviations and Symbols

|                      |   |
|----------------------|---|
| $\emptyset$          | Diameter [m]  |
| 3 D                  | Three dimensional   |
| A                    | Area [m <sup>2</sup> ]  |
| <i>A. diadematus</i> | <i>Araneus diadematus</i>   |
| <i>A. mellifera</i>  | <i>Apis mellifera</i>   |
| <i>B. mori</i>       | <i>Bombyx mori</i>  |
| BSH                  | Bosch und Siemens Hausgeräte GmbH                                 |
| <i>c</i>             | Concentration [g/l]   |
| <i>C. carnea</i>     | <i>Chrysoperla carnea</i>   |
| ChryC1               | <i>Chrysoperla carnea (Protein) 1</i>                             |
| CEN                  | European communications, entertainment & technology law committee |
| CES                  | Centrifuge electrospinning  |
| CV                   | Rayon   |
| <i>d</i>             | Diameter [m]  |
| <i>d<sub>x</sub></i> | Spinning height [mm]  |
| DMF                  | Dimethylformamide   |
| <i>e</i>             | Vapor pressure [bar]  |
| <i>E. coli</i>       | <i>Escherichia coli</i>   |
| <i>eADF4(C16)</i>    | <i>Engineered Araneus diadematus fibroin 4</i>                    |
| $\vec{E}$            | Electrostatic field strength [kV/mm]                              |
| ECM                  | Extracellular matrix  |
| ES                   | Electrospinning   |
| <i>F</i>             | Force [N]   |
| FSD                  | Fourier self-deconvolution  |
| GdmSCN               | Guanidinium thiocyanate   |
| <i>H</i>             | Hairiness Index [ $\mu\text{m}^2/\text{cm}^2_{\text{yam}}$ ]      |
| HFIP                 | Hexafluoro-2-propanol   |
| <i>k</i>             | Thousand  |
| <i>l</i>             | Length [m]  |

|            |   |
|------------|---|
| LI         | Linen   |
| $m$        | Mass [kg]   |
| $m_a$      | Area dependent protein coating mass [ $\text{g}/\text{m}^2$ ] |
| $M$        | Torque [Nm]   |
| MW         | Molecular weight [g/mol]                                      |
| $n$        | Rotational speed [rpm]  |
| $n_s$      | Quantity of tested samples                                    |
| N          | Fabric, mainly from natural resources                         |
| NaCl       | Sodium chloride   |
| $\Delta p$ | Pressure drop [Pa]  |
| $p_{air}$  | Air pressure over atmospheric pressure [bar (g)]              |
| P (1, 2)   | Fabrics, mainly from polymeric resources                      |
| PAN        | Poly(acrylonitrile)   |
| PCDT       | Poly(-1, 4-cyclohexylene-dimethyle terephthalate)             |
| PEG        | Poly(ethylene glycol)   |
| PEO        | Poly(ethylene oxide)  |
| PET        | Poly(ethylene terephthalate)                                  |
| PETG       | Glycol modified Poly(ethylene terephthalate)                  |
| PI         | Isoelectric point   |
| PLA        | Poly(lactic acid)   |
| QF         | Quality factor  |
| $r$        | Radius [m]  |
| $rH$       | Relative humidity [%]   |
| $rpm$      | Revolutions per minute [n]                                    |
| SEM        | Scanning electron microscopy                                  |
| t          | Time [s]  |
| $T$        | Temperature [ $^{\circ}\text{C}$ ]                            |
| TC         | Technical committee   |
| TR         | Technical report  |
| TRIS       | Tris(hydroxymethyl)-aminomethane                              |
| $\Delta U$ | Voltage [V]   |
| $v$        | Flight velocity [m/s]   |
| V          | Volume [L]  |

|                |   |
|----------------|---|
| $\dot{V}_a$    | Air flow rate [L/s]                                       |
| $\dot{V}_e$    | Dope volume stream in electrospinning [ $\mu\text{l/s}$ ] |
| $\alpha$       | Cone pitch angle [rad]                                    |
| $\dot{\gamma}$ | Shear rate [1/s]  |
| $\eta$         | Dynamic viscosity [Pa s]                                  |
| $\pi$          | Circular number [-]                                       |
| $\rho$         | Density [ $\text{g/cm}^3$ ]                               |
| $\omega_r$     | Rotational velocity [m/s]                                 |

---

# **1 Introduction**

## **1.1 Polymers in modern production processes and the need of surface modification**

From simple products like cutlery or cases, to highly complex products such as aircraft and cars, a variety of materials are utilized. Polymers often represent the main component, becoming indispensable during the last decades.<sup>[1,2]</sup> In regards to global warming and eco-friendly lifestyles in recent years, special emphasis has been placed on sustainable development of novel polymers from renewable resources.<sup>[3]</sup> The selection of the particular polymer in the production process of an object is mainly influenced by its properties, such as thermal stability, tensile strength, elastic modulus, resistance to solvents or acids as well as transparency. Yet, the surface properties of the product after processing rarely fit the applications' needs. To overcome this deficit, surface modification is employed to facilitate desired properties, such as reduced friction or sensibility to chemicals and surfactants, improved wettability or adhesion and special optical features.<sup>[4-6]</sup>

Surface modification techniques differ, depending on the product. For soft and moldable materials, physical methods affecting the surface structure are preferred. Those methods comprise embossing, impulsive peening, rolling, fretting and stressing amongst many others.<sup>[7]</sup> The main disadvantage of those treatments is the destructive nature with plastic deformation and ablation of the products' material. Hence, to provide a certain level of protection against mechanical stress or degradation, protective layers have to be added.<sup>[8]</sup> Such protective coating layers are mainly obtained via chemical treatments using additional substances.<sup>[9]</sup>

By definition of O. S. Parmaj and Prof. Dr. M. D. Teli, both experts on the subject of fiber and textile processing from the Institute of Chemical Technology in Mumbai: "Coating is an application of an appropriate chemical system to form a layer of coating compound on the substrate".<sup>[10]</sup> The proper application of a coating onto a subject is a crucial procedure, with either solid phases (lining/ lamination, melt extrusion, calendaring) or liquid phases (dimethylformamide (DMF) coagulation/ wet processing, roller coating, doctor blading, dip coating/ Foulard-process, pressure-/ spray coating) typically being em-

ployed. Solid phase coatings mainly affect the template surface. In contrast to that, wet coatings are more homogeneous throughout the total material at the expense of extensive amounts of coating solution required. Remaining solvents and excessive coating substance have to be removed mechanically, increased drying temperatures are required and additionally they are comparably time consuming.<sup>[11-14]</sup> Such highly effective, but costly coating methods are most frequently utilized for efficient treatment of highly porous and voluminous mass-produced articles like textiles.<sup>[15,16]</sup>

Manufacturing of yarn and fabric for furniture has been optimized over several centuries. Especially, high quality furniture fabrics, which are mainly built from polymer filaments, processed into yarns and subsequently arranged to fabrics, need an extraordinary quality and long lifetime.<sup>[12]</sup> For such mass-product articles with several structural levels commonly combinations of mechanical treatment with subsequent chemical coatings are utilized. In terms of textile processing O. S. Parmaj and Prof. Dr. M. D. Teli refine the definition of coatings to: "...a process in which a polymeric layer is applied directly on one or both the surface of a fabric."<sup>[10]</sup> Fabrics are exposed to high extends of mechanical stress but are supposed to remain their appearance as long as possible besides special requirements, such as dirt repellency or flame resistance. In that regard, mechanical treatment is stretched to its limits, emphasizing the need of protective coatings.<sup>[13,14,17]</sup> Unfortunately, those basic coating substances providing flame retardancy usually comprise harmful substances, such as fluorochlorinated hydrocarbons amongst others. This factor strongly contrasts with sustainable development goals.<sup>[18,19]</sup> Therefore, the need for novel green coatings, derived from ecologically friendly materials and solvents is obvious and research on this topic, steadily gains importance.<sup>[20-23]</sup>

## 1.2 Filtration

Wherever mechanical processes are carried out and two different media are in contact, interactive motions between the media generate friction. Consequentially, particles and fragments are extracted from the materials' surfaces, which distribute in the surrounding medium. In case of air, light particles either occur in the form of an aerosol or, if a certain particle weight is overcome, build sediment. Such particles commonly are called dust. Additionally, this term comprises all kinds of mineral dirt and sand particles, biological remains, such as hair, skin scales, pollen or mite feces, as well as, ashes in consequence of combustion process. It is well known, that inhaling such particles carries an enormous risk to the human body.<sup>[24]</sup> Hence, it is crucial to extract them from the surrounding matter to clean the living environment - this process is called filtration. By definition of the Encyclopedia Britannica: "Filtration is the process in which solid particles in a liquid or gaseous fluid are removed by the use of a filter medium that permits the fluid to pass through but retains the solid particles. Either the clarified fluid or the solid particles removed from the fluid may be the desired product."<sup>[25]</sup> Focusing the cleaning of the gaseous media, such as air or combustion gases in industrial processes, often cyclones and settling chambers are employed. In human daily routine still predominantly vacuum cleaners, using vacuum cleaner bags are used. Also in medical surroundings and places where clinical purity is demanded, high-efficiency particulate air (HEPA) or ultra-low penetration air (ULPA) filter media are employed. Those filter bags and media are composed of polymer fibers, assembled in the form of woven or nonwovens. Depending on the process requirements, the production conditions, the processing and in particular the material itself are precisely chosen.<sup>[26]</sup>

In the following chapters polymer types and their typical representatives are introduced. Those examples are relevant either regarding the production volume and therefore importance for the human daily life or concerning the polymers' suitability for fiber production.

### 1.3 Synthetic polymers

Well known over centuries for their versatility, as well as, cost- and weight-efficiency, crude oil based synthetic polymers are found most prominently in almost all production processes. From astro- and aeronautics to home- and textile industries, synthetic polymers are omnipresent in the human life and gain even more importance in modern technical development.<sup>[27,28]</sup> After immense oil field discovery during the conquest of the North American continent in the late 19<sup>th</sup> century, crude oil became abundant. Petroleum, which was initially used as lamp oil since the antiquity, subsequently accelerated the industrial revolution in the form of production machinery fuel. After the First World War, construction materials and metals were consumed for the manufacture of war machinery, and above all had become very rare and expensive for daily products. Hence, the search for new materials, meeting the requirements of the citizens' convenience goods, was accelerated. From this demand, a manifold of petroleum-based polymers were developed and molded to all kinds of elements, vessels, cases and surfaces.<sup>[1,29]</sup>

From a chemical point of view, polymers are long repetitive molecules, comparable to chains, built up from several thousands of repeating single units of macromolecules that comprise structural basic units. Defined by Mark, for synthetic polymers made from crude oil, those core units consist of carbohydrates either in basic form, modified by functional groups or alternating with characteristic molecules, such as aromatics.<sup>[30]</sup> The main chain, forming the backbone, exemplarily consists of repeating carbon units (in vinyl-derived polymers) or carbon combined with non-carbon units (other condensation derived polymers).<sup>[31,32]</sup> One of the polymers' main benefits might be located in inter- and intra-chain bonding, which alternate with the nature of the backbone, the chain size and geometry, molecular weight and additives amongst others and enables the versatility in appearance and mechanical properties.<sup>[33,34]</sup> The major drawback of synthetic polymers is the limited residual amount of their raw material. Crude oil originates from ancient biomass, which has been chemically converted in a millions-of-years-long process and still cannot be produced artificially in the required amounts. Since human life and industrial processes now depend considerably on synthetic polymers, the artificial production of crude oil is researched intensely.



The Norwegian company Nordic Blue Crude AS in cooperation with Sunfire GmbH and others, have announced the development of an industrial scale plant for the synthesis of this valuable raw material from water, carbon dioxide and eco electricity starting in 2020.<sup>[35]</sup>

Some of the best known and most employed synthetic polymers in the textile industry, hygiene products and healthcare are presented in the following. Amongst the industrial polymers especially polyesters are highly prominent due to their extensive usage in the textile industry. Chemically the main premise for Polyesters is the presence of an ester group in their main molecule (see Figure 1.1).

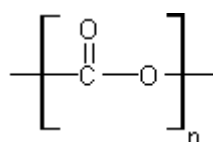


**Figure 1.1:** Characteristic ester group (monomer) in polyester molecules, derived from poly-condensation reactions between acids and alcohols or phenols.

Even though Polyesters are a whole subcategory of synthetic polymers, labels of textiles contain this term, as well as, the abbreviation PES in the material composition section, mostly without further specifications. Consequently, in the textile industry two types of polyester fibers are used, the more prominent poly(ethylene terephthalate) (PET) and the rarely used Poly(-1, 4-cyclohexylene-dimethyle terephthalate) (PCDT). Whilst PET is more durable and strong, and therefore is used alone, as well as, in blends, PCDT has a higher elasticity and resilience and is processed in blends only.<sup>[36-38]</sup>

### 1.3.1 Poly(ethylene terephthalate)

Poly(ethylene terephthalate) (PET) is a thermoplastic, produced via poly-condensation reaction between ethylene glycol and dimethyl terephthalate or terephthalic acid. Industrial applications range from plastic bottles, foils, food and household containers to textile fibers, which were developed in 1941 by J. R. Whinfield and J. T. Dickson in Great Britain.<sup>[39,40]</sup> In a first step, ethylene is synthesized from petroleum and oxidized to glycol monomers.

Those are then combined with monomeric terephthalic acid in vacuum, and at high temperatures in the second step in a catalytic reaction to obtain the final polymer (see Figure 1.2).<sup>[41]</sup>

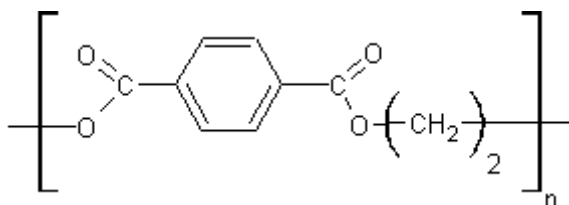


**Figure 1.2:** Monomer of PET, derived from poly-condensation reaction between ethylene glycol and dimethyl terephthalate or terephthalic acid.

Fibers made from PET feature high mechanical strength, which is based on the molecules polar character and the resulting intermolecular interaction. Additionally, the linear structure of the chains yields semi-crystalline regions, without preliminary cross-linking. Therefore, the fibers feature an increased fracture strength and shape stability perfectly suited for fibrous or planar applications.<sup>[42]</sup> New attempts of PET, modified with glycol (PETG), use its low viscosity for advanced fused deposition molding in 3D-printing applications.<sup>[41]</sup>

The major drawback of PET is its low resistance against strong mineral acids, especially sulfuric, nitric and hydrochloric acid. Due to the intensive industrial production of PET, the total production volume still increased steadily to 56 million tons in 2016 alone and therefore the importance of recycling has been steadily growing during the first decades of the 21<sup>st</sup> century.<sup>[43]</sup>

### 1.3.2 Poly(acrylonitrile)

Another polymer that is well-known in textile industry and additionally for serving as a precursor in carbon fiber production is poly(acrylonitrile) (PAN). The semi-crystalline molecule is derived from polymerization of polar acrylonitrile (see Figure 1.3) and features a high young's modulus (stiffness) and tensile strength due to strong intermolecular interactions, mainly brought forth by the attached nitrile group.<sup>[44]</sup>

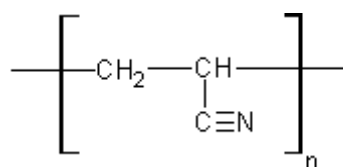


**Figure 1.3:** Characteristic acrylonitrile monomer in PAN molecules.

Furthermore, PAN is resistant to most solvents and chemicals, burns slowly and has a low permeability to gases. Therefore, PAN fibers are for example used in industrial hot gas filtration systems.<sup>[45]</sup> Fibers made from PAN feature a smooth touch and a shiny surface. The main amount of the world's annual output is employed in the production of highly stressed outdoor textiles like sails for yachts or tents, as well as, in knitted clothing- and furniture textiles acting as wool replacements. Most prominent textile fibers made from PAN are sold using trademarks such as Dralon and Dolan and many more.<sup>[46]</sup>

### 1.3.3 Poly(ethylene oxide)

Chemically, Poly(ethylene oxide) (PEO) belongs to the group of polyethers in the form of -R1-O-R2-O-R3- and might be considered as their representative build from the simplest monomeric unit (see Figure 1.4).<sup>[47]</sup>

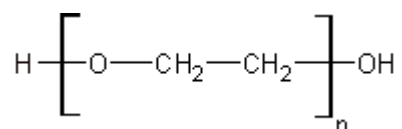


**Figure 1.4:** Monomeric unit (ethylene oxide) of PEO.<sup>[47]</sup>

This polymer is also referred to as poly(ethylene glycol) (PEG). Both names are treated synonymously, whereas historically PEG was used for molecules up to a molecular weight of 20 kg/mol and PEO for larger molecules. Depending on the chain length PEO is available as liquids or low-melting solids. The latter are highly soluble in water and are hygroscopic and therefore used as thickener or dispersant in numerous cosmetic products such as lotions, creams or as anti-foaming agent in food.<sup>[48,49]</sup> PEO is generally considered to be biologically inert, highly biocompatible and safe. Hence, in medical industry it is applied as a biomaterial for the production of hydrogels or building blocks in copolymers, as non-degradable polymeric carrier materials in drug delivery or as enhancer of

the osmotic pressure in gastrointestinal cleaning fluids.<sup>[50-52]</sup> Also in industrial scale PEO is used, exemplarily as binder in precursor for production of ceramics.<sup>[53]</sup> Because of its versatility PEO is one of the most prominent and common polymers and, in addition to its comparatively safe and easy handling and preparation, often employed as a demonstrative model for the processing of water-soluble polymers.

## 1.4 Biopolymers

Polymers from natural origin, plants and animals as well, in the first place are widely important for human daily nutrition. In form of carbohydrates and proteins, such as gelatin or silks of arthropods, polymers are ingredients in most foods. Additionally, polyesters such as cutin and suberin, both found as insoluble epidermal cell wall components in higher plants also are subsumed under the term biopolymer.<sup>[54]</sup>

Since the components of those materials may be metabolized and completely degraded after the internal application, many studies focused on broad medical approaches and therefore their employment as *Biomaterial*. Especially polysaccharides are well known, and easy to modify for different purposes offering a wide field of applications.<sup>[55]</sup> One of those polysaccharides, cellulose, is called rayon in one of its regenerated form and is also widely used in industrial scale textile production and even as bio-textile in medical implants.<sup>[56-58]</sup>

Biopolymer applications were made in the field of drug delivery for example with orally applied chondroitin sulfate for treatment of articular pathology.<sup>[59]</sup> Here, the degradation of the carrier and therefore the consumption dynamic is mainly influenced by the degree of sulfation.<sup>[60,61]</sup> Other studies focused on the cross-linking of chitosan to create loadable microparticles or liposomes and granules to benefit from low density cholesterol-lowering and weight-loss supporting effects of chitosan.<sup>[62-64]</sup> Definitions of biopolymers differ in terms of the origin of the raw material and their application. The technical report 15932 (CEN/TR 15932) for bio-based products, which was published from the technical committee 249 of the European Communications, Entertainment & Technology Law committee (CEN/TC 249) included a recommendation for the terminology and characterization of biopolymers and bioplastics as depicted in Figure 1.5.

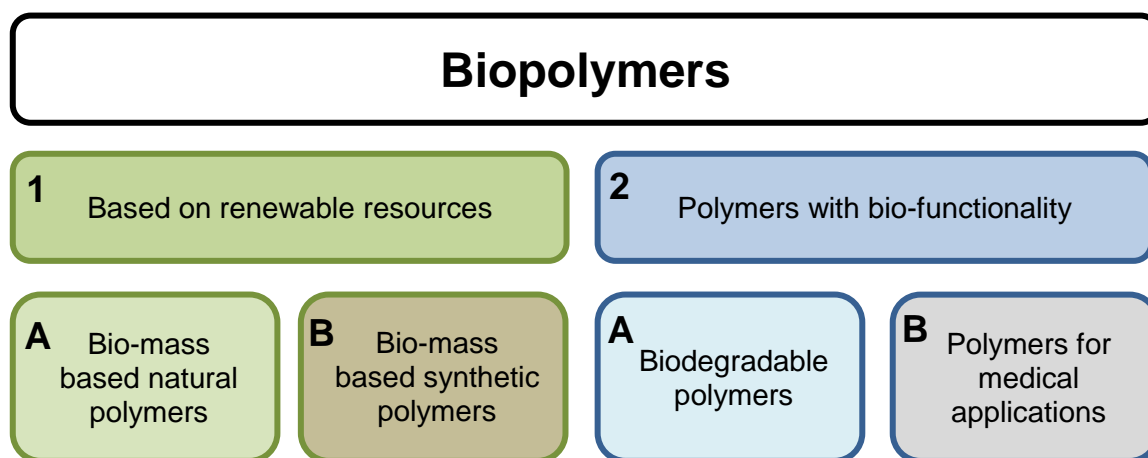


**Figure 1.5:** Definition of biopolymers modified after CEN/TR 15932.<sup>[65]</sup>

Regarding this definition, biotechnologically derived polymers such as poly(lactic acid) (PLA), for the production of bioplastics in food packaging, belong to category 1B. On the other hand, natural polymers, such as collagen, as well as, polysaccharides like cellulose and starch, used in cosmetics, belong to category 1A.<sup>[65-68]</sup> Despite their versatility, the main drawbacks of the latter polysaccharides are source-related variations in material properties, microbial contaminations, poor mechanical properties on top of both water uptake and uncontrolled degradation.<sup>[69]</sup>

One of the most prominent examples for bioplastics based on renewable resources is biodegradable thermoplastic poly(lactic acid) (PLA) (Figure 1.6), also referred to as “polylactide”, made from renewable resources, such as starch from corn, sugarcane, tapioca roots or yeast. It cannot be harvested in nature directly. The aliphatic molecule is mostly prepared industrially in a step-wise polymeric growth from renewable resources.<sup>[70,71]</sup> This can either be done by direct polycondensation in high boiling solvents or direct polymerization in bulk followed by chain extension with reactive additives.<sup>[72]</sup> Despite of its name PLA belongs into the category of polyesters rather than polyelectrolytes (polyacid).

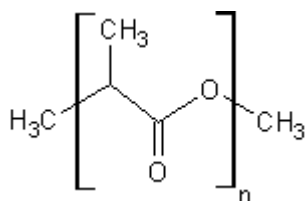


**Figure 1.6:** Monomeric unit (lactic acid) of PLA.<sup>[73]</sup>

PLA might be employed as mulch-films in ecological friendly farming or as cups, bags or similar, acting as degradable plastics replacements.<sup>[73]</sup> Because of the mostly autocatalytic degradation poly(lactic acid) is mainly applied in medical products. Whilst degrading, the material induces an acidic milieu, harmful in some tissues. PLA is often applied in bone plugs, screws or fracture fixation plates. Yet, the applications are limited because of a rapidly reducing material strength *in vivo*.<sup>[74]</sup>

Silks, another well-known example for biopolymers, in scientific terms are fibrous proteins, containing repetitive amino acid sequences, which are spun or pulled under shear forces. According to Craig (2003), some male myriapoda produce fibrous proteins from accessory glands, which could be called silk, for mating purposes (sperm stalks, sperm webs, mating threads).<sup>[75]</sup> The coiling millipede (*Glomeris marginata*), or the chilipod centipede (*Orphnaeus brasilianus*) produce sticky and toxic secretions, but the main silk producing organisms are found amongst the arthropoda-classes of insecta (insects) and arachnida (arachnids).

#### 1.4.1 Natural Polymers

##### 1.4.1.1 Spider silks

In the subphylum of chelicerates, only the all-terrestrial class of arachnida, comprising the silk producing orders true spiders or araneae (web-building spiders, tarantulas and wolf spiders), acari (mites and ticks), as well as, pseudoscorpiones (false scorpions), are able to secrete silks.<sup>[76]</sup> Whilst acari and pseudoscorpiones are using glands in their trophi attached to their head, spiders are in particular specialized on silk production through glands placed at the end of their abdomen. These spiders are capable of producing up to

seven different types of silk.<sup>[75]</sup> To produce fibers, these spiders developed unique specialized protrusions, called spinnerets as depicted in Figure 1.7.<sup>[77,78]</sup>

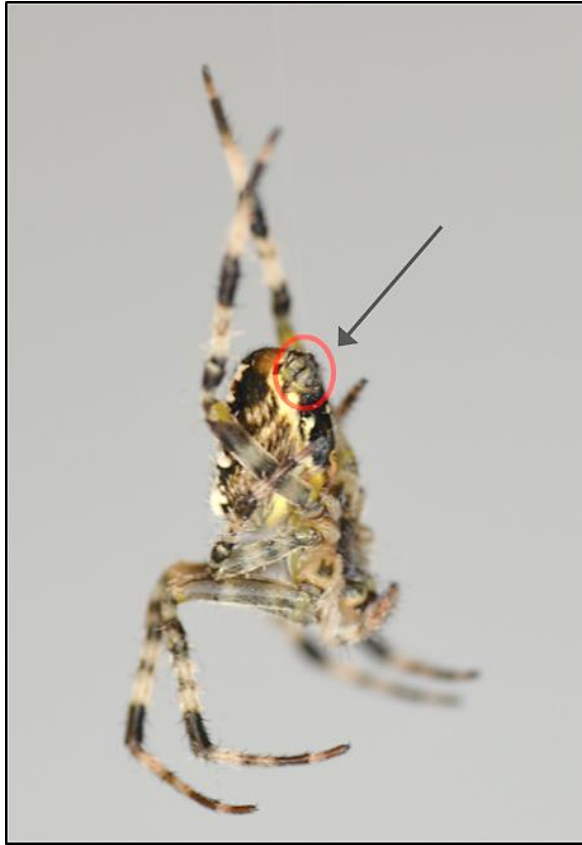


**Figure 1.7:** European garden cross spider (*A. diadematus*) while rappelling using its dragline with highlighted spinneret.

True spiders use silk in a manifold of ways to catch prey by building highly structured webs (web weaving spiders), to enhance their tactile sense and to protect their offspring.<sup>[79]</sup> Orb-weaving spiders may produce up to seven different types of silk from which araneidae use tubuliform silk for the deposition of their eggs and the sheathing in a protective cocoon (Figure 1.8, white, 1/2). The remaining five types are used for the construction of their webs, one of the most effective and economical methods of catching prey in the animal kingdom.<sup>[80-82]</sup>

The proteins of each silk are produced in their individual gland inside the spider's abdomen and pulled out of the storage by attaching the end of the thread to a fixed point and dragging the thread while walking in the desired direction.<sup>[83,84]</sup> The main frame of the web, as well as, the stabilizing outer construction (Figure 1.8, 3.1)

and the spider's dragline (Figure 1.8, 3.2), used for self-protection while rappelling, is composed of major ampulate silk. It is characterized by exceptional tensile strength and mechanical toughness.<sup>[85]</sup> During the web construction the spider builds an assistant-spiral (Figure 1.8, 4) using minor ampulate silk, to facilitate the following buildup of the catching spiral (Figure 1.8, 5), composed of flagelliform silk. The extraordinary extensibility of this silk type is necessary for the intake of the kinetic energy of an impinging flying insect without ripping and its subsequent dissipation into the web structure. To prevent the repulsion from the web and to fix the prey on the impact spot, the threads of the catching spiral are covered with sticky droplets of aggregate silk (Figure 1.8, 6).

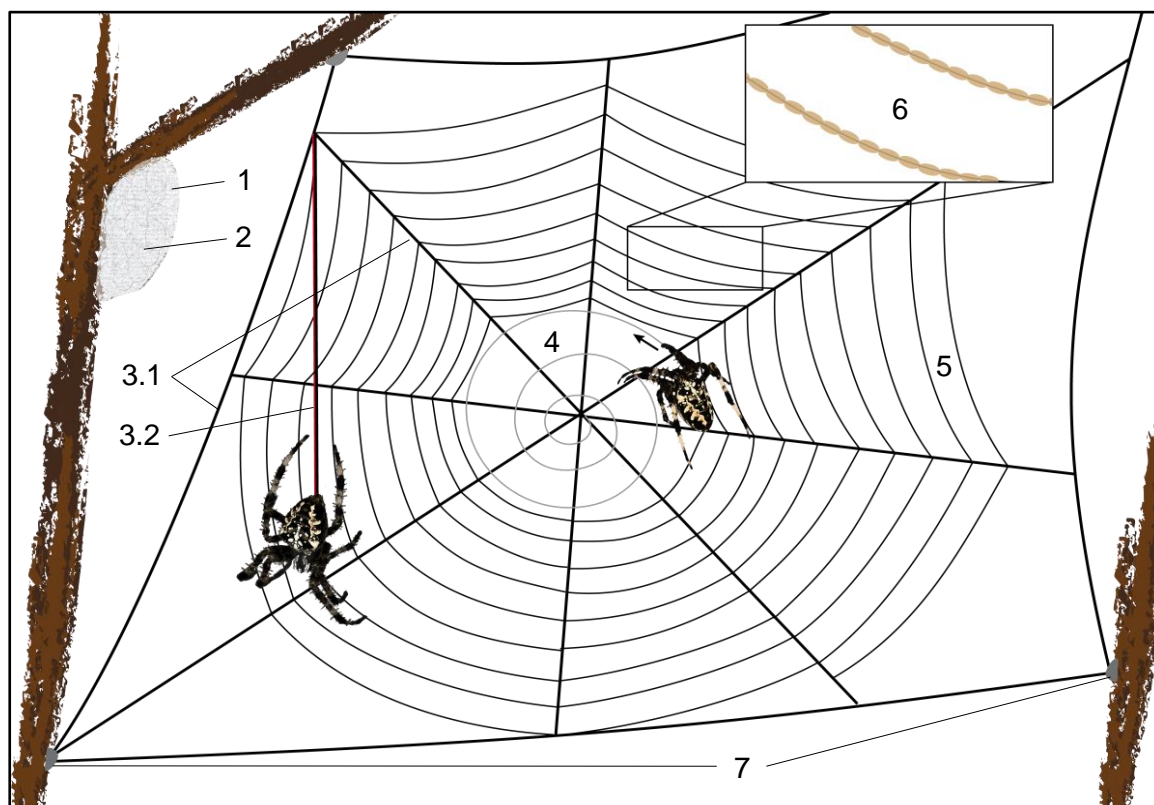


**Figure 1.8:** Web construction of orb-weaving spiders from different silk types with outer and inner shell of their cocoon (white, 1/2), the framework of the web (bold black, 3.1), the spiders dragline (bold black/red, 3.2), the supporting spiral (light grey, 4) which is used by the spider to build up the catching spiral (black, 5) covered with sticky silk droplets (brown, 6); the whole web constructions are fixed on surfaces via the frame construction using cement silk dots (grey, 7).

The last silk-type used for the web construction is named piriform silk and acts as cement, attached to the ends of the web's frame structure and connects it to the environmental fix points (Figure 1.8, 7). Many spider families have developed two identical spinnerets placed next to each other, which enable them to spin double threads in case of emergency to reinforce their dragline even more or while wrapping of their prey with aciniform silk.<sup>[86]</sup>

#### 1.4.1.2 Recombinant production of silk proteins

Due to the desirable mechanical properties of silks numerous applications in human healthcare and industrial purposes have been published.<sup>[87-91]</sup> Those properties comprise



extraordinary toughness (spider silk) or high bending stiffness (egg stalk silk of lacewings). One major drawback is the limited access to naturally sourced spider silks, due to their cannibalistic and territorial behavior, hampering their large-scale farming.<sup>[92]</sup> To overcome this hurdle, recombinant production of silk proteins has been auspiciously established in the past.<sup>[90,93-95]</sup> For recombinant production spider silk proteins (spidroins) consensus sequences, based on repetitive motives of the core sequences of dragline silk-spidroins were created. In a following step the genetic information was adapted to the codon usage of the host organism, e.g. *Escherichia coli* (*E. coli*). Furthermore, multimerization via cloning steps was performed, and the transfer of the genetic information into a vector resulted in a plasmid.<sup>[96]</sup>

Recombinant production of insect silk proteins is comparable to that of spider silk. In this process the lacewing *Chrysoperla carnea* (*C. carnea*) served as model organism. In a first approach consensus sequences were created as well. Yet, for the following production of recombinant egg stalk protein consensus sequences were not needed anymore, since the usage of natural sequences was facilitated.<sup>[97,98]</sup>

### **1.4.1.3 Insect silks**

Within the class of insecta, in the subphylum hexapoda amongst arthropods the larvae of the silkworm *Bombyx mori* (*B. mori*) is the best-known producer of silk. Because of its touch, shine and good availability, it is used for textile production by men since millennia.<sup>[99]</sup> Similar to other silk secreting organisms, *B. mori* - silk proteins are produced in glands, placed in the prosoma, the front part of the body, and secreted by their differently shaped mandibles.<sup>[100]</sup> Other insects like lacewings and most spiders use secretion protrusions or spinnerets connected to their specialized glands at the end of their opisthosoma, the abdomen.<sup>[77,78]</sup> To generate a fiber out of the highly concentrated silk dope, most organisms use pultrusion rather than extrusion to apply the necessary tension. Regarded separately, *B. mori* silkworms attach their silk to a prior produced layer of randomly spun silk threads between sticks and then pultrude the silk out of their storage using a lying-eight-movement to enwrap themselves in a final cocoon.<sup>[84]</sup> Less known, honey bees like *Apis mellifera* (*A. mellifera*), or wasps (apocrita) include silky threads in the highly hydrophobic waxy structure of combs inside their hives to reinforce the structure.

Underwater insects are also able to produce sticky silks such as caddisflies (trichoptera) whose larvae collect debris and stick it to their abdomen using their silk as cement to yield an underwater shelter.<sup>[101]</sup> The lacewing *Chrysoperla carnea* (*C. carnea*) places a silky droplet on leaves and lifts its abdomen to produce an extraordinary bending stiff thread. On its lower end it is attached to an egg, hanging from the leaf to be protected from predators. Especially the notable mechanical properties of lacewing silk, induced by cross-beta structures, were extensively studied.<sup>[89,97,98,102,103]</sup>

## 1.5 Properties of synthetic and natural polymers

Due to the multitude of conversion and synthesis possibilities of petroleum into all kinds of industrially utilized polymers, they are highly used for a variety of convenience goods. Yet the source material is limited, which is the greatest drawback of synthetic polymers. Additionally, oil production will become more difficult due to depleted easy accessible resources.<sup>[104]</sup> Hence, replacements must be found, which may be derived from renewable resources. Even though scientific research and technical development offer the usage of renewable polymers, most of them are produced with the need to care for distinct production methods, conditions and treatments. Hence, the costs are much higher compared to their synthetic counterparts. The second major drawback dulling the enthusiasm for polymers from renewable resources, is the still much lower mechanical resilience.<sup>[105]</sup> These facts represent the greatest disadvantages compared to synthetic polymers. Synthetic ones furthermore might be “grafted”, modified chemically on a molecular level by substitution or insertion of molecules and thereby altering the polymer backbone to adjust their properties as desired in respect of the distinct application.<sup>[106,107]</sup> The development of synthetic polymers culminated in a multifold assortment providing various chemical and mechanical properties, as well as, geometric shapes as displayed in Table 1.1 that comprises a selection of synthetic polymers with high production volumes and their typical morphologies, properties, features and potential application.

Most prominent materials are deployed in all fields of daily life from medical therapies and pharmacy to industrial textiles.<sup>[108-110]</sup> Important factors regarding fiber applications are the lateral contraction, elasticity, young’s modulus, the total appearance, including touch, look and surface morphology, in addition to durability, and abrasion resistance. Polyamide (PA) fibers for example provide low density and thereof produced lightweight products featuring a low water uptake and reduced swelling.<sup>[111]</sup> A nature-like optic at the expense of moderate mechanical stability might be obtained by employing Poly(acrylonitrile) (PAN) fibers with a woolen soft and warm touch, as well as, Cellulose Acetate (CA) fibers with a silky shine and minor wrinkle propensity.<sup>[112]</sup> Yet, if water repellency is demanded for production of woven outdoor textiles, shoes or electrical insulations Poly(vinyl chloride) (PVC) is the raw material of choice. Altogether, polymeric materials are most prominent for their versatility due to thermoplastic behavior amongst others. In that context Polycarbonate (PC) is a well-known example used in planar applications such as lenses for sun glasses or disks.<sup>[113]</sup>

**Table 1.1:** Overview of a selection of the most common and best known synthetic polymers used for industrial scale applications.

| Material                                | Application   | Features                                   | Properties   | Morphology                        |
|---|---|--|--|-----------------------------------|
| Poly(acrylonitrile) (PAN)               | Yarns in textile industry/ carbon fiber precursor                     | Wool like aesthetics (warm and soft touch) | Moderate abrasion resistance, well colorable                 | Filaments/ Fibers, Yarns          |
| Polyacrylate sodium salt (PA)           | Super-absorber (diapers)  | High porosity                              | May take up water of more than 300 times the bulk mass       | Highly porous particles           |
| Polycarbonate (PC)                      | Sunglasses, eye lenses, disks   | High fracture strength                     | Two benzene rings stabilize monomer                          | Planar objects                    |
| Poly(ethylene oxide) (PEO)              | Medical formulations, lubricant                                       | Highly hydrophilic, well soluble in water  | Different molecular weights, solutions up to gels obtainable | Particle powders, pellets         |
| Poly(ethylene terephthalate) (PET)      | Packaging, plastic bags, plastic bottles                              | Flexibility, highly (re)formable           | Thermoplastic, therefore highly versatile                    | Films and foils                   |
| Poly(p-phenylene terephthalamid) (PPTA) | “Kevlar” in bullet resistant vests, immensely stress resistant fibers | High tensile strength and toughness        | Two benzene rings and nitrile group strengthen monomer       | Fibers                            |
| Poly(vinyl chloride) (PVC)              | Pipes, outdoor textiles, sport shoes, electric insulation             | Water repellency, pressure resistance      | Chloride ion in monomer raises stability                     | Planar objects, Filaments/ fibers |

Yet, the certainly most widely used polymeric material in everyday life are Poly(ethylene terephthalate) (PET) due to its processability into tear-resistant and tenacious foils and films for the manufacturing of all kinds of bags, as well as, for (food) packaging purposes and plastic containers and bottles.<sup>[114]</sup>

Polymers from natural resources on the other hand are increasingly utilized in applications due to improved processing methods and the increasing production rate. The most prominent naturally derived polymers, as well as, their origin, possible application, properties and typical product morphology are displayed in Table 1.2. The use of some of those naturally derived polymers are not recent inventions, but known for decades such as rubber, which became one of the most important resources in the production of tires

induced by the discovery of the vulcanization reaction of natural rubber and sulfur by Charles Goodyear in 1839. The reaction, also called curing, is used to crosslink the natural rubber molecules with sulfur resulting in a remarkable tenacity and flexibility.<sup>[115-117]</sup>

Wood has been used as strong construction material for thousands of years, and the strength of plant fibers has been known for long. Hence, the highly robust cellulose fibers, derived from herbal cell walls, as the most prominent representative of polysaccharides, is utilized in textile production, and as a solid fuel. Lately, this material is also gaining more importance in modern medical research, drug delivery, as well as, tissue engineering. In the field of polysaccharides also chitin, derived from marine crustacean shells, and its more water-soluble derivate chitosan, are candidate materials in this field of research. For bone replacement applications also mammal collagen is promising.<sup>[55,118-120]</sup> Moreover, another aspect of modern research is the development of genetic engineering and biotechnological manufacturing methods, which enable the large scale production of natural derived polymers, such as PLA for textile industry or spider silk proteins. Yet, PLA is barely used in medical application, due to its acidic metabolites.<sup>[70,121]</sup>

Spider silk is a multifaceted material with various desirable properties. Those range from fibrosis reducing effects when used as a component or coating in medicine and prosthetics, embodying an efficient water vapor and oxygen shield utilized in food packaging, to providing high toughness and elasticity when employed as fiber.<sup>[122-125]</sup> The development of biotechnological production methods overcomes the lack of natural availability further pushing investigation of possible applications.<sup>[90,93-95]</sup> Additionally, the material might be metabolized completely into harmless amino acids by most living creatures.<sup>[87,88,126]</sup> Hence, silk proteins might be considered as one of the most promising bio-derived materials when it comes to sustainability in combination with extraordinary mechanical properties. But also other highly specialized animal proteins besides spider silks serve as templates for research and biotechnological production, such as the mechanically gradually altering mussel byssus or other insect silks, for example from honey bees.<sup>[90,127-130]</sup> As soon as research and implementation of multiple technical applications overcomes the hurdle of mass production, biologically derived recombinant proteins, headed by spider silk protein, might guide the way into a new industrial revolution of materials.<sup>[131]</sup>

**Table 1.2:** Overview of the renewable polymers under research and their properties as well as possible applications.

| Material          | Derived from   | (Possible) Application   | Properties  | Morphology  |
|-------------------|--|--|---|---|
| Cellulose         | Plants (Wood), biosynthetic synthesis                    | Wooden constructions, textiles (lyocell), tissue engineering, drug delivery                    | Highly stable molecule                                      | Raw material (wood), fibers and textiles, films, capsules |
| Chitin/ Chitosan  | Crustacean shells  | Outdoor clothing, food packaging, cosmetics  | Solvable in acidic aqueous media, resistant                 | Films and foils, particles                                |
| Collagen          | Mammal corpses (human, pig)                              | Tissue engineering, regenerative medicine, cosmetics   | Elasticity, adaptable mechanical properties                 | Particle powders, fibers, hydrogels                       |
| Pectin            | Protopectin from plant cells/ fruits                     | Hydrogels in industry and medicine   | High molecular weight - viscosifier, high natural presence  | Particles/ powders to form gels                           |
| Poly(lactic acid) | Lactic acid from plants (e.g. corn)                      | Textile industry, food packaging, implants   | Versatile, UV- and flame resistance, low moisture regain    | Fibers, films, foils, medical implant connection elements |
| Rubber            | Natural rubber as latex (milky colloid) from rubber tree | Tires, sealing gaskets, Control interfaces, Anti-shock elements                                | Large stretch ratio, flexibility, elasticity and resilience | Volume bodies, blocks, sleeves                            |
| Silk proteins     | Recombinant production                                   | Fibers for textiles/ industrial purposes, drug delivery, protective and biocompatible coatings | High tensile strength, toughness, versatility               | Fibrils, fibers, films, foils, particles                  |

## 1.6 Fiber production methods

Fibrous materials from natural resources have been long utilized by mankind to create textiles for protection, warming, camouflage or fashion purposes. Prominent examples are the fur or wool of mammals, as well as, silk from arachnids and insects - from animal origin - on one hand, or fibers from herbal origin (linen (Li) made of flax, cotton, hemp, bamboo) on the other. Technological development has allowed mimicking these by using basic materials from alternative resources, available in larger scale, such as synthetic polymers made of crude oil. Through modern research and technology, many artificial fibrous products even surpassed the natural ones, in terms of mechanical or optical

properties. To customize fiber parameters, such as surface morphology, fiber strength, diameter and appearance, different processes were invented. The herein used categorization is based on a combination of the solvent or physical solvating force of the raw material respectively, as well as, the driving force of the spinning process. Earth and reddish colors are displaying spinning methods based on polymer melts; yellow and greenish colors stand for electrically driven spinning processes and blue colors decrypt solution spinning methods (Figure 1.9).<sup>[132]</sup>

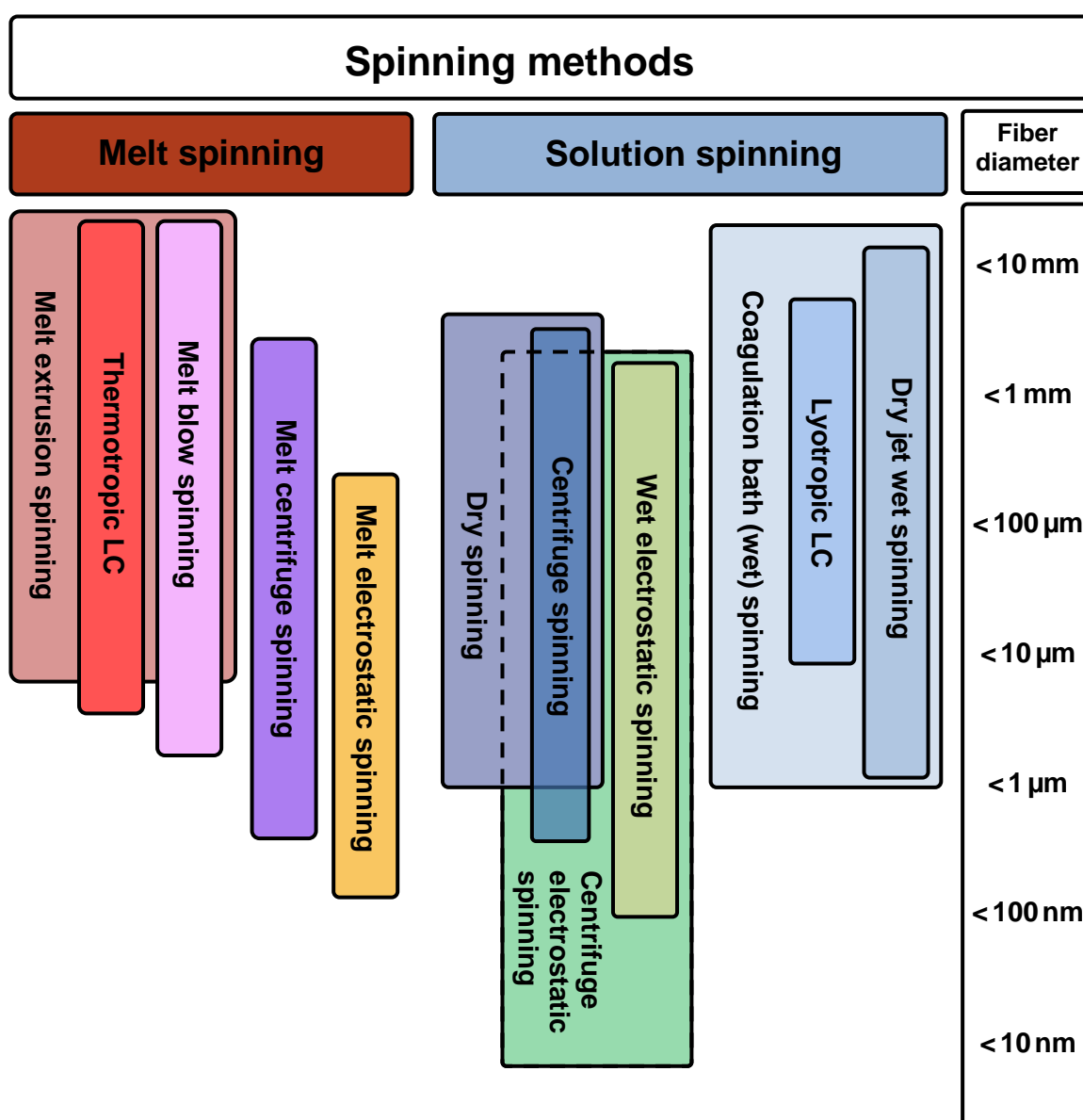


**Figure 1.9:** Overview of the mainly industrially employed spinning methods and the respective fiber diameter range.<sup>[128-143]</sup>

### **1.6.1 Melt spinning**

The name of these spinning methods refers to the preparation of fibers from the melt. Heat is used to melt the employed thermoplastics. In its most basic form, the melt extrusion spinning, the highly viscous liquefied polymer-melt is extruded and further transported via a gear pump (Figure 1.10 A). Subsequently, the viscous melt is led into a dye block to further supply a subsequent (multifilament) spinneret. In the simplest form, the emerging filaments of the molten polymer that are extruded from the spinneret, enter a hardening zone, which is composed of a space cooled by quenching air (Figure 1.10 A). The filaments thereby cool down and solidify.

Following this, the emerging fibers are led through stretching pipes and either taken up to be post-stretched in a second step (two step continuous filament spinning, Figure 1.10 B) and finally collected on a bobbin, or deflected to create randomly oriented nonwovens, directly being deposited upon a receiver mat using suction-air (spunbonded fabric process, Figure 1.10 C). Both methods are versions of classical melt extrusion spinning.<sup>[133]</sup>

#### **1.6.1.1 Melt-blown spinning**

The most common and most frequently employed spinning method to produce synthetic fiber nonwovens for textile industry is melt-blowing (Figure 1.10 D). The basic form of this subcategory of melt spinning processes is carried out by feeding the polymer melt to a nozzle structure instead of a multifilament spinneret. Cooling air is then streamed in high velocities at the nozzle tip, resulting in a spray-like jet of multiple fibers. Deposition on a rotating drum results in nonwoven fiber mats.<sup>[133]</sup>



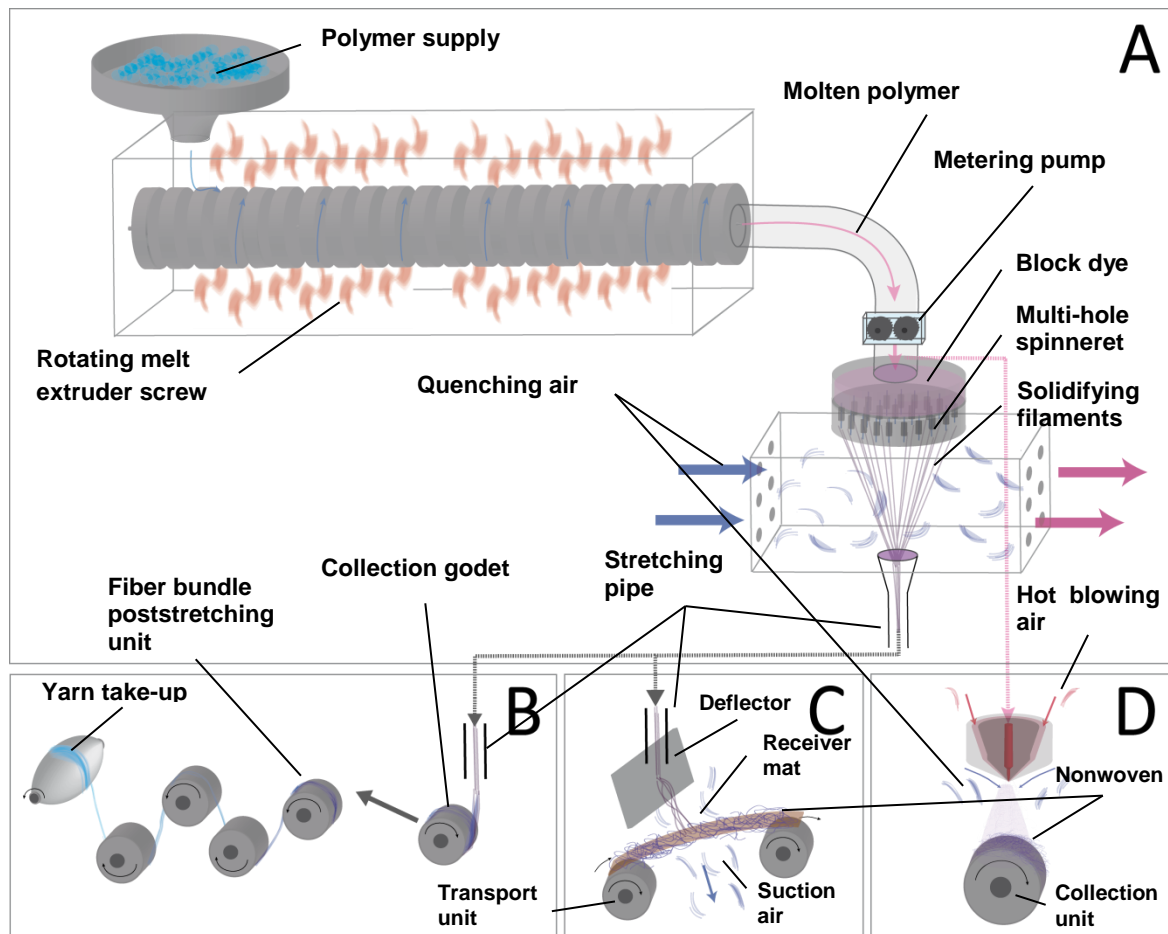


**Figure 1.10:** Basic scheme of melt spinning method; a polymer is led into a heated extruder screw where the material is molten and then extruded with a constant flow through a multifilament spinneret with the help of a metering pump (A). In classical melt spinning, the fibers are cooled and hardened by quenching air and let into a stretching pipe. Subsequently, the filament bundles are either collected to be post-stretched with altering rotational velocities, followed by a yarn take-up (B) or deflected to be randomly deposited on receiver mat using suction-air via a spunbonded process (C). For melt blow processes the polymer melt is directly pumped into a blowing nozzle, here hot air is used to accelerate multiple fiber jets. These fly towards a collection unit and solidify due to cooling by the quenching air (D).<sup>[133-135]</sup>

### **1.6.1.2 Special melt spinning methods**

Due to their special behavior, melt spinning of liquid crystals with thermoplastic character is regarded as special subcategory. Furthermore, the careful choice of working parameters provides a controlled spinning of uniform fibers. For example, researchers were able to produce melt spun single fibers in a one-digit micrometer range from liquid crystalline carbon.<sup>[135]</sup>

### **1.6.2 Solution spinning methods**

In contrast to melt spinning methods, in solution spinning methods, the utilized polymeric raw materials are dissolved in the organic or inorganic solvents. Most preferably aqueous solutions are employed to maintain a stable dope concentration by reduced evaporation at room temperature. Though, often polymers require aggressive and highly volatile solvents which demand a considerably increased amount of precaution, as well, as attention during handling and processing. Low viscous dope solutions are stored in tanks and transported using liquid pumps (Figure 1.11 A), while high viscous polymers are prepared using extruder screws and transported via gear pumps (Figure 1.11 B).<sup>[133,136-139]</sup>

#### **1.6.2.1 Dry spinning**

In its simplest version, solution spinning is performed by extruding the polymer solution through a multi-hole spinneret, and solidification of the emerging polymer is forced by the employment of hot drying air, in a special chamber. This method is called dry spinning (Figure 1.11 C). Provided, that the used solvent is highly volatile, this method is preferred due to its simplified fiber curing. The fiber production is relatively slow compared to other spinning methods. Typically fiber diameters obtained from dry spinning are in the range from 1  $\mu\text{m}$  to several micrometers.

The take-up has to be performed in reduced velocities due to the risk of a fiber break. A poststretching step can subsequently be added to produce high performance fibers (Figure 1.11 E).<sup>[133,140]</sup>

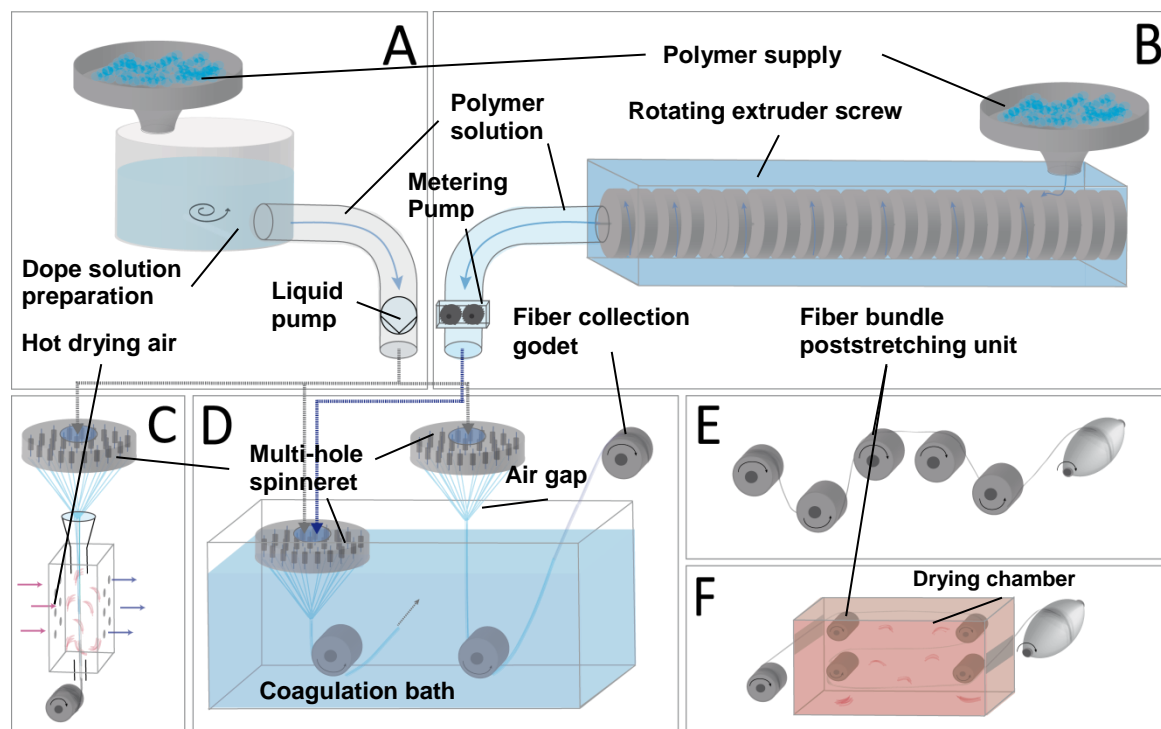


**Figure 1.11:** Basic scheme of solution spinning methods; a polymer is dissolved in a proper solvent; either a low viscous polymer solution is pumped, using a liquid pump (A), or a highly viscous high molecular weight polymer solution is extruded, using a rotating extruder (B), into multi-hole spinnerets. Hot drying air is directly streamed at the emerging filaments, which solidify and are subsequently collected, using godets regarding dry spinning (C). Emerging fibers might be led into a coagulation bath, either sub-liquid level (C1, classical wet spinning), or using an air gap (C2) and collected upon solidification. The fiber bundles from dry or wet spinning may be poststretched, using godets with slightly increasing rotational velocities, if desired (E). Regarding ultra-high molecular polyethylene poststretching is performed in a heated drying chamber with fibers in a gel state to create high modulus polyethylene filaments (F).<sup>[133,136-138,140-147]</sup>

### **1.6.2.2 Coagulation bath (wet) spinning**

The most common and widely known wet spinning method is the basic coagulation bath spinning, also commonly referred to as “wet” spinning (Figure 1.11 D). Herein, the dope material is dissolved using a proper solvent and extruded through a nozzle or spinneret directly into the coagulation bath (Figure 1.11 D, left). This bath is filled with a liquid in which the dope material shows a lower solubility compared to the solvent. The solidifying filaments are extracted from the bath and subsequently dried using hot air, infrared radiation or similar, and poststretched, if desired (Figure 1.11 E).

#### **Dry-jet / air gap wet spinning**

In some processes it is beneficial to provide a short stretching phase after the fibers emerge from the spinneret. The filaments first dry in air and then subsequently pass the coagulation or quenching bath. Therefore, the fibers are led through an air gap before coagulation (Figure 1.11 D, right). Thus, the molecular chains are less separated by hydration spheres, and intermolecular attraction is increased. The fiber bundles are usually pre-stretched in the bath and post-stretched until finally cured during drying (Figure 1.11 E).

#### **Gel spinning**

To produce strong fibers from polyethylene (PE), which is one of the most important commercial polymers, gel spinning is performed. Ultra-high molecular weight polyethylene (UHMW PE,  $MW > 10^6$  g/mol) is dissolved in proper solvents such as decalin (bicyclo[4,4,0]decane) and extruded by a (twin) screw (Figure 1.11 B). A metering pump further squeezes the highly viscous suspension through a multi-filament spinneret. After passing an air gap and a subsequent quenching, or extraction bath filled with water, the filaments remain in a gel-like state, with a low entanglement of polymer chains, rendering them highly drawable (Figure 1.11 D right). Subsequently, the fibers are led through a

heated chamber and cure during solid-state drawing (Figure 1.11 F). The inherent crystals are thereby aligned to obtain high modulus fibers that further are collected on a bobbin.<sup>[142,143]</sup>

### **Lyotropic liquid crystal spinning**

One prominent product made by dry-jet wet spinning is Kevlar, processed from aromatic polyaramid. This lyotropic liquid crystal material is processed using sulfuric acid as solvent and a cold water coagulation bath. After extrusion, the emerging filaments are dried at the surrounding or hot drying air. The subsequent employment of an air gap contributes to the orientation of the liquid crystals. Parallel oriented crystals stabilize the fiber noticeably, and therefore the dry-jet directly influences the tensile strength and performance of the fibers. The filaments pass a coagulation bath, where solidification occurs. To further improve the product, a subsequent post-stretching step at temperatures ranging from  $T=300\text{ }^{\circ}\text{C}-400\text{ }^{\circ}\text{C}$  is added. The obtained fibers are finally collected and exhibit strong inter-chain forces due to the inherent hydrogen bonds aligned alongside the fiber axis, contributing to an extraordinary degree of orientation and strength.<sup>[144,145]</sup>

#### **1.6.2.3 Special solution spinning methods**

One special subcategory of coagulation bath spinning is matrix-spinning, which is performed during the production of PTFE-Fibers. Neither melt spinning, nor standard coagulation bath wet spinning methods are suited to process PTFE due to its resistance to most solvents and its high melt-viscosity. To overcome these hurdles, an aqueous PTFE-dispersion is mixed with a rayon matrix dope in a ratio of 3:1 - 24:1 and extruded into a highly acidic coagulation bath.

Subsequently, the emerging mixed fibers, containing PTFE and rayon, are sintered in order to thermally decompose the rayon and mechanically improve the fibers. Nevertheless, the residues of the sintering process lead to a brownish coloring of the fibers.<sup>[147]</sup>

### 1.6.3 Centrifugal spinning methods

The method of centrifugal spinning is a spinning method to generate fibers with small diameters in the lower micrometer range by a rotating orifice and subsequently occurring centrifugal forces. The utilized dope material is either dissolved by a proper solvent and transported via a liquid pump or molten and extruded by a gear pump, when using thermoplastics, as described before. This method is rarely used in industrial applications due to difficult fiber collection in its basic form. In laboratory experiments, polyamide 6 (Nylon 6) fibers were obtained with diameters below  $1\ \mu\text{m}$ , using centrifugal solution spinning.<sup>[146]</sup> With polypropylene melts also fibers in the lower micrometer range could be produced in laboratory experiments.<sup>[134]</sup>

The setup includes a container for dope storage, as well as, a pump for the extrusion of the dope through a nozzle. The latter is situated in or on a device capable of rotating around its axis of symmetry with the rotational speed  $\omega_r$  [m/s]. The droplet of the mass  $m$  [kg] emerging at the nozzle tip is thereby accelerated with a centrifugal force  $F$  [N], which can be expressed by Equation 1.1, and stretched due to its inherent inertia. During the flight time of the polymer jet either the solvent evaporates or the melt cools down and the jet solidifies, resulting in a fiber. Due to the centrifugal force, the fiber then is tossed towards a planar collector surface, mounted perpendicular to the axis of the nozzle in the distance  $r$  [m] and collected thereon.

$$F = m * \frac{\omega_r^2}{r} \tag{1.1}$$

Depending on the molecular weight of the dope material and the dope concentration, the degree of molecular entanglements shifts. Likewise, the fiber diameters, as well as, the degree of stretching alter.

The biggest disadvantage of centrifugal spinning is the limited length of the collector, with a maximum deposition length of its circumference. Due to a mostly necessary opening of the collector-ring the filaments have to be cut open, representing a severe handicap regarding the production of endless fibers. So far, limited studies focused on the improvement of the method itself, as well as, the large-scale production of nanofibers or thin submicron fibers of outstanding porosity.<sup>[148-151]</sup>

### 1.6.4 Electrospinning methods

Even though these methods use the surrounding air or atmosphere as solidification forces, and therefore belong to dry spin, the usage of an electric potential difference as the driving force for fiber formation enforces an exclusive categorization. The first requirement for these production methods was the description of the electric field by Charles-Augustine de Coulomb in 1784 in its scalar form, where  $\vec{E}$  is the electric field strength [V/m],  $k_e$  is the Coulomb's constant ( $k_e = 8.99 \cdot 10^9$  [Nm<sup>2</sup>/C<sup>2</sup>]),  $q_1$  and  $q_2$  [V] are the directional magnitudes of the charges and  $d_x$  [m] is the distance between these charges, as depicted in Equation 1.2.<sup>[152,153]</sup> This equation is valid for electrostatic fields that remain constant over time.

$$\vec{E} = k_e \frac{|q_1 q_2|}{d_x^2} \quad (1.2)$$

#### 1.6.4.1 Electrostatic (dry) spinning

The production of fibers with the smallest diameters down to the nanometer scale using an electric field as a driving force has been performed since 1902. The first observation of the movement of a liquid droplet due to a charged object was described by William Gilbert in the late 16<sup>th</sup> century.<sup>[154]</sup> It took several hundred years until the process of electrospinning (ES) was published in 1902 by John F. Cooley.<sup>[155]</sup> The basic setup is oriented vertically or horizontally.

The latter is beneficial if larger droplets are built during the spinning process, which here cannot fall on collected fibers and dissolve them, but are drawn to the ground by gravity. A standard vertical setup is displayed in Figure 1.12. High electric voltage is applied to a flattened capillary tip, which is attached to a container - mostly a syringe, filled with a spinning dope.

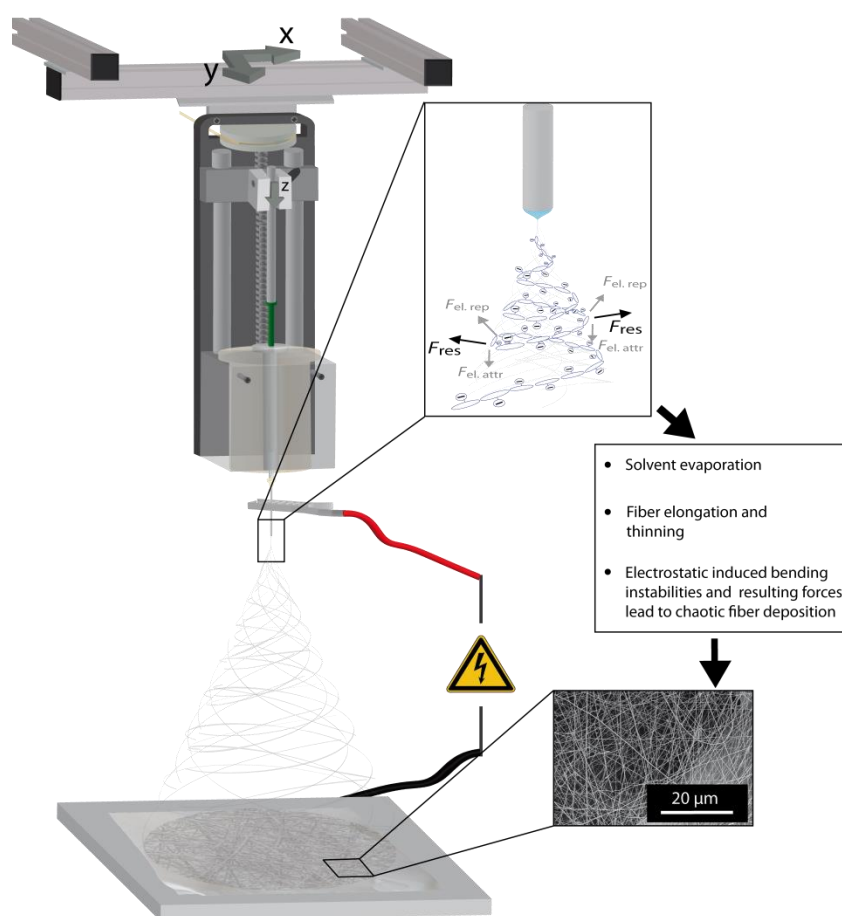


**Figure 1.12:** Schematic of a standard electrospinning device; a high electric potential is applied to a capillary tip acting as an electrode and a collector plate acting as a counter electrode. The latter is placed in a distance of 1 - 40 cm, using high electric voltage (0-45kV) which leads to a strong electrostatic field. Dope solution is extruded through the capillary tip. The electrostatic field induces repulsive forces inside of the emerging droplet forming a Taylor cone. If the attractive forces of the electrostatic field overcome the surface tension of the solvent, then a thin jet erupts from the cone, which is affected by bending instabilities causing loops and turbulences, and therefore stretching the fiber while traveling to the collector plate and solidifying them. Multiple chaotically deposited fibers form a nonwoven mesh.

Mostly polymer dispersions are employed due to simplified handling, but also melt-electrospinning is performed using thermoplastic polymers. A counter electrode is placed in a certain distance, regularly in between a range of 0 - 20 cm.<sup>[156-160]</sup> This set-up yields a strong triangular shaped electrostatic field. Whilst the polymer solution is extruded from the capillary, the potential applied to the capillary induces repulsive forces within the charged solution. The created droplet deforms into a cone shape (Taylor cone) due to



the repulsive forces and the attraction of the counter electrode on the molecules, which assemble at the tip of that cone.<sup>[161-166]</sup> If the surface tension is exceeded, a thin jet of enchaind polymer molecules erupts from the cone surface. Depending on the raw material used, the solvent and the setup itself, multiple jets may erupt from the cone or the jet, which also might split up during their flight leading to a variety of side-jets. After formation, induced by electrostatic interactions, bending instabilities (Rayleigh-Plateau/Weber instabilities) occur within the jet, causing whipping and further stretching as the solvent evaporates, and a solid fiber is formed.<sup>[167-169]</sup> Finally, the fiber is randomly deposited on the counter electrode in the form of a nonwoven mesh. This might be collected by a proper substrate placed on the counter electrode, as long as it is not disturbing the electrostatic field.

### Theoretic Background

The basic set-up can be considered as a two plate capacitors, with a constant total surface of  $A$  [mm<sup>2</sup>], and placed in a certain distance  $d_x$  [mm] building up the capacity  $C$  [F]. The material-specific dielectric constant  $\epsilon_R$  [-], the electric constant  $\epsilon_0$  [As/Vm], and the electric charge  $Q$  [As] are given and constant. The resulting capacity, influenced by a variable potential difference and therefore voltage  $\Delta U$  [kV] is calculated by Equation 1.3.

$$C = \frac{(\epsilon_0 * \epsilon_R * A)}{d_x} = \frac{Q}{\Delta U} \quad (1.3)$$

Furthermore, the present surface charge density  $\sigma$  [As/m<sup>2</sup>] on the capacitor plates can be expressed as in Equation 1.4.

$$\sigma = \frac{Q}{A} \quad (1.4)$$

Subsequently, the strength of the electric field which develops between those charged capacitors is in direct dependency of the surface charge density and therefore of the electric charge divided by capacitor surface area and the electric constant (Equation 1.5).

$$\vec{E} = \frac{\sigma}{\varepsilon_0} = \frac{Q}{A * \varepsilon_0} \quad (1.5)$$

Considering the constants, and combining Equations 1.3 to 1.5 leads to the simplified Equation 1.6 for calculation of the electric field strength, which only has to be enhanced by a form factor  $k$  [-], since these equations are valid for two ideal plate capacitors, which are infrequent for standard electrospinning setups. The standard set-ups presented and used in this work build up a pyramid shaped electric field, due to a point-like electrode and a plate capacitor as collector plate electrode, placed from each other in a certain distance  $d_x$  [mm]. Such an electrostatic field in a pyramid shape is associated with a form factor of  $k=1$  and a constant voltage  $U$ .<sup>[170]</sup>

$$\vec{E} = \frac{\Delta U}{d_x} * k \quad (1.6)$$

### **Influencing parameters**

Many parameters have a massive impact on the resulting fiber quality. The most obvious ones comprise the molecular weight (MW [g/mol]) of the raw material itself, the dope concentration  $c$  [g/l] of the spinning dope, and its resulting viscosity  $\eta$  [Pas], as well as, the solvent, and its volatility expressed by the vapor pressure  $e$  [bar]. Also the surrounding conditions, like temperature  $T$  [°C] or relative humidity  $rH$  [%] directly influence the vapor pressure, and therefore the fiber solidification process.

The higher the local temperature, and the lower the relative humidity, the faster the solvent evaporates, which can cause a drying out of the ideal Taylor cone (Figure 1.13 A) and may interrupt the spinning process.

The electric field strength  $\vec{E}$  [kV/mm] impacts the spinning process the most and results from the potential difference between the spinning electrode and the counter electrode that acts as collector plate. The underlying applied electric voltage has to be adjusted thoroughly in respect to the distance between the electrodes as displayed in Equation

1.6. Excessive electric field strengths in the first place lead to inconsistent spinning process and a stretched and elongated Taylor cone, representing the uncontrolled material removal if the dope extrusion remains constant. A further increase of the electric field strength leads to a retraction of the solution droplet into the cannula, resulting in a negative meniscus and the subsequent drying of the local solvent, as well as, the clogging of the cannula and the interruption of the spinning process (Figure 1.13 C). In contrast to that, insufficient electric field strength, as well as, a massive extrusion volume stream  $\dot{v}_e$  [ $\mu\text{l/s}$ ], may cause an overflow of the Taylor cone. The additional amount of material then cannot be carried away by the emerging jets, and whole droplets are tossed onto the collector plate, dissolving the produced nonwovens through the spilled solvent (Figure 1.13 B).

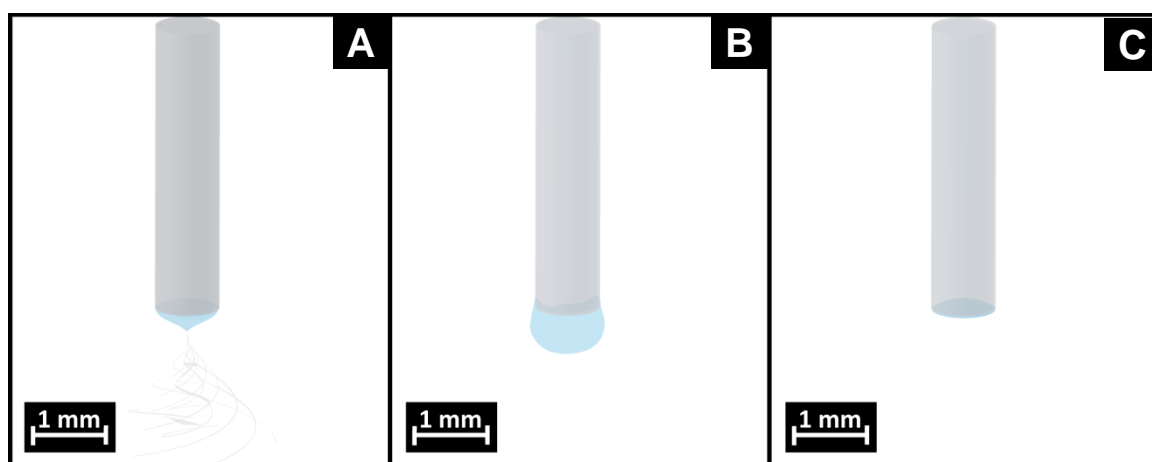


**Figure 1.13:** Schematic of a Taylor cone in proper form (A), an overflowing Taylor cone with emerging droplet (B), and the cannula electrode with retracted and dried out Taylor cone (C).

#### 1.6.4.2 Centrifugal electrospinning (CE)

Since this processing method represents a special modification of electrospinning, their basic setups are alike. Mainly the upper electrode in the form of a capillary tip is exchanged for a rotating bell shape (centerbell, Figure 1.14). Due to a high number of revolutions (0-50krpm) the extruded spinning dope is distributed in the inner bell wall and gathered at the lower edge. The repulsive forces in between the dope molecules, affect-

ed by the applied potential, and the subsequent accumulation of charges, as well as, the strong attraction to the counter electrode in the electrostatic field, yield a ring-like torus shape with multiple emerging Taylor cones (Figure 1.14, magnification). Once the electric field strength, as well as, the attractive forces exceed the surface tension of the solvent, numerous jets erupt from these cones along the torus. Their exact number depends on the repulsive forces, and therefore on the amount of accumulated charges.<sup>[171]</sup> The massive amount of evolving fibers and electrostatic interactions combined with the centrifugal force, due to the rotary movement, result in a radial acceleration of the fibers. To reduce a widespread fiber deposition, guiding air is led through a slit opening between the centerbell and the casing, building up a surrounding barrier and an additional force towards the deposition electrode.<sup>[172-177]</sup>

### **Influencing parameters**

In addition to the influencing parameters already described in 1.6.4.1, the method of centrifugal electrospinning (CES) comprises additional forces, and therefore additional influencing parameters. Mainly the revolutions per minute *rpm* [n] influence the lateral or centrifugal forces on the emerging jets. For highly viscous dope solutions a too slow rotational velocity can lead to an inhomogeneous distribution of dope solution in the centerbell and subsequently to inhomogeneous spinning results. Also, a local solution overflow in the centerbell and liquid drops on the resulting nonwoven meshes are possible risks for low viscous dope solutions. Maximal rotational speeds on the other hand, can cause drying out during the extrusion of high viscous dope solutions, whereas for lower viscosities, the emerging fibers are distributed over a broad area and the chance of receiving entangled fibers is increased, impairing the overall spinning result. Another parameter present for the described standard centrifugal spinning device is the guiding air pressure  $p_{air}$  [bar]. This air curtain reduces the spreading of emerging fibers by forcing them into the direction of the collector. Additionally, this air contributes to the solidification process of the fibers by accelerating the solvent evaporation.

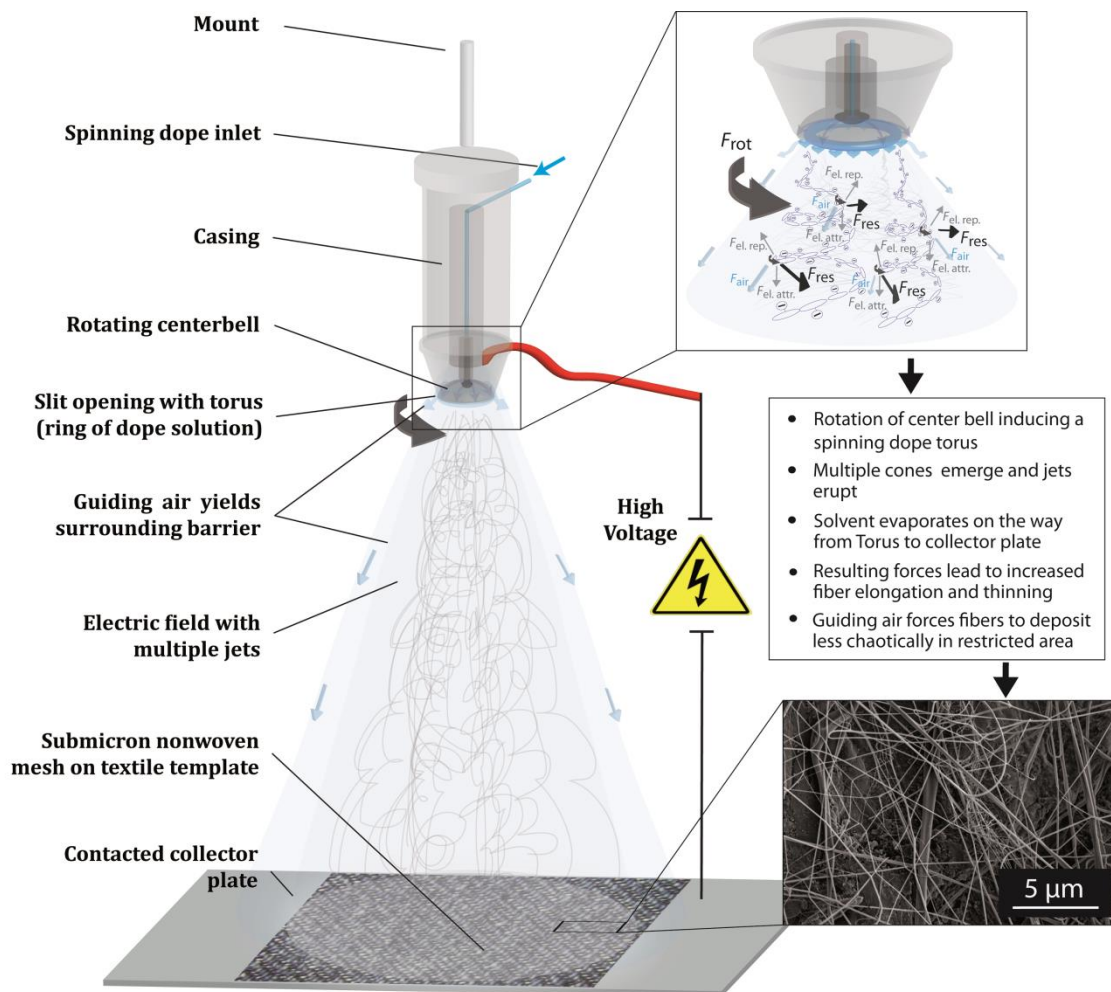


**Figure 1.14:** Schematic of a centrifugal electrospinning device where a high electric voltage (0-90kV) is applied to a rotating center bell, a syringe filled with a spinning dope solution, and a grounded collector plate electrode is placed in a distance (spinning height  $d_x$ ) of 20-100 cm. This setup leads to a strong electrostatic field, inducing attractive and repulsive forces to the dope solution, which forms a torus that emerges at the inner wall edge of the center bell. If the surface tension is exceeded, thin jets erupt from the highest points of the torus which are affected by rotational forces and bending instabilities, causing further stretching as the solvent evaporates. Numerous solid fibers are formed, which are finally randomly deposited on the counter electrode in the form of a nonwoven mesh.

## **1.7 Mechanical textile processing**

After production of fabrics via weaving, knitting or other methods, the product usually does not fully fit the customer's expectation. Physical or chemical post-processing modification is utilized to adjust the textiles' properties. Another approach would be the pre-production treatment of the used yarns, but in that case the possibilities are limited, and the processing proves to be difficult and expensive with incalculable outcome. Additionally, the treatment has a high risk of being harmed during any mechanical production step.

[132,178]

The first approach in post manufacturing textile processing regularly is represented by mechanical treatment methods, which are necessary to provide the fabric with typical features, such as improved optical features, compactness or soft and fleecy touch.<sup>[132]</sup>

### **1.7.1 Compacting**

Compacting, as well as, heat setting or steaming (polyester and nylon), or fulling (wool), is used to densify the fabrics structure by shrinking the total volume and increasing the mechanical stability. This is commonly performed using heat, such as hot steam in combination with compression and friction (wool). Additionally, the treatment influences the surface structure and morphology, yielding a crepy and raw look or altering the color-shade.<sup>[179]</sup>

### **1.7.2 Calendering**

Calendering is sometimes also referred to as a wet finishing method, but herein calendering is presented as a compacting-related mechanical finishing method for textiles using two cylindrical rollers, which are passed by the textile under carefully controlled temperature and pressure to adjust the textiles surface texture. The gap width in between the rollers, as well as, their surface structure, and its profile enable specific effects in the fabric such as smoothness, suppleness or luster. Generally, the calendering rolls regularly consist of a plain highly polished surface heated metal drum, sometimes provided with small and numerous exaltations. Three and four-roll calender set-ups are the

most popular types. The rolls rotate in the opposite direction and are individually driven at different speeds, which provide a flexibility of the applied friction ratio, which is defined as the ratio of the peripheral speed of the faster roll in respect to the slower one and is normally set from 1.5 - 3. The weaving process results in heterogenic yarn interlacing heights and diverging intersections and cavities. Calendering flattens the fabric structure and fibers are pressed into a cylindrical shape yielding a flat and compact fabric. A special sub-process of letting the textile pass specialized heated metal rolls, which feature a certain relief or an elevated pattern to integrate this pattern on the fabric surface, is also known as embossing.<sup>[180-182]</sup>

### **1.7.3 Raising or napping**

In contrast to compacting purposes, the raising of fibers at the surface of the cloth to increase wearing comfort, induce a fleecy feeling on the skin and warmth of the wearer, is done via raising/napping. The textiles are led over cylindrical rollers, whereby the surfaces are modified by card clothing of about 10-15 cm long steel wires. The protrusive fibers on the fabrics surface are cut and elevated, resulting in an increased surface area and expanded gap area between the upper fiber-interlacings.<sup>[179,183]</sup>

### **1.7.4 Sueding**

Similar to raising/napping this mechanical treatment method is carried out using modified cylindrical rollers coated with abrasive material on produced fabrics. The brushing of the textile's surface lifts the exposed fibers and yields loops and pills. These generate a soft and fluffy touch and improve insulating capacities of the fabric due to the enlarged, entrapped, inner air volume.<sup>[182-184]</sup>

## **1.8 Coating methods**

Mechanical treatment is followed by textile-finishing using special substances and chemicals to add desired properties. Amongst those, flame inhibition (public service offices), dirt repellency, anti-crease (often for cotton, linen or rayon), anti-pilling, anti-static, water- and oil-repellent finishes, colorfastness and antibacterial finishes are the most prominent. The application methods for these chemicals still offer a variety of modifications to adjust the finishing process, as well as, the overall result.<sup>[185]</sup>

### **1.8.1 Protective planar coatings in form of closed layers**

Industrial goods, in the form of solid materials, mostly feature closed surfaces and casings to improve handling and cleaning, as well as, protection of inner elements. Therefore, these surfaces are perfectly suited for the application of protective coatings. The greatest difficulty hereby is in the infiltration of cavities and pockets in complex three-dimensional objects, as well as, pores or roughly structured surfaces. Hence, layered coatings based on highly fluid dopes or aerosols are employed.<sup>[186]</sup>

#### **1.8.1.1 Dip coating/ Foulard process**

Dip coating, also known as impregnation, saturation or Foulard process (named after a thin type of fine, mostly silken, cloth) is the standard method for finishing of textiles, due to its simple setup.<sup>[187]</sup> The textile is led into a tank and immersed in the coating substance for a defined period of dwell time. Subsequently, flexible doctor blades or nip rolls are used to squeeze out excess substrate from the passing textile. The rolls are either perforated or placed in certain distances to yield a distinct gap width and enable a predefined net pickup of the liquid. In a final step, the improved textile is dried. The transportation velocity, the drying temperature, as well as, the drying time have to be adjusted carefully in dependence of the thickness and structure, and therefore of the absorbing capacity of the textile.



The setup itself requires a comparable high amount of provided substrate and resultantly increased drying energy due to a soaking of the complete textile.<sup>[12]</sup>

#### **1.8.1.2 Kiss-roll coating**

One possible modification of the dip coating process is the passive application of the substrate using a transport roll covered with an absorptive material, being in contact to a liquid bath on one side, and the fabric to coat on the other. Because of the peripheral movement, the roll confers the substrate on the fabric at the point of contact, which is called the kiss. Subsequent drying requires less energy, because of a decreased wetting of the fabric and stabilizes the coating.<sup>[188,189]</sup>

#### **1.8.1.3 Spray coating**

A more energy friendly and efficient method for liquid coating of fabrics is spray coating. Here the cloth is led through one or more sprinkling showers of substrate, which is sprayed through nozzles from above in a certain distance (typically 5-60 cm).<sup>[190]</sup> Less material is needed to cover a larger surface area of textile, and soaking is additionally reduced at the expense of a less homogenous coating. For textile drying, the energy consumption is noticeably lower in comparison to dip coating methods, since required temperature and exposure time can be reduced.<sup>[191]</sup>

#### **1.8.1.4 Foam coating**

One of the most efficient textile coating, yet also highly difficult methods regarding the applicative setup is the foam coating process. The substrate has to fulfill distinct requirements in terms of viscosity, shear resistance and chemical stability, since the dope has to be prepared thoroughly and foaming agents have to be added. The ideal mixture of both, yielding the dope, is purged by foaming gas followed by the application of high shear forces to generate stable foam with small volume bubbles, high surface area and highest foam to liquid ratio possible. The foam is further transferred onto the fabric sur-

face, distributed equally and cut to a certain height by a doctor blade, comparable to the Foulard process. Subsequently, the foam is sucked through the textile by vacuum applied from underneath the fabric, for example by using a perforated drum roller. The foam collapses and a liquid film is built on the fabrics surface. Excessive and removed liquid is recycled. Finally, the fabric has to be dried. Compared to other coating methods the required drying energy after foam coating is minimized, since the residual moisture in the textile is lowered drastically at the benefit of optimized coating homogeneity.<sup>[192]</sup>

### **1.8.2 Special coatings in form of nonwoven meshes**

Besides of the already named examples of classic coating methods, modern processing techniques offer a variety of unusual coatings. Advanced electrospinning processes allow the production of submicron nonwoven meshes from a variety of materials and the direct deposition on different surfaces. In comparison to protective planar coatings, multi-layered submicron fiber meshes, based on tubular shaped electro-spun fibrils, offer an excessive increase in specific surface area, due to their small diameter and very low volume-to-surface area ratio. Nonwoven meshes additionally offer a virtually endless character of the basic threat at low material deployment.<sup>[193]</sup> These characteristics lead to potential applications as a carrier for pharmaceutical, chemical and other goal-driven reactants in active coating, as well as, applications being in need of extensive adhesive or separating surfaces - for example to purify oily industrial waste water or polluted oceanic water.<sup>[194,195]</sup>

In medical research nonwoven coatings are analyzed to prevent attachment of microbes to implants and others by the usage of antibacterial dope material and blends thereof. Other approaches analyze the loading of the fibers with medically active substances by mixing those into the dope solution in order to obtain anti-infective material surface coatings capable of releasing.<sup>[196,197]</sup> Recently increasing numbers of studies focus on submicron nonwoven fibers as scaffolds in tissue engineering. For the production of ultra-thin and flexible cell sheets, fibroblasts are first seeded on chitin nonwoven meshes, which were subsequently combined to complex tissue replacements. Micro-pores and connected channels in the fiber network reassemble the topography of extracellular matrix, which facilitates cellular growth by supporting cell proliferation and differentiation.<sup>[198,199]</sup>

Other approaches utilized nanofiber nonwoven coatings from cellulose to reduce the air permeability and raised heat resistance of textiles, desired factors for functional sports and outdoor clothing.<sup>[200]</sup> Wool and jute cloths coated with electrospun PAN nano-fibrous membranes featured increased sound absorbency proving useful for the development of lightweight noise canceling cloths and curtains.<sup>[201]</sup> Due to their minimal diameter-to-length ratio and the chaotic deposition during standard electrospinning processes, sub-micron nonwoven meshes also exhibit smallest gaps and complex pores, when multiple meshes are stacked, perfectly suited for particle filtration purposes. Though, the mechanical stability of submicron nonwoven meshes barely allow their unattached employment. Acting as a fine dust filtration layer, in combination with supportive layers, nonwoven meshes are a promising enhancement for high performance filter elements.<sup>[11,202]</sup>

## **1.9 Motivation and aim of the thesis**

Numerous studies have focused on the properties of recombinant spider silk proteins in regards to their applications in daily care, healthcare, and drug delivery.<sup>[11,125,202-214]</sup> Yet, technical applications are barely found in large-scale realizations, due to the complex transition of promising scientific discoveries to industrial scale. Hence, the investigation of the applicability of recombinant spider silk proteins for the improvement of everyday products and to reinforce their weak-spots is standing to reason.

The aim of the work was the comparison and evaluation of the upscaling potential of two technical processes to improve two existing types of characteristic mass products. In a first approach a spider silk protein foam coating of furniture textiles was performed. The second project focused on the processing and comparison of fine dust filter materials using green polymers in comparison to synthetic ones. Therefore, precisely fabricated nonwoven meshes made of poly(ethylene oxide) (PEO), poly(lactic acid) (PLA), eADF4(C16) (engineered recombinant spider silk protein) and ChryC1 (recombinant lacewing silk protein) were used in a submicron regime using electrospinning.

The scope of this work is divided into three consecutive main parts as displayed in Figure 1.15.

- 1 Preliminary studies: Production and characterization of spider silk protein dope solutions adjusted for foam coating and electrospinning processes.

In the beginning of this work, two different types of spider silk protein dope solutions should be developed, produced and characterized, meeting the requirements of foam production, as well as, electrospinning. Therefore, a low concentrated aqueous spider silk protein solution with low viscosity, low vapor pressure and foaming agent for foam production was necessary. On the other part higher concentrated electrospinning dopes containing different crude oil-derived, as well as, green polymers (spider and lacewing silk protein), should be analyzed using highly volatile organic solvents.

- 2 Small-scale experiments with basic elements: Foam coating of single yarns, electrospinning of nonwoven fiber meshes and analysis of beneficial effects.

In the subsequent step, the solutions should be used to perform laboratory scale experiments. Concerning furniture textile improvement, spider silk protein foam coating on single yarns of different raw materials should be performed, followed by process optimization to enhance homogeneity. In addition, characterizations regarding coating stability and protective effects in the presence of abrasive strain should be carried out. Submicron nonwoven meshes for filtration applications should preliminary be produced by electrospinning on polyamide supports and analyzed in terms of particle deposition and air permeability.

- 3 Upscaling experiments: Processing of foam coated textiles and centrifugal electrospun nonwoven fiber meshes and evaluation of results and practicability.

In a final step, the preliminary gathered results should be used to perform upscaling experiments. Regarding the finishing of textiles, the foam coating of complete furniture textile fabrics should be performed in various numbers of cycles and analyzed in respect of the protective effects and durability. The production of spider silk protein nonwoven meshes, limited by the batch operating electro spinning process, should be initially transferred to a novel centrifugal electrospinning method, capable of producing large amounts of nonwoven meshes continuously. Then, all working parameters should be transferred and adjusted accordingly, followed by the characterization of their interaction and the impact of additional inherent parameters, such as rotational speed.

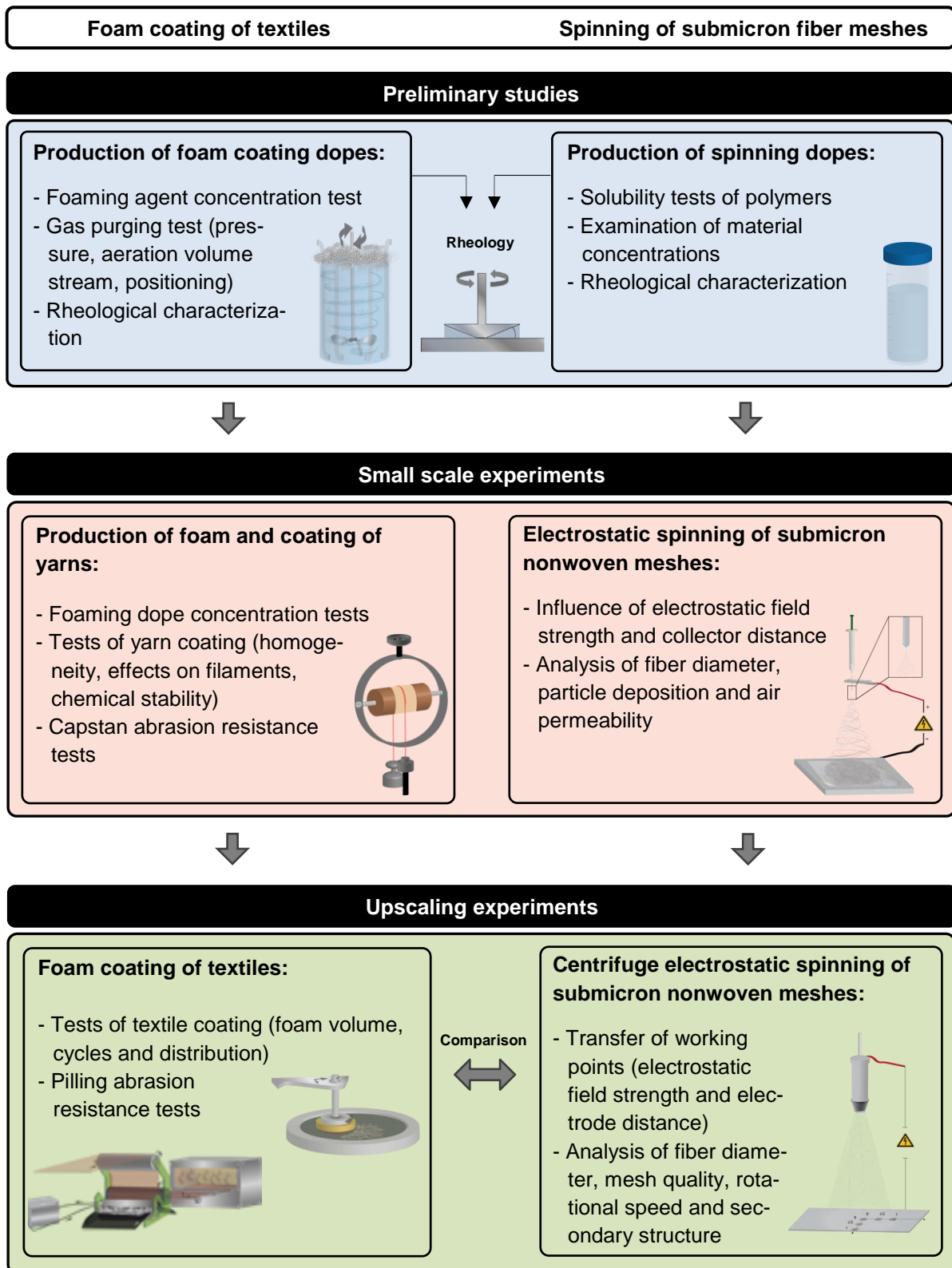


Figure 1.15: Flowchart of the outline of the work of this thesis.

## 2 Materials and Methods

### 2.1 Materials and instruments

#### 2.1.1 Chemicals and Consumables

**Table 2.1:** Overview of all used chemicals and consumables.

| Name  | Modell/ Type/ Molecular weight | Producer/ Company                                  |
|---|--------------------------------|--|
| 1,1,1,3,3,3-hexafluoro-2-propanol (HFIP)                    | -                              | Alfa Aesar (Karlsruhe, Germany)                    |
| 5/6-carboxyfluorescein succinimidyl ester (NHS-fluorescein) | 46410                          | Thermo Fischer Scientific (Waltham, USA)           |
| 2-propanol  | ≥ 99,5%, p.A.                  | Carl Roth (Karlsruhe, Germany)                     |
| Arizona fine dust A2  | 0.2 – 8.9 µm, ISO 12103-1      | PTI Powder Technology (Arden Hills, USA)           |
| Cannula flattened (electrode)                               | Sterican (19Gx2", 30 mm)       | B. Braun Melsungen (Melsungen, Germany)            |
| Dust Bag (commercial)                                       | AEG/ AE120                     | MicrofiltPlus (Frankfurt am Main, Germany)         |
| Ethanol (EtOH)  | 96%                            | Carl Roth (Karlsruhe, Germany)                     |
| Poly(lactic acid) (PLA)                                     | 39 kDa                         | Toray (Düsseldorf, Germany)                        |
| Poly(ethylene oxide) (PEO)                                  | 400 kDa                        | Sigma-Aldrich (St. Louis, USA)                     |
| Conductive adhesive carbon dots (Ø: 12 mm)                  | G3347                          |  |
| Conductive adhesive aluminum tape (25 mm x 5 m)             | G3350C                         | PLANO (Marburg, Germany)                           |
| Conductive adhesive aluminum tape (12 mm x 5 m)             | G3349C                         |  |
| Foaming agent   | Ultravon JUN, non-ionic        | Huntsman Textile Effects GmbH, (Langweid, Germany) |
| Guanidinium-thiocyanate                                     | -                              | Carl Roth (Karlsruhe, Germany)                     |

|  |                         |   |
|--|-------------------------|---|
| Hydrochloric acid                            | -                       | Carl Roth (Karlsruhe, Germany)  |
| Methanol                                     | ultra-pure              | VWR International (Radnor, USA)   |
| Pin sample holder (Ø: 12.5 mm)               | G301                    | PLANO (Marburg, Germany)  |
| Recombinant lacewing silk protein (ChryC1)   | 82 kDa                  | Martin Neuenfeldt, Lehrstuhl Biomaterialien, Universität Bayreuth (Bayreuth, Germany) |
| Recombinant spider silk protein (eADF4(C16)) | 48 kDa                  | AMSilk (Planegg, Germany)   |
| Sodium Chloride                              | -                       | Merck (Darmstadt, Germany)  |
| Standard cotton testing fabric               | SM25                    | Rohleder (Konradsreuth, Germany)  |
| Syringe (dope storage)                       | Inkjet (0.01 mL - 1 mL) | B. Braun Melsungen (Melsungen, Germany)   |
| Trichloromethan (TCM, chloroform)            | -                       | Merck (Darmstadt, Germany)  |
| Tris(hydroxyl-methyl)-amino-methane (TRIS)   | -                       | Carl Roth (Karlsruhe, Germany)  |
| Ultra-pure water (H <sub>2</sub> O)          | MilliQ                  | Merck Millipore (Darmstadt, Germany)  |
| Urea   | -                       | BDH Prolabo (Darmstadt, Germany)  |

#### Spider silk enhanced dust bag - Filter layer and support Material

| Name                             | Pore size [µm] | Producer/ Company  |
|----------------------------------|----------------|--|
| Polyamide woven (PA-80/105)      | 80             | Schwegmann Filtrations-Technik (Grafschaft-Gelsdorf, Germany). |
| Polypropylene fleece (spun bond) | 500            | Sandler AG (Schwarzbach a. d. Saale, Germany)                  |
| Polyester fleece (staple fibers) | 2000           |  |

### 2.1.2 Textiles and yarns

Textile fabrics and yarns in different fineness (1 tex = 1 g/km) were acquired from Rohleder GmbH, (Konradsreuth, Germany). The used materials contained a rayon-linen mixture (CV/Li, 70/30, staple fiber yarn, Art. 69, 111 tex), pure linen (Li, staple fiber yarn, Art.



927, 71 tex), poly(acrylonitrile) (PAN, staple fiber yarn, Art. 355, Nm 31 tex) and poly(ethylene terephthalate) (PET, filament yarn, Art. 66, Nm 48 tex).<sup>[215,216]</sup>

### 2.1.3 Instruments and devices

**Table 2.2:** Overview of used devices for analytics and material processing.

| Type of device                               | Modell                                    | Producer   |
|--|---|--|
| Akustron air permeability tester             | ALD-150                                   | rycobel group (Uffenheim, Germany)               |
| Balance                                      | ALC-3100.2                                | Acculab (Göttingen, Germany)                     |
| Cell disruption device                       | Sonopuls HD3200 with KE76 ultrasonicator  | Bandelin GmbH (Berlin, Germany)                  |
| Centrifuges                                  | Haereus Pico 17                           | Thermo Fischer Scientific Inc. (Waltham, USA)    |
|  | Haereus Pico 17                           |  |
|  | Haereus Multifuge 3SR+                    |  |
|  | Haereus Multifuge 1S-R+                   |  |
|  | Sorvall RC6+                              |  |
| Dip coating device                           | WPTL5-0.01                                | MTI (Richmond, USA)                              |
| Fermenter                                    | BIOSTAT B plus 5 L                        | Sartorius (Göttingen, Germany)                   |
| Foil-spraying / Foam-coating-device          | V1  | Central Workshop (Universität Bayreuth, Germany) |
| Fourier-transformation infrared spectrometer | Tensor I with IR Microscope Hyperion 3000 | Bruker Corporation (Billerica, USA)              |
| Freeze dryer                                 | Alpha 1-2 LDplus                          | Christ GmbH (Osterode im Harz)                   |
| Heating chamber                              | OV-SS-00AB                                | MTI (Richmond, USA)                              |
|  | Haereus Function Line                     | Thermo Fischer Scientific Inc. (Waltham, USA)    |
| Light and fluorescence microscope            | DMI3000B                                  | Leica Microsystems GmbH (Wetzlar, Germany)       |
|  | DMI1                                      |  |
|  | DMI8                                      |  |
|  | HXR-R 120W/45C VIS lamp                   |  |

|                                    |   |   |
|------------------------------------|---|---|
| Magnetic stirrer (with heating)    | RCT basic   | IKA GmbH (Staufen, Germany)                             |
| Martindale testing device          | NU-Martindale 864 with SM25 (standard cotton textile) | James H. Heal & Co. Ltd., (Halifax, Great Britain)      |
| Microbalance                       | Discovery   | Ohaus Inc. (Pine Brook, USA)                            |
| Particle counter/ analyzer         | Palas MFP 2000  | PTI Powder Technology Inc. (Arden Hills, USA)           |
| Rheometer                          | ARG2  | TA Instruments Waters GmbH (Eschborn, Germany)          |
| Scanning electron microscope (SEM) | Gemini, Sigma 300 VP/ 1540 ESB Cross Beam, LEO1530    | Carl Zeiss Microscopy GmbH (Jena, Germany)              |
| Sputtering device                  | 208HR   | Cressington Scientific (Watford, GB)                    |
| Stirrer (laboratory)               | RZR 2020  | Heidolph Instruments GmbH & Co. KG (Schwabach, Germany) |
| Tensile testing device             | ElectroForce 3220                                     | Bose Corporation (Eden Prairie, USA)                    |
| Ultracentrifuge                    | Optima MAX-XP   | Beckman Coulter Inc. (Brea, USA)                        |
| UV-Vis Spectrophotometer           | NanoPhotometer P330                                   | Implen Inc. (La Baya Drive, USA).                       |
|                                    | Nanophotometer NanoDrop 1000                          | Thermo Fischer Scientific Inc. (Waltham, USA)           |
|                                    | Varian Cary 50  | Agilent Inc. (Santa Clara, USA)                         |

### 2.1.4 Software

**Table 2.3:** Overview of used software for device operation, analysis, and graphic processing.

| Name                     | Specification                                       | Developer/ distributor                                 |
|--------------------------|---|--|
| Acrobat                  | 9Pro  | Adobe Systems Inc.<br>(San Jose, USA)                  |
| Endnote                  | X4  | Thomson Reuters<br>(New York City, USA)                |
| Illustrator<br>Photoshop | Creative Suite (CS)5                                | Adobe Systems Inc.<br>(San Jose, USA)                  |
| ImageJ                   | 1.47v   | Wayne Rasband,<br>(Bethesda, MD, USA)                  |
| Leica Application Suite  | V4.3  | Leica (Wetzlar, Germany)                               |
| Mathematica              | 10.3  | Wolfram Research<br>Inc. (Champaign, USA)              |
| Office                   | Professional Plus 2010                              | Microsoft Corporation<br>(Albuquerque, USA)            |
| Opus                     | Quant, V 6.5  | Bruker AXS Inc.<br>(Madison, USA)                      |
| Paint                    | V6.1 SP1  | Microsoft Corporation<br>(Albuquerque, USA)            |
| Particle Analyzer        | Palas MFP 2000                                      | PTI Powder Technology<br>Inc. (Arden Hills, USA)       |
| ProtParam                | -   | Swiss Institute of Bioinformatics<br>(Lausanne, Swiss) |
| PVC application          | 5.11.1.3  | Implen Inc.<br>(La Baya Drive, USA).                   |
| Rheology Advantage       | Data Analysis V.5.8.2<br>Instrument Control V.5.8.2 | TA Instruments<br>(New Castle, USA)                    |
| Varian UV Scan           | 3.00(339)   | Agilent Inc.<br>(Santa Clara, USA)                     |
| Wintest                  | 4.1   | Bose (Eden Prairie, USA)                               |

## 2.2 Recombinant production of ChryC1 lacewing and eADF4(C16) spider silk proteins

Recombinantly engineered *Araneus diadematus* fibroin 4 (eADF4(C16), Figure S1) was purchased from AMSilk GmbH (Munich, Germany).<sup>[217]</sup> *Chrysoperla carnea* (*C. Carnea*) (ChryC1, Figure S2) lacewing silk protein was recombinantly produced in *Escherichia coli* (*E. coli*) BL21-Gold (DE3) pLysS from Novagen (Madison, WI, USA), and gene expression was induced by adding 0.5 mM isopropyl- $\beta$ -D-thiogalactopyranoside (IPTG) at an optical density (600 nm) between 3.0 and 3.5. Cells were harvested after expression for 4 h at 30 °C. After cell disruption, the lysate was treated with heat (80 °C for 20 min), acetic acid (pH 4.2 for 2 h) and  $(\text{NH}_4)_2\text{SO}_4$  (fractional precipitation by using 0.8 M and 1.5 M final concentration). The obtained pellets were washed with 1.6 M  $(\text{NH}_4)_2\text{SO}_4$ , 25 mM sodium phosphate, pH 8.0, solubilized in 6 M guanidinium thiocyanate (GdmSCN), dialyzed against 10 mM  $\text{NH}_4\text{HCO}_3$  and lyophilized. Incubating eADF4(C16) silk protein with NHS-fluorescein ( $\beta_{\text{NHS}} = 1 \mu\text{g}/\text{mL}$ ) for 2 h, followed by dialyzes against aqueous 50 mM Tris/HCl (pH 8) dissolved in ultra-pure water yielded fluorescently labeled silk protein. The labeling efficiency was 0.6 mol/ mol<sub>silk</sub>.

## 2.3 Foam processing from spider silk solutions

In a first step eADF4(C16) silk protein was dissolved in 6 M guanidinium thiocyanate (GdmSCN,  $\beta_{\text{silk}} = 75 \text{ g}/\text{L}$ ), and dialyzed against aqueous 50 mM Tris/HCl (pH 7.5, 100 mM NaCl) dissolved in ultra-pure water (MilliQ, Merck Millipore, Darmstadt, Germany), followed by a centrifugation step (20k rpm, 30 min). In a beaker (1000 mL) combined with four tubes ( $d = 3 \text{ mm}$ ) for aeration, the aqueous protein solutions were placed and purged at a pressure of 1 bar (g) and a flow rate of  $\dot{v} = 3000 \text{ mL}/\text{h}$ . Foaming agent (Ultravon Jun) was added at a concentration of 30 g/L. Foaming of the solutions was further induced by mixing the air bubbles and solutions using a Heidolph RZR 2020 (Heidolph Instruments GmbH & Co. KG, Schwabach, Germany) with a three bladed propeller stirrer (PR 30) and a diameter of 58 mm, a shaft diameter of 8 mm, and a length of 400 mm at 1000 rpm for 5 min each. Subsequently, the resulting foam was transferred into the foam application chamber. To perform fluorescent coatings, labeled foams were produced. Therefore, a

dope solution was prepared by mixing non labeled and labeled silk protein solutions at a ratio of (200:1).

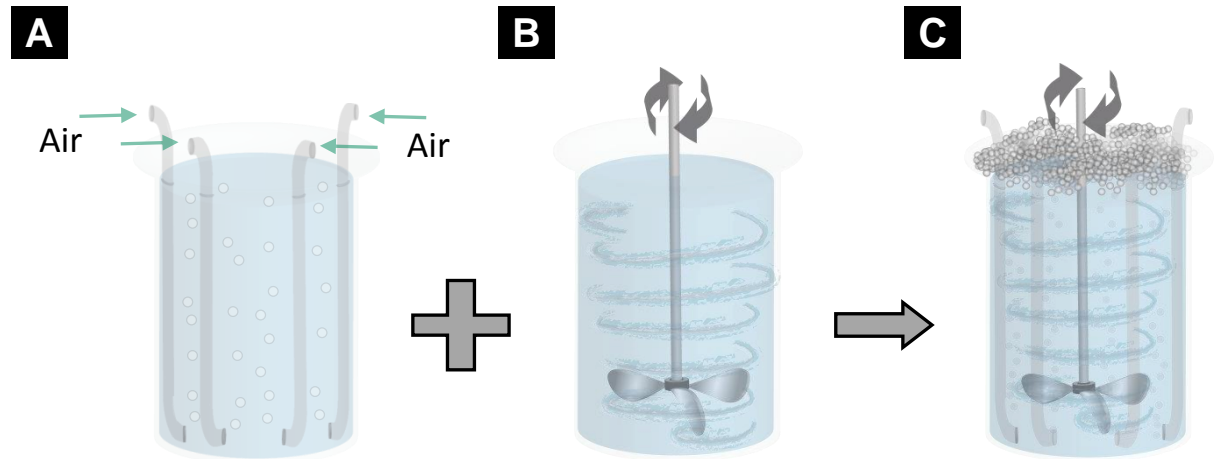


**Figure 2.1:** Foam production; A: aeration of coating solution, B: shearing of silk solution with mixing rotor, C: combination leads to foam creation with air flow rate  $\dot{v}$  [L/h], air pressure  $p_{air}$  [bar (g)] and number of revolutions  $\omega$  [rpm].

## 2.4 Foam coating of fibers and fabrics

Foam coatings were performed in a closed chamber. Initially, textile fabrics and single fiber yarns were placed and fixed on a transportation foil with a width of 150 mm. The coating was performed using a transportation velocity of 0.1 m/min. A doctor blade was adjusted to cut the foam at a height of 3 mm above the sample. Due to the linear motion and a sufficient amount of silk foam, all samples were coated homogeneously and ran over a perforated cylinder. A vacuum was applied to cause the collapse of the foam and enabled the suction of remaining foaming dope through the textile, which could be collected and upcycled. Drying of the coated samples was performed using heat radiation by infrared lamps at a distance of 100 mm and a temperature of 40 °C for 30 min.

## **2.5 Processing of spider silk protein and polymer solutions for production of nonwoven meshes**

### **2.5.1 Electrospinning**

The electrospinning device was equipped with an x-y-axis movable spinning head to provide a homogeneous and widespread surface coating of up to 1.5 m<sup>2</sup>. Three equal filters (100 cm<sup>2</sup>) were made from each material to produce improved fine dust filtration layers on PA support and measured thereafter to determine one particle deposition data set. Both silk materials were dissolved in HFIP; PEO was dissolved in ultra-pure water, and PLA in TCM to achieve dope solutions. Before transferring into 1 mL syringes, serving as a dope reservoir and connected to blunt grinded cannulas used as spinning electrode, all solutions were shaken for 48 hours. Spinning of submicron fiber meshes onto the poly-amide support mesh with a gap-width of 80 μm was carried out on a rectangular table (1100 mm x 600 mm), which acted both as counter electrode and collector table. Submicron fiber nonwovens were electro-spun using a constant flow rate of 4.4 μL/min for all dope solutions. The electric field strength combining the voltage difference between both electrodes and the spinning height were both set individually for each material and dope concentration (see 3.2).

### **2.5.2 Centrifuge electrospinning**

As a new application of electrospinning methods, centrifuge electrospinning combines centrifugal forces and electrostatic fiber production in one method, which is described in detail under 1.6.4.2. All spinning experiments were carried out at 20 °C and relative humidity from 30% to 60%. Spinning dopes and solvents (PLA and TCM; PEO and water) were filled into respective storage containers and transported using a micro annular gear pump with 0.6 cm<sup>3</sup> per revolution and 1.5 - 15 mL/min. Spinning dopes from eADF4(C16) in HFIP were induced using a syringe pump modification with 25 mL filling volume and 0.1 - 10 mL/min at 8 mL/min for 1 min. Spinning tests were performed at a preset combination of rotational velocity/number of revolutions [krpm], spinning voltage [kV], and electrode distances from 200 nm to 600 mm, for 60 s on polyamide mesh supports (100 cm<sup>2</sup>).

## 2.6 Processing of nonwoven meshes for filter production

Submicron fibers from silk protein with increased  $\alpha$ -helical and random coil structures are more fragile and dissolved by air humidity over time.<sup>[202]</sup> Ethanol, as well as, water vapor posttreatments were carried out to induce and maximize crucial  $\beta$ -sheet secondary structure as previously published.<sup>[122,202]</sup> Additionally, partial melting of fiber crossings at their surface and subsequent re-solidification is a side effect of the posttreatment, strengthening the fiber-networks and enhancing filtration capability since fiber slipping is minimized, and pores remain constant in size. Spider silk protein (eADF4(C16)) nonwoven samples were placed hanging freely inside a sealable vessel (Figure 2.2, Step 1). Employing a syringe attached to a tubing system, the vessel was filled from the bottom with 50 mL of ethanol and placed on a heater to induce 60 °C for 120 min. After 10 min of cooling time, the collected liquid was extracted using the respective syringe. The procedure was then repeated with a water-filled syringe attached to a second tubing system (Figure 2.2, Step 2).

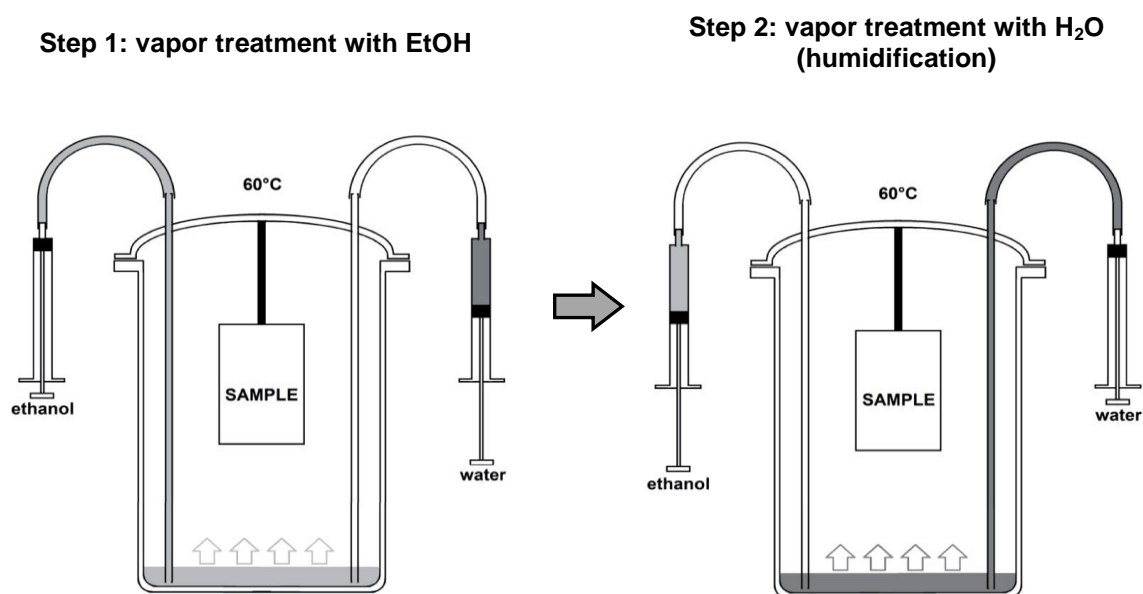


**Figure 2.2:** Schematic procedure of post-treatment of electro-spun eADF4(C16) and ChryC1 nonwoven meshes. Regarding eADF4(C16), the chamber was preliminary filled with ethanol and the sample was steamed at 60 °C for 120 min. In order to soften the nonwoven meshes for subsequent handling, ethanol was removed in a second step, and the fibers were treated with water vapor according to step 1. For ChryC1, the post-processing is carried out with water vapor (Step 2) only, modified from.<sup>[202]</sup>

## **2.7 Analytical methods**

### **2.7.1 Spectroscopic methods**

#### **2.7.1.1 UV-Vis spectroscopy (foam coating efficiency)**

Analysis of textile foam coating efficiency, and therefore the analysis of the amount of spider silk protein on yarn material, was carried out using a Varian Cary 50 UV-Vis spectrometer by initially washing five samples (5 cm<sup>2</sup>) of each coated textile in a saturated urea solution (8 M, 25 mL) for 48 h. The solution was subsequently centrifuged at 20krpm for 30 min to remove fiber residues. A drop of the solution was transferred to a cuvette with integrated dilution of factor 50. All textile samples were tested in triplicates at 280 nm and concentrations were calculated by Equation 2.1, with absorbance,  $E$  [AU]; path length,  $d=1$  cm;  $\epsilon=47680$  L/(mol cm).

$$E = \epsilon * c * d \tag{2.1}$$

#### **2.7.1.2 Fourier transform infrared spectroscopy (FTIR)**

Secondary structural properties, as well as, structural changes upon posttreatment of silk protein nonwoven meshes were detected using FT-IR and subsequent Fourier self-deconvolution (FSD). For each spectrum, accumulations of 60 scans were measured and averaged in transmittance-mode at wavenumbers ranging from 800 to 4000 1/cm. One reference per spectrum was measured at surrounding conditions with dried air. For quantitative analysis of the data, FSD of amid I bands (between 1590 and 1705 1/cm) was performed. The process includes baseline correction and a local least square fit to analyze single contribution peaks according to the corresponding peak positions previously published (1611, 1619, 1624, 1630, 1640, 1650, 1659, 1666, 1680, 1691, 1698 1/cm).<sup>[218]</sup>



## **2.7.2 Microscopy**

### **2.7.2.1 Polarized light or bright field microscopy**

Polarized light (PLM), as well as, bright field (LMBF) microscopy were both carried out using a stereoscopic microscope with light sources in the visible spectrum (halogen lamp, 100W, 2900K). To obtain bright field images, the samples were illuminated and observed from beneath, yielding images of the samples built-up from light reduced areas.

Regarding PLM, the light was primarily polarized by  $90^\circ$  using a first polarizing lens before being led on the samples, subsequently passing a second polarizing filter (analyzer). The polarized light is unable to pass the analyzer and the field of view therefore appears dark. Highly ordered crystalline structures offer the feature of double refraction due to birefringence. Therefore, these structures are able to split light in a parallel and perpendicular polarized component.<sup>[98]</sup> When passing samples containing such highly ordered crystalline structures, the already polarized light is again refracted, and the double polarized fraction is now able to pass the analyzer. Hence, the structures of interest, and as a result the image of the analyzed sample, now appear bright in contrast to the shaded image in standard bright field microscopy.

### **2.7.2.2 Fluorescence microscopy**

The distribution of spider silk on textile fabrics and yarn materials was studied by fluorescence microscopy. Therefore, samples of coated textiles and yarns before washing, as well as, after washing (see 2.7.4), were illuminated at an excitation wavelength of 494 nm using a mercury lamp. Subsequently, the reflected light was analyzed at an emission wavelength of 518 nm.

### 2.7.2.3 Scanning electron microscopy (SEM)

The prepared samples were attached to aluminum sample holders using double sided, adhesive carbon dots, wrapped laterally using aluminum tape and subsequently sputtered with a 2 nm thick platinum layer by vacuum evaporation for 2 min.

The morphology of the coated yarn or textile surfaces, as well as, all fiber meshes were characterized using scanning electron microscopy at a voltage of 3 kV.

### 2.7.3 Rheological characterization of foaming and spinning dopes

Silk protein solutions were rheologically characterized using a rotational rheometer, a cone-plate system ( $d=40$  mm,  $0.5^\circ$ ), and a sample volume of  $180\ \mu\text{L}$ . A flow procedure with a logarithmic shear ramp at shear rates ( $\dot{\gamma}$  [ $1/\text{s}$ ]) ranging from  $2.86$   $1/\text{s}$  to  $286.4$   $1/\text{s}$  was set up and ten points were collected and averaged per decade (100 points). All samples were pre-heated to  $25^\circ\text{C}$ .

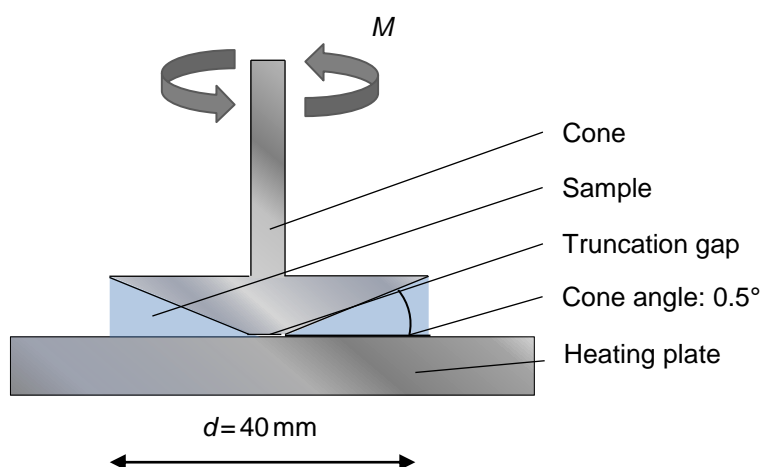


**Figure 2.3:** Schematic illustration of the cone-plate system implemented in the rheological characterization set-up with a truncation gap between cone and heating plate, a sample placed between both components with a sample volume of  $V = 180\ \mu\text{L}$ , a cone diameter of  $d = 40$  mm and a cone angle of  $0.5^\circ$ .

#### **2.7.4 Analysis of coating stability and efficiency**

To evaluate the stability and efficiency of the coating process, tests were performed using fluorescently labeled silk protein coated yarn or fabric. In the first step, all coated textile samples were flushed with 1 mL ultra-pure water or ethanol with subsequent drying step at 40°C for 30 min. This procedure was repeated three times. The amount of silk protein applied to the textile fabric was further washed off the samples by incubating 5 pieces of 25 cm<sup>2</sup> surface area per textile in 8 M urea for 48 h. The solution was centrifuged at 20 krpm for 30 min to remove textile residues. The amount of dissolved protein was finally analyzed using UV-Vis spectroscopy at a wavelength of 280 nm.

#### **2.7.5 Mechanical analytical methods for foam coated yarns and textiles**

In reference to furniture textile improvement, the resistance to mechanical stress represents the most important factor. Since the single yarns, as well as, the complex woven textiles were foam coated in this work, both types were analyzed in regards to their stress behavior in the form of friction, using standard testing textiles.

##### **2.7.5.1 Characterization of yarn to fabric friction (capstan test)**

A testing standard for analyzing the friction coefficient after *capstan* was modified to characterize coated yarns.<sup>[219-221]</sup> Briefly, a wooden cylinder with a diameter of 22 mm was fixed in a traverse and covered with a stripe of standardized cotton fabric (SM25). The yarn was connected to a weight (10 mN/tex) on one end and fixed on the other. The yarn was then wrapped around the standard fabric on the wooden cylinder perpendicularly. Vertically reciprocating movements (6 mm, 0.33 mm/s, n=10) were generated by a movable framework of a tensile testing device inducing pills and knots on the yarn surface. Subsequently, profile plots were made by computational transferring visual images, created by light microscopy, into black and white pictures. The hairiness index ( $H$  [ $\mu\text{m}^2\text{cm}_{\text{yarn}}^{-2}$ ]) was implemented and used to describe the total black pixel surface area

regarding the strained yarn [ $\mu\text{m}_{\text{black pixel}} / \text{cm}_{\text{yarn}}$ ]. This allows the numerical comparison of fraying reduction.<sup>[222]</sup>

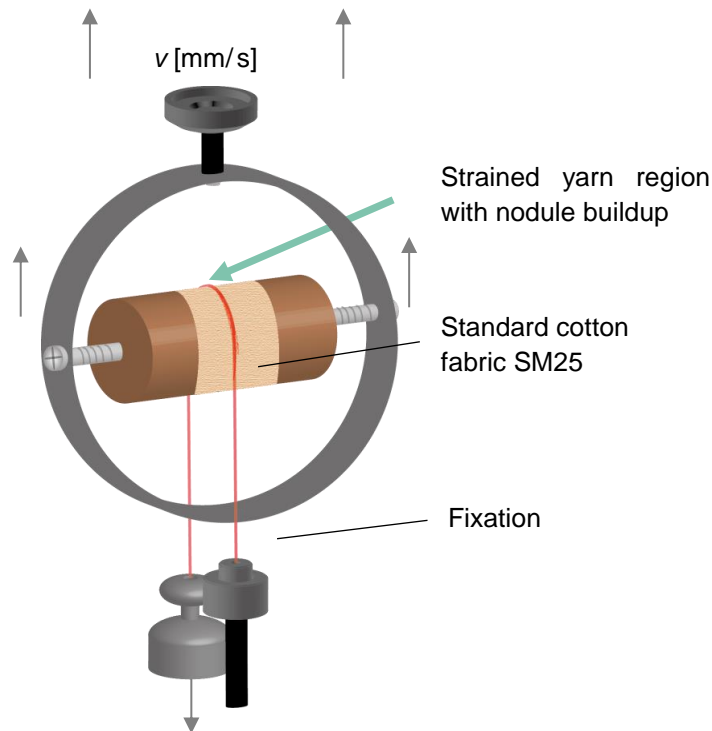


**Figure 2.4:** Schematic illustration of yarn to fabric characterization modified after Capstan test with a standard cotton textile SM25 attached to a cylinder, the fiber is connected to a weight on one end and to a force sensor on the other; a vertically reciprocating movement of the construction caused a scrubbing and the induction of nodules on the yarn indicating its destruction; modified after sources <sup>[219]</sup> and <sup>[220]</sup>.

### 2.7.5.2 Fabric to fabric characterization - abrasion resistance (pilling)

Pilling was tested for coated textile fabrics modified after a Martindale abrasion resistance test according to norm EN ISO 12945-2, using a NU-Martindale testing device as depicted in Figure 2.5.<sup>[223]</sup> A standard cotton textile (SM25) was attached to a stamp and pressed onto the textile sample ( $d=140\text{ mm}$ ) with a contact force of 3.8 N. Pilling of the fabric was visually evaluated after defined revolutions (500, 1000, 2000, 5000) in 5 main and 8 sub quality categories.<sup>[224]</sup>

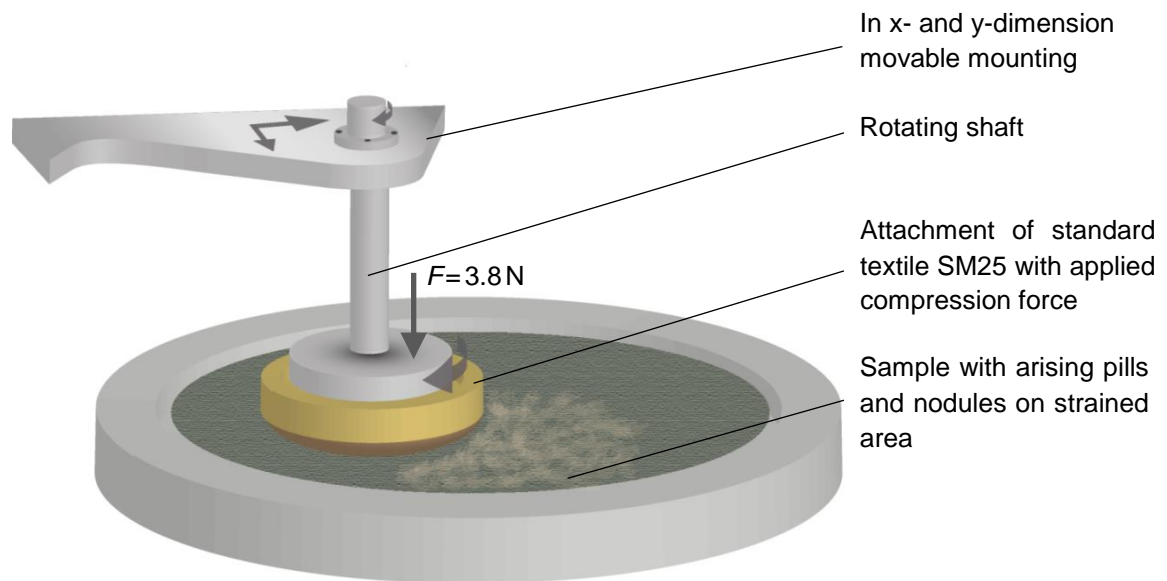


**Figure 2.5:** Schematic abrasion resistance (pilling) test module after Martindale in accordance with EN ISO 12945-2 with a SM25 cotton standard textile attached to a stamp-like mounting which is pressed onto the textile sample and rotated; the suspension is moving in x and y direction to cover the whole surface; the rotational movement destroys the textile surface integrity by the build-up of pills and nodules.

## 2.7.6 Filtration efficiency tests

### 2.7.6.1 Air permeability measurements

All filter-set-ups were tested in triplicate and ten points per sample. Air permeability of the filter layers was determined using an Akustron air permeability tester at a pressure drop of 200 Pa in a range of 30 - 3000 L/m<sup>2</sup> volumetric air stream. Values of ten different spots per filter layer were used to determine the arithmetic mean of air permeability.

### **2.7.6.2 Particle deposition measurements**

Particle deposition was evaluated in triplicates using a Palas particle analyzer. Fine dust (A2 - Arizona fine test dust), according to ISO 12103-1, was used with particle sizes ranging from 0.2 - 8.9  $\mu\text{m}$ . Filters of 28.3  $\text{cm}^2$  circular testing surface were analyzed using 300  $\text{mg}/\text{m}^3$  of dust. The inflow velocity was set to 0.025  $\text{m}/\text{s}$  for 30 s leading to a total dust volume of 42.5 L/min. The pressure drop was determined automatically between clean and dust-filled filter layers to maintain the constant inflow velocity.

Initially, single filter layers (electro-spun nonwoven on PA support) were tested and compared. Their applicability as fine particle layers was tested in a dust-filled air stream. Best performing fine particle filter layers were implemented in a stacked setup of three filter layers for raw, intermediate, and fine dust particle filtration (see 3.2.2.3), representing a filter bag set-up and subsequently characterized in a dust filled air stream, as well.

## **3 Results**

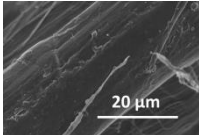
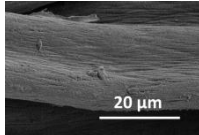
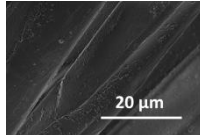



### **3.1 Protective effects of spider silk foam coatings on furniture textiles**

The first aim of this work was to evaluate the benefit of a spider silk protein foam coating on textiles and therefore analyze the capability of strain reduction. The foaming dope was characterized using a rotary viscometer, followed by the screening of optimal foaming parameters, the coating of sample textiles, and strain experiments.

#### **3.1.1 Textiles and yarns for coating**

The textiles, which were aimed to be coated and improved, are displayed subsequently in Table 3.1. The textiles were supplied by the Rohleder GmbH (Konradsreuth, Germany) and contained different combinations of the basic materials rayon (CV) and linen (Li) (CV/Li, 70/30, staple fiber yarn, Art. 69, 111 tex), poly(acrylonitrile) (PAN, staple fiber yarn, Art. 355, 31 tex), and poly(ethylene terephthalate) (PET, filament yarn, Art. 66, Nm 48 tex).<sup>[215,216]</sup>

**Table 3.1:** Overview of used fabrics; fabric (N) containing 2/3 of natural material based LI and CV as well as 1/3 PET yarn with intermediate surface roughness, polymeric material fabrics based on PAN and PET yarns with high (P1) and low (P2) surface roughness, modified from.<sup>[216]</sup>

| Textile index                              | Natural   | Polymeric  |   |
|--|---|--|---|
|  | N   | P1   | P2  |
| Material composition [wt %]                | LI / PET / CV<br>47 / 34 / 19   | PAN / PET<br>56 / 44   | PAN / PET<br>56 / 44  |
| Textile mass $m_A$ [g/m <sup>2</sup> ]     | 346   | 299  | 299   |
| Yarn fineness [g/km]                       | 2.4   | 3.3  | 1.3   |
| Manufacturing technique                    | Ring yarn   | Combed yarn  | Ring yarn   |
| Fabric treatment                           | Steam pressed   | Wet stretched  | Steam pressed   |
| Resulting surface texturization            | Intermediate  | High   | Low   |
| SEM  |  |  |  |
| Resulting surface texturization pictograph |  |  |  |

### 3.1.2 Rheological analysis of spider silk foaming dopes

Since viscosity is one of the most important inherent parameters and has a major impact on the foamability of a solution, the shear dependent dynamic viscosity of the foaming solutions was initially measured. The analysis of foaming dopes using a rotational rheometer revealed a similar curve shape of the tested solutions. At low shear rates (< 50 1/s), viscosities appear to be about one magnitude higher than water (see Figure 3.1). With increasing shear rates above 100 1/s, an asymptotic approximation to constant viscosity values, slightly higher than that of water, can be observed for all solutions.



The relation between the shear rate  $\dot{\gamma}$  [1/s] and the number of revolutions  $n$  [rpm] in a cone-plate rheometer system with a cone pitch angle  $\alpha$  [rad] is described by Equation 3.1.<sup>[225,226]</sup> For the given rheometer parameters (see Chapter 2.2) and propeller revolutions of 600-800rpm, the calculative shear rates were about 6200 1/s (800rpm)-10500 1/s (1000rpm). Since these values are higher than the operating range of the used rheometer, the maximum shear rate of 300 1/s was applied and the resulting viscosities were measured. The resulting number of revolutions of 24.2 rpm was also taken into consideration.

$$\dot{\gamma} = \frac{2 * \pi * n}{60 * \tan \alpha} \quad (3.1)$$

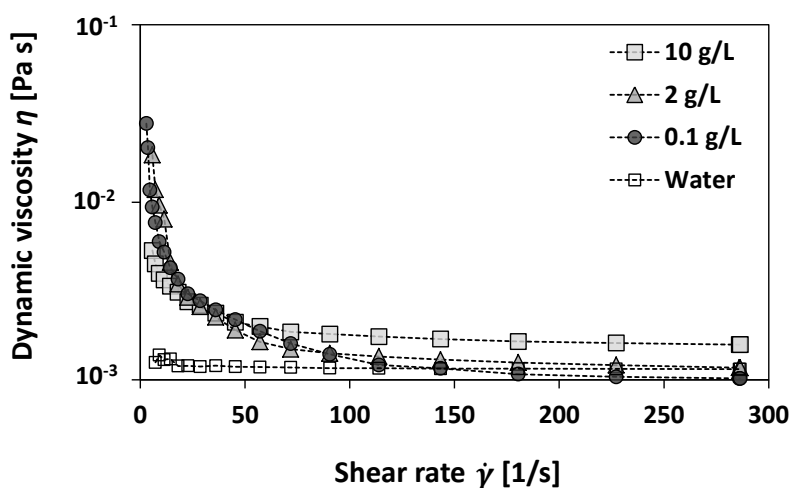


**Figure 3.1:** Dynamic rheology of foaming dopes with different silk protein concentrations, 10g/L (A), 2g/L (B), 0.1g/L (C), each solution contains the foaming agent Ultravon Jun (3g/L).

The highest silk protein concentration resulted in the highest viscosity (0.002 Pa/s) for all tested solutions. The overall low values that were tested led to the assumption that foam dope concentrations are not likely to have a significant impact on foaming results. Hence, for all following tests, the highest tested concentrated foam dope (A) was chosen.

### 3.1.3 Analysis of foam coating parameters

To find the best foaming parameters at laboratory conditions, 10 g/L silk solution was foamed (see Chapter 2.3) at different air pressures and at altering numbers of revolutions. To describe the quality of the foaming process, the blow ratio, which describes the ratio of the dope solution mass to the mass of the generated foam displayed in Equation 3.2, was used.<sup>[227]</sup>

$$\text{blow ratio} = \frac{m_{\text{dope}}}{m_{\text{generated foam}}} \quad (3.2)$$

The air pressure ( $p_a$  [bar (g)]) had a specific influence on the foamed medium (Figure 3.2 A). Lowest (0.5 bar(g)) and highest (2 bar(g)) air pressures resulted in similar amounts of foamed medium, while an air pressure of 1 bar (g) resulted in the maximum amount of foam with about 38% at 3.5 L/h air flow rate ( $\dot{V}_a$  [L/h]). Subsequently, the amount of foamed medium was tested at different rotational speeds ( $n$  [rpm]) and at the optimum air pressure of 1 bar (g), regarding the air flow rate. The amount of foam clearly increased with higher numbers or revolutions and had a distinct peak at 3.5 L/h air flow rate in all tests (Figure 3.2 B). Since 1000 rpm was the highest possible number of revolutions in the given setup, this value was chosen for all further laboratory scale tests. The air flow rate of 3.5 L/h, which lead to the highest amounts of foam in both tests, was fixed for all further steps.

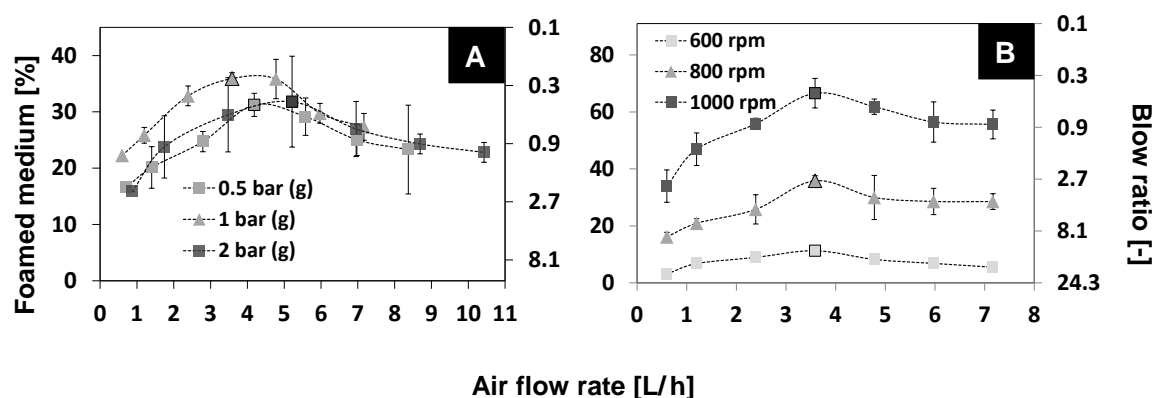


**Figure 3.2:** Foamed spider silk media (10 g/L) amount and the blow ratio at 800 rpm (A); and at 1 bar (g) (B).

### 3.1.4 Distribution of spider silk foams on furniture textiles

A textile mostly composed of natural components (N, linen and rayon) with intermediate roughness was coated with aqueous spider silk protein foams and compared to a smooth (P2), as well as rough (P1), polymeric textile, treated likewise. The coating resulted in a smoothing of the surface roughness on all tested fabrics (Figure 3.3 A1-A3 and B2).

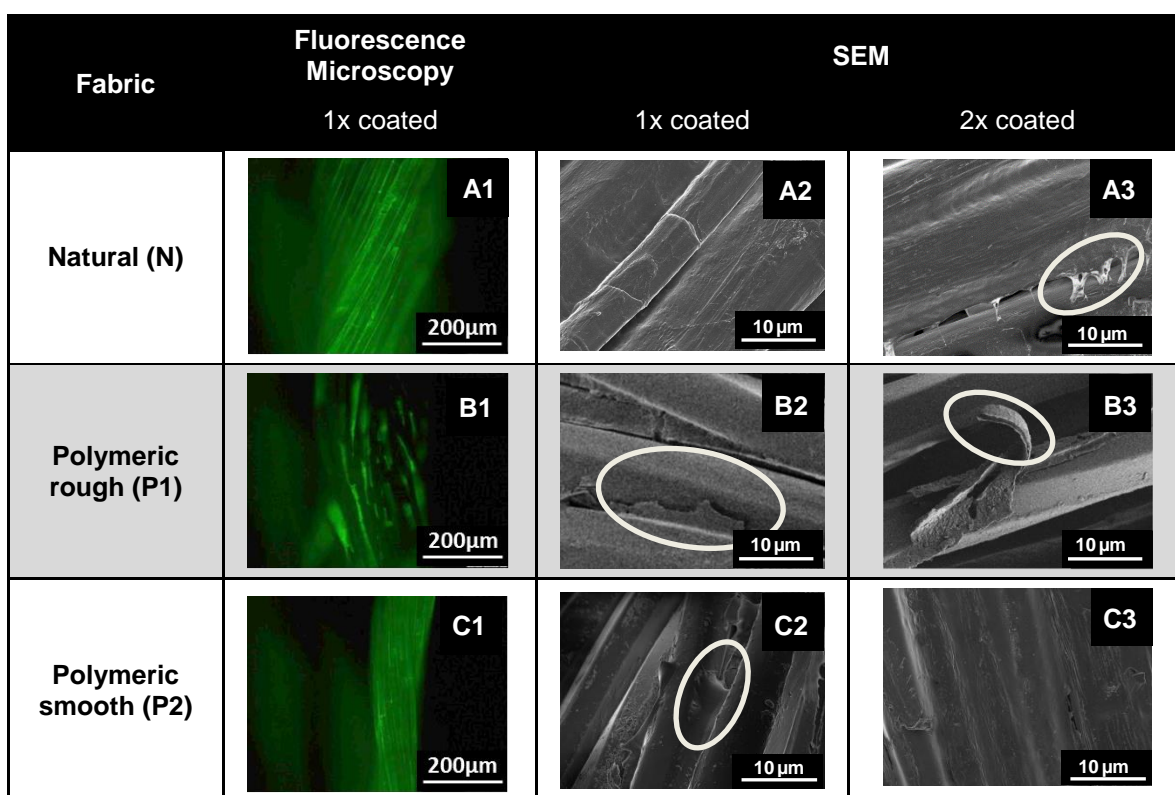


**Figure 3.3:** Overview of fluorescence and scanning electron microscopy images of coated natural (N, A1-A3), rough polymeric (P1, B1-B3) and smooth polymeric (P2, C1-C3) yarns after single and double coating. Fluorescence images indicating homogeneous coverage of all tested textiles (A1, B1 and C1) not providing inherent fluorescence. Film-like coatings cover single fibers of the yarn (A2, C3) and fiber-interconnecting bridges (A3, C2) are depicted. Increasing film thickness is reached upon a second coating step (B2, B3), modified from.<sup>[216]</sup>

Coating efficiency differed according to the surface roughness of the fabric (Figure 3.4). Whilst the rough polymeric fabric took up 87 % (w/w) of the total amount of silk included in the coating foam, the smoothest fabric (P2) only took up 29 % (w/w) in the first coating step. A second coating step resulted in a decreased absorbance of silk on the surfaces.

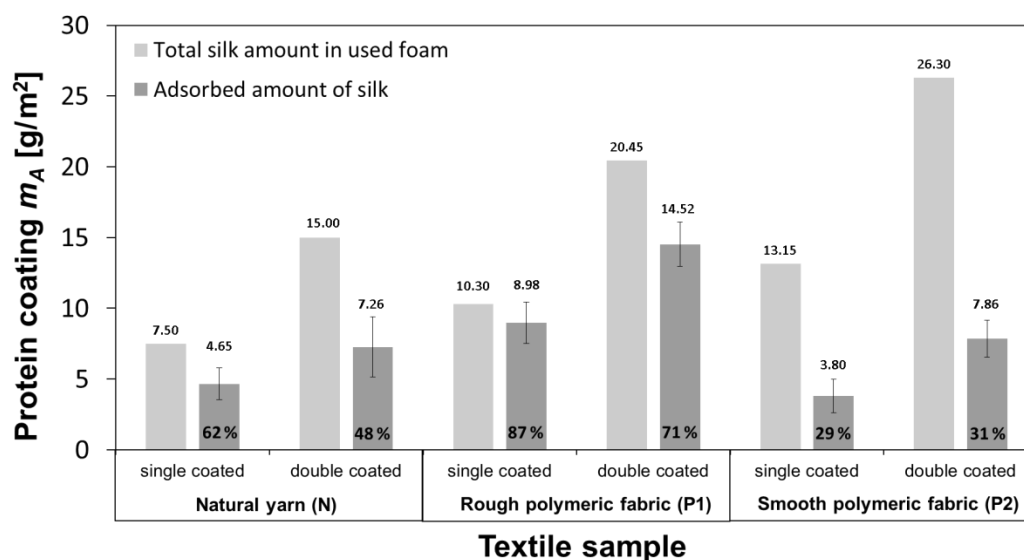


**Figure 3.4:** Analysis of the protein amount in the used foam vs. the adsorbed protein amount on the fabric for single-coated and double-coated (repeated first coating step) textiles.

### 3.1.5 Coating stability and protective effects of spider silk on single yarns

Yarn fraying tests were carried out to investigate the impact of silk foam coating on single yarns. Silk coated yarns showed a reduced fraying behavior compared to uncoated ones as depicted for linen yarn in Figure 3.5 and in Table 3.2. Compared to uncoated yarn (Figure 3.5 A), fewer fibers were ripped out of the matrix (Figure 3.5 B). A conversion into black/white pixel with subsequent ratio analysis revealed a wider peak after fraying in case of the uncoated samples, compared to silk coated yarns (Figure 3.5 C-E). The numerical comparison of fraying reduction upon silk coating was achieved by determining the hairiness index  $H$  [ $\mu\text{m}^2/\text{cm}^2_{\text{yarn}}$ ]. This ratio describes the total black pixel area in square- $\mu\text{m}$  per square-centimeter of yarn (Table 3.2).<sup>[222]</sup>

The reduction of fraying differed in dependence of the surface roughness of the used textile fibers. It was less for smooth fibers like PET (6%) or CV (13%), compared to the highest values for structured fiber materials like LI (36%) or PAN (51%).

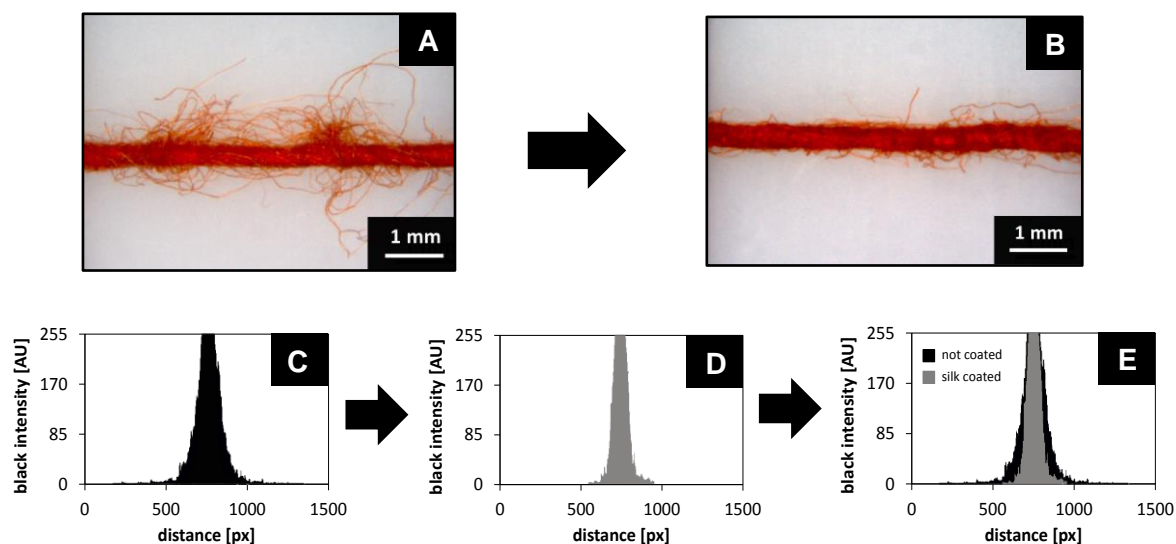


**Figure 3.5:** Fraying test of a LI fiber yarn, Art. 927 (textile N), uncoated yarn after fraying test (A), spider silk coated yarn after fraying test (B); Examples of yarn fraying test analysis using black/white pixel ratio analysis of uncoated yarn volume after fraying (C), silk coated yarn volume after fraying (D) and overlay of C and D for direct comparison (E), modified from.<sup>[216]</sup>

**Table 3.2:** Single fiber fraying test and reduced single fiber fraying upon coating, modified from.<sup>[216]</sup>

| Yarn material                      | Hairiness index $H$<br>[ $\mu\text{m}^2/\text{cm}^2_{\text{yarn}}$ ] |        | Reduction of<br>fraying [%] |
|------------------------------------|--|--------|-----------------------------|
|                                    | Uncoated   | Coated | Coated                      |
| Linen (LI)                         | 279  | 206    | $36 \pm 13$                 |
| Rayon (CV)                         | 339  | 301    | $13 \pm 3$                  |
| Poly(acrylonitrile) (PAN)          | 503  | 333    | $51 \pm 21$                 |
| Poly(ethylene terephthalate) (PET) | 268  | 253    | $6 \pm 1$                   |

The coating stability was tested by washing with water and ethanol (Table 3.3). The water washing test and ethanol washing test led to no destruction of the coating on the individual fibers. Only connecting points between single fibers were diminished in yarn materials with smooth surfaces like polyester (with water, as well as, with ethanol) and rayon (ethanol).

**Table 3.3:** Coating stability, tested by washing with water and ethanol; ten independent samples were tested ( $n_s=10$ ), modified from.<sup>[216]</sup>

| Yarn material                      | Water washing test |                 | Ethanol washing test |                 |
|------------------------------------|--------------------|-----------------|----------------------|-----------------|
|                                    | Film               | Fibrous Bridges | Film                 | Fibrous Bridges |
| Linen (LI)                         | +                  | +               | +                    | +               |
| Rayon (CV)                         | +                  | +               | +                    | -               |
| Poly(acrylonitrile) (PAN)          | +                  | +               | +                    | +               |
| Poly(ethylene terephthalate) (PET) | +                  | -               | +                    | -               |

### 3.1.6 Abrasion tests of spider silk coated fabrics

The textile quality was measured by the application of strain and the subsequent appearance of pilling for untreated textiles compared to the reduction of pilling after silk coating. In all cases, natural textile fabrics showed a low tendency of pilling (Figure 3.6 A). Spider silk coating slightly improved the textile integrity regarding intermediate strain. An additional coating step (i.e. double coating) led to a further improvement of the long-term resistance by 17%. The polymeric fabrics, both comprising PAN-filaments and PET-staple yarn fibers arranged in combed yarn matrix, showed increased basic roughness. Upswelling stress led to a direct drop of integrity in the case of uncoated fabrics. Regarding the spider silk coating, the fabric quality was significantly increased after strain by up to 200% (see Figure 3.6 B (P1), 5000 rounds uncoated vs. double coated) throughout all numbers of revolutions. Especially at long-term abrasion (5000 rounds) the tendency to pill was significantly reduced. An additional second coating step had no additive effect.

Regarding the smooth polymeric textile P2, the initial strain on uncoated textile had a similar destructive effect compared to that on P1 in the case of short-term strain (Figure 3.6 C (P2)). Upon silk coating, the abrasion resistance was significantly improved by more than one quality category throughout the complete range of strain (revolutions). For long-term strain the quality was seen to nearly doubled. In addition, for coated textile P2, an initial gradual decrease in remaining textile quality could be recorded. As seen previously, the second coating step showed no further effects on the textile integrity.

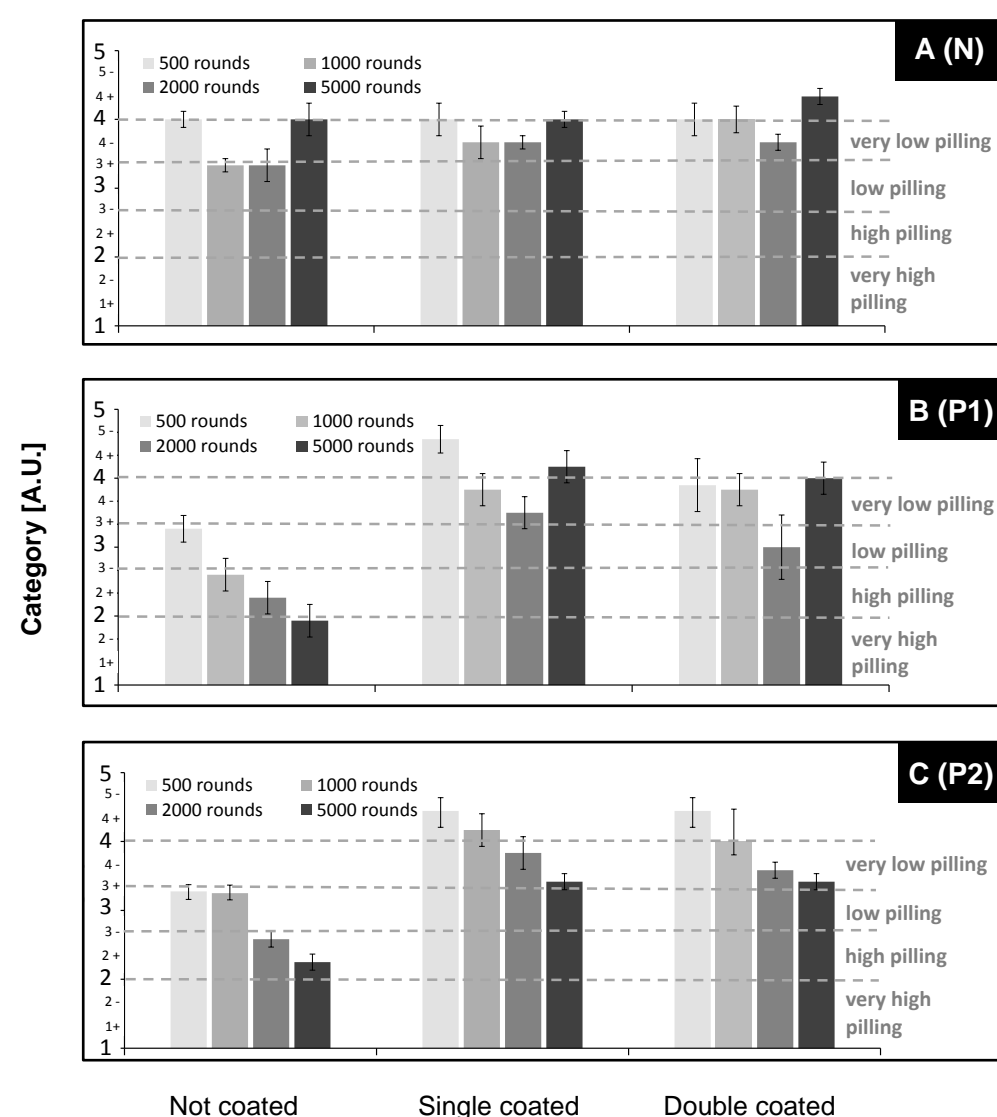


**Figure 3.6:** Pilling abrasion test; A: rough partially natural fiber textile (N); B: rough polymeric textile (P1); C: smooth polymeric textile (P2). Three independent samples were tested for each material and level of strain/ number of revolutions ( $n = 3$ ), modified from.<sup>[216]</sup>

### 3.2 Electrospun nonwoven mesh for the improvement of a filtration surface

The second aim of this work was processing of nonwoven fiber meshes for the production of filter materials using electro spinning. One intention was the establishment of an upscaling process for standard electrospinning.

#### 3.2.1 Preliminary analyzes

The analysis of spinning dopes, including their viscosities and the resulting fiber diameters (see Table 3.6), were preliminarily focused.

##### 3.2.1.1 Rheological characterization of spinning dopes

The rheological analysis of the used polymeric and biomaterial spinning dopes revealed three regimes. The solvents with lower viscosities (about 1 mPa s), the biopolymers ChryC1 and eADF4(C16) with a constant viscosity at 0.1 Pa s and the PLA and PEO polymer dopes with the highest final viscosities at 1 Pa s (Figure 3.7).

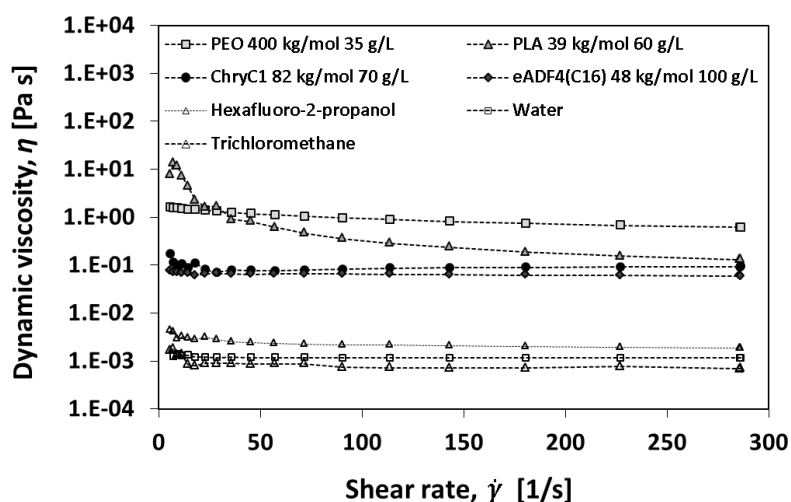


**Figure 3.7:** Mean viscosity of spinning dopes under increasing shear forces from 0 to 286 1/s.



In electrospinning processes, the dope solutions are extruded through cannula acting as an electrode and build droplets. Due to the electrostatic field strength those droplets are conically deformed (Taylor cone). Thereon polymer jets are emerging from the extruded droplet and solidify during their flight towards the collector plate. The shear rate of fluids in a cylindrical system is expressed by Equation 3.3. Lang described a required linear velocity of  $v = 33$  m/s for an accelerated cylinder roll to enable aligned collection of electrospun silk protein submicron fibers.<sup>[228]</sup> For an inner cannula diameter,  $d = 0.8$  mm, and the given speed of the polymer jets,  $v = 33$  m/s, a resulting shear rate of  $\dot{\gamma} = 330.000$  1/s might be assumed. As a consequence, the tested viscosities after asymptotic approximation were set for each dope, in steady state at the highest shear rates (286 Pa s).

$$\dot{\gamma} = \frac{8 \cdot v}{d} \quad (3.3)$$

**Table 3.4:** Asymptotic approximation values of rheological analysis of electrospinning dopes with dynamic viscosities of all used spinning dopes at highest tested shear rate.

| Steady state dynamic viscosity $\eta$ [Pas] |                     |                     |                     |                     |                     |                     |                       |
|---|---------------------|---------------------|---------------------|---------------------|---------------------|---------------------|-----------------------|
| Shear rate $\dot{\gamma}$ [1/s]             | TCM                 | Water               | HFIP                | PLA<br>60 g/L       | PEO<br>35 g/L       | ChryC1<br>70 g/L    | eADF4(C16)<br>100 g/L |
| 286   | $7.0 \cdot 10^{-4}$ | $1.1 \cdot 10^{-3}$ | $1.8 \cdot 10^{-3}$ | $1.3 \cdot 10^{-1}$ | $6.1 \cdot 10^{-1}$ | $0.9 \cdot 10^{-1}$ | $1.1 \cdot 10^{-2}$   |

### 3.2.1.2 Comparison of the dynamic dope viscosities and E-spun fiber diameters

The comparison of the dope viscosities in relation to the employed dope concentrations revealed three different tendencies (Figure 3.8). For aqueous PEO solutions, a steep linear increase could be observed, whereas the dynamic viscosity of PLA showed a flat part and a steeper increase above 140 g/L.

In contrast to that, both recombinant proteins showed a similar increase over a broad range of dope concentrations not exceeding 1 Pas.

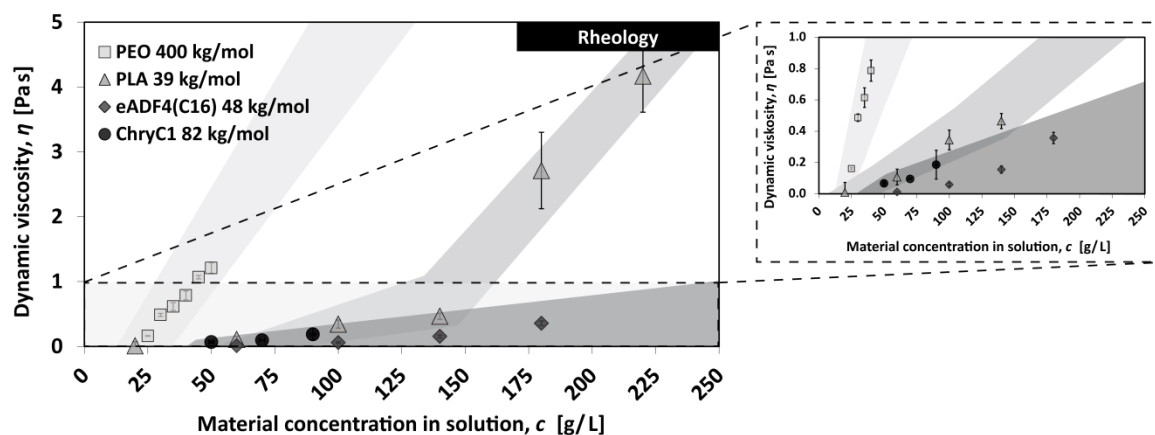


**Figure 3.8:** Overview of resulting dynamic viscosities after rheological characterization of the used synthetic polymer (PEO, 400 kg/mol and PLA, 39 kg/mol) and the recombinant proteins (eADF4(C16), 48 kg/mol and ChryC1, 82 kg/mol) at different dope concentrations.

The analysis of the fiber diameter in relation to the dope viscosities revealed two different regimes. Dopes of synthetic polymers yielded a linear diameter increase with a maximum at 450 nm for PEO and more than 5  $\mu\text{m}$  for PLA. Spinning of the recombinant proteins resulted in overall smaller fiber diameters with a flat increase (Figure 3.9).

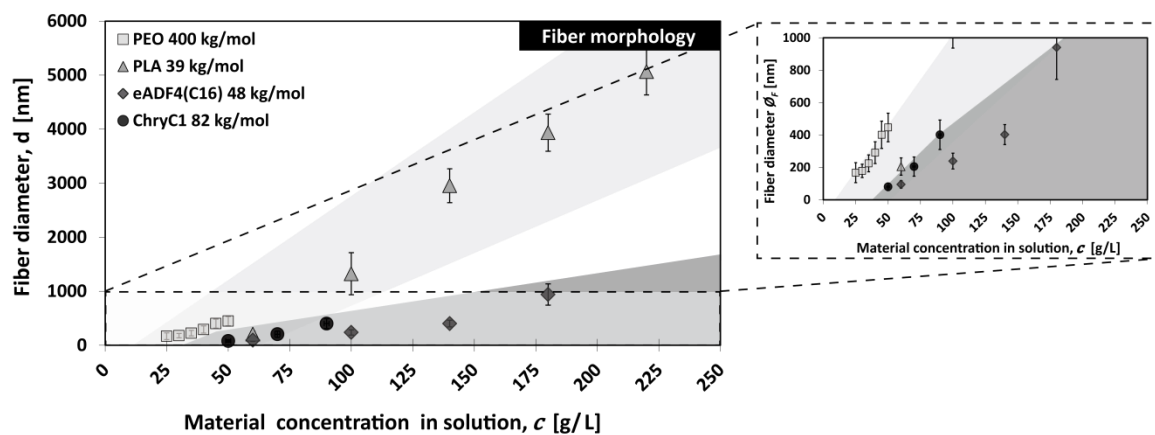


**Figure 3.9:** Overview of resulting fiber diameters after electrospinning of the synthetic polymer (PEO, 400 kg/mol and PLA, 39 kg/mol) and the recombinant proteins (eADF4(C16), 48 kg/mol and ChryC1, 82 kg/mol).

### **3.2.2 Electrospun nonwoven fiber meshes for filtration purposes**

To obtain fiber meshes of constant quality regarding fiber diameter and mesh thickness, optimal processing parameter setups were investigated for electrospinning fiber meshes, to include voltage and electrode distance. In a second step, the electrostatic field strength was calculated and analyzed. The parameters yielding best results were analyzed, and the fabricated fiber meshes were tested regarding their applicability for filtration purposes.

#### **3.2.2.1 Processing parameters for electrospinning**

The most effective electrode distance was analyzed by producing fiber mats from each dope, exhibiting the same deposition area. Therefore, the electrode distance and voltage difference had to be adjusted accordingly for each spinning dope. The mesh diameter of 125  $\mu$ m, obtained from the best spinning of eADF4(C16) dissolved in HFIP, 100 g/L at 15 kV, 50% rH and a spinning distance of 125 mm (Figure 3.10 A), was set as reference.

To meet similar mesh diameters for other spinning dopes, the ideal spinning distance for each dope concentration was evaluated by alternating the collector electrode distance until a nonwoven diameter of 125  $\mu$ m was gained within 5 s of spinning. The ideal voltages (see Chapter 3.2.2.2) and spinning heights (see Figure 3.10 B-D) were then taken as standard parameters for spinning fiber meshes (Figure 3.10). The relative humidity was set to 50% (rH) in case of PLA, PEO and recombinant spider silk protein eADF4(C16), and 30% (rH) for recombinant lacewing silk protein (ChryC1).

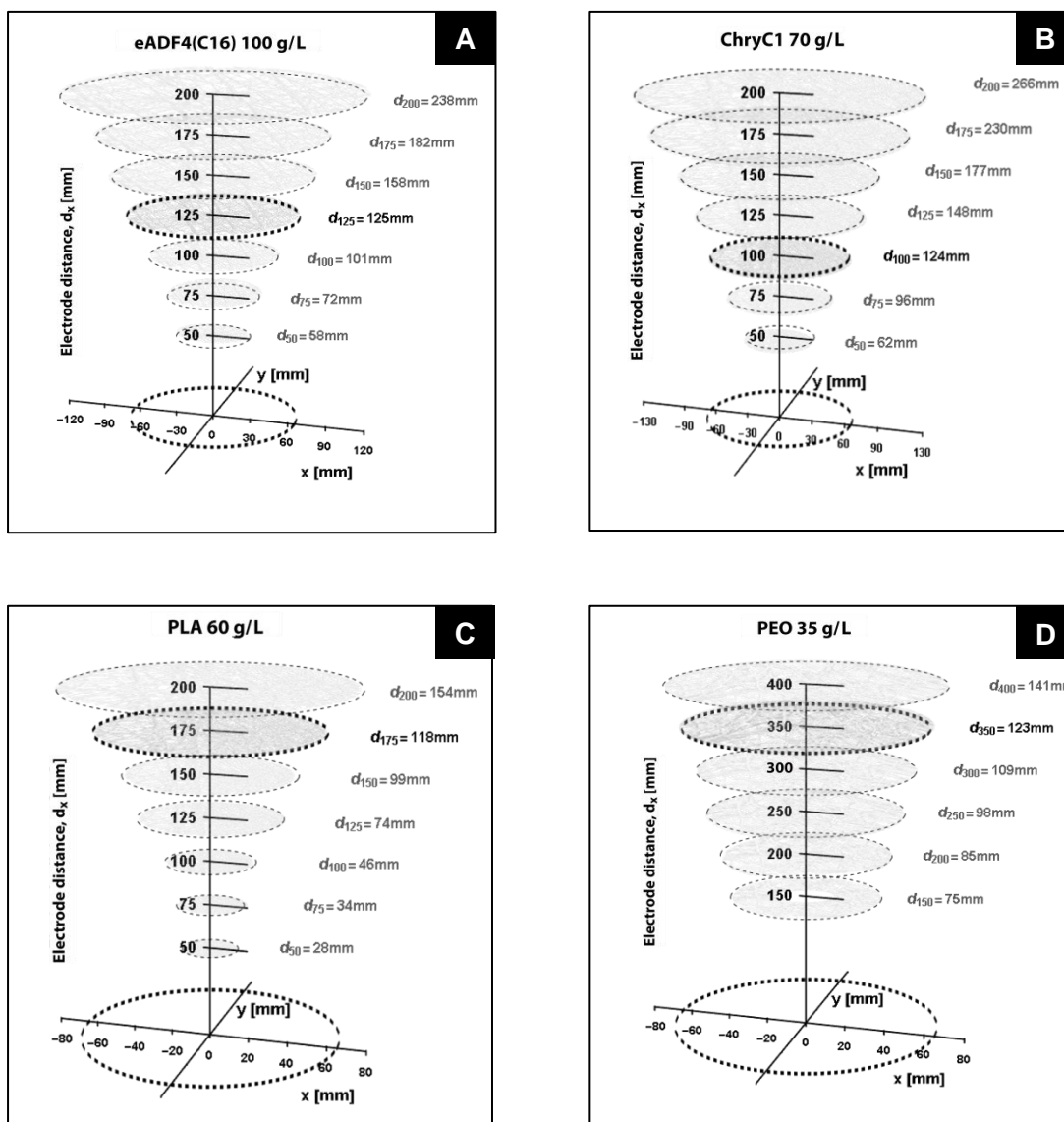


**Figure 3.10:** Electrode distance comparison for electrospinning of different polymer solutions; eADF4(C16) 100 g/L (A), ChryC1 70 g/L (B), PLA 60 g/L (C), PEO 35 g/L (D) at voltages 15 kV (A), 12.5 kV (B), 12.5 kV (C) and 27.5 kV (D).

### 3.2.2.2 Relation between voltage and spinning distance (electrostatic field strength)

The electrostatic field strength is defined as the voltage difference per electrode distance (Equation 3.4). It is one of the main parameters that influence the spinning processes.

$$\vec{E} = \frac{U}{d_x} \left[ \frac{kV}{mm} \right] \quad (3.4)$$

The range of applicable spinning parameters (electrode distance and voltage difference), and the resulting electric field strength for all materials used in electrospinning processes at different dope concentrations in this work are depicted in Table 3.5. Highlighted values were used to generate the best fiber meshes. Additionally, the highlighted fields represent spinning experiments at spinning dope concentrations that yielded similar fiber diameters. Electrospinning of those dopes was possible over a broad range of electric field strengths, but best results were obtained at 0.13 kV/mm for ChryC1, 0.12 kV/mm for eADF4(C16) and 0.10 kV/mm for PLA (all dissolved in high volatile organic solvents), as well as, 0.08 kV/mm for PEO (dissolved in water). The resulting electric field strength was dropping relative to the materials molecular weight and was dependent on the type of solvent. For those dissolved in organic solvents, the voltage difference remained almost identical and the necessary collector distances increased in an inversely proportional fashion. Considering each material separately, the required electric field strength for electrospinning of the dopes was also directly proportional to the dope concentration.

Regarding electrospinning, the possible operating parameters for each polymer and dope concentration were displayed in a matrix and were adjusted accordingly. After optical evaluation of the processed nonwoven meshes, the electric field strength yielding best nonwoven fiber meshes were collected and highlighted for each set (Table 3.5). The necessary electric field strengths were: 0.13 kV/mm for ChryC1, 0.12 kV/mm for eADF4(C16), 0.10 kV/mm for PLA and 0.08 kV/mm for PEO.

**Table 3.5:** Comparison of required electric field strengths for electrospinning of the tested materials, highlighted values depict dope concentrations, voltage differences, collector distances and resulting electric field strengths to obtain best results and similar fiber diameters.

|            |                              | Collector distance, $d_x$ [mm] |  |      |             |             |      |             |      |      |             |      |
|------------|------------------------------|--------------------------------|--|------|-------------|-------------|------|-------------|------|------|-------------|------|
|            |                              | 50                             | 75   | 100  | 125         | 150         | 175  | 200         | 250  | 300  | 350         | 400  |
|            | Dope concentration $c$ [g/L] | $\Delta U$ [kV]                | Electrostatic field strength $\bar{E}$ [kV/mm] |      |             |             |      |             |      |      |             |      |
|            | CryC1                        | 50                             | 10   | 0.10 |             |             |      |             |      |      |             |      |
| <b>70</b>  |                              | <b>12.5</b>                    | 0.25   | 0.17 | <b>0.13</b> | 0.10        | 0.08 | 0.07        | 0.06 |      |             |      |
| 90         |                              | 15                             | 0.15   |      |             |             |      |             |      |      |             |      |
| eADF4(C16) | 60                           | 10                             | 0.08   |      |             |             |      |             |      |      |             |      |
|            | <b>100</b>                   | <b>15</b>                      | 0.30   | 0.20 | 0.15        | <b>0.12</b> | 0.10 | 0.09        | 0.08 |      |             |      |
|            | 140                          | 25                             | 0.16   |      |             |             |      |             |      |      |             |      |
|            | 180                          | 20                             | 0.20   |      |             |             |      |             |      |      |             |      |
| PLA        | 20                           | 10.0                           | 0.08   |      |             |             |      |             |      |      |             |      |
|            | <b>60</b>                    | <b>12.5</b>                    | 0.25   | 0.17 | 0.13        | 0.10        | 0.08 | <b>0.10</b> | 0.06 |      |             |      |
|            | 100                          | 15.0                           | 0.12   |      |             |             |      |             |      |      |             |      |
|            | 140                          | 17.5                           | 0.14   |      |             |             |      |             |      |      |             |      |
|            | 180                          | 20.0                           | 0.16   |      |             |             |      |             |      |      |             |      |
|            | 210                          | 22.5                           | 0.18   |      |             |             |      |             |      |      |             |      |
| PEO        | 25                           | 22.5                           | 0.06   |      |             |             |      |             |      |      |             |      |
|            | 30                           | 25.0                           | 0.07   |      |             |             |      |             |      |      |             |      |
|            | <b>35</b>                    | <b>27.5</b>                    | 0.18   |      |             |             |      | 0.14        | 0.11 | 0.09 | <b>0.08</b> | 0.07 |
|            | 40                           | 30.0                           | 0.09   |      |             |             |      |             |      |      |             |      |
|            | 45                           | 32.5                           | 0.09   |      |             |             |      |             |      |      |             |      |
|            | 50                           | 35.0                           | 0.10   |      |             |             |      |             |      |      |             |      |

### 3.2.2.3 Assembly and analysis of filter systems based on polymer and silk nonwoven mesh fibers

Electro-spun fiber mats were deposited on polyamide mesh support (Figure 3.11 A) to cover the gaps and obtain an uniform fine dust filter layer on the support, as depicted in Figure 3.11 B. The amounts of fiber meshes, laid down per time interval, and hence the fiber mesh thickness, were adjusted by the spinning time, as well as, the dope concentration.

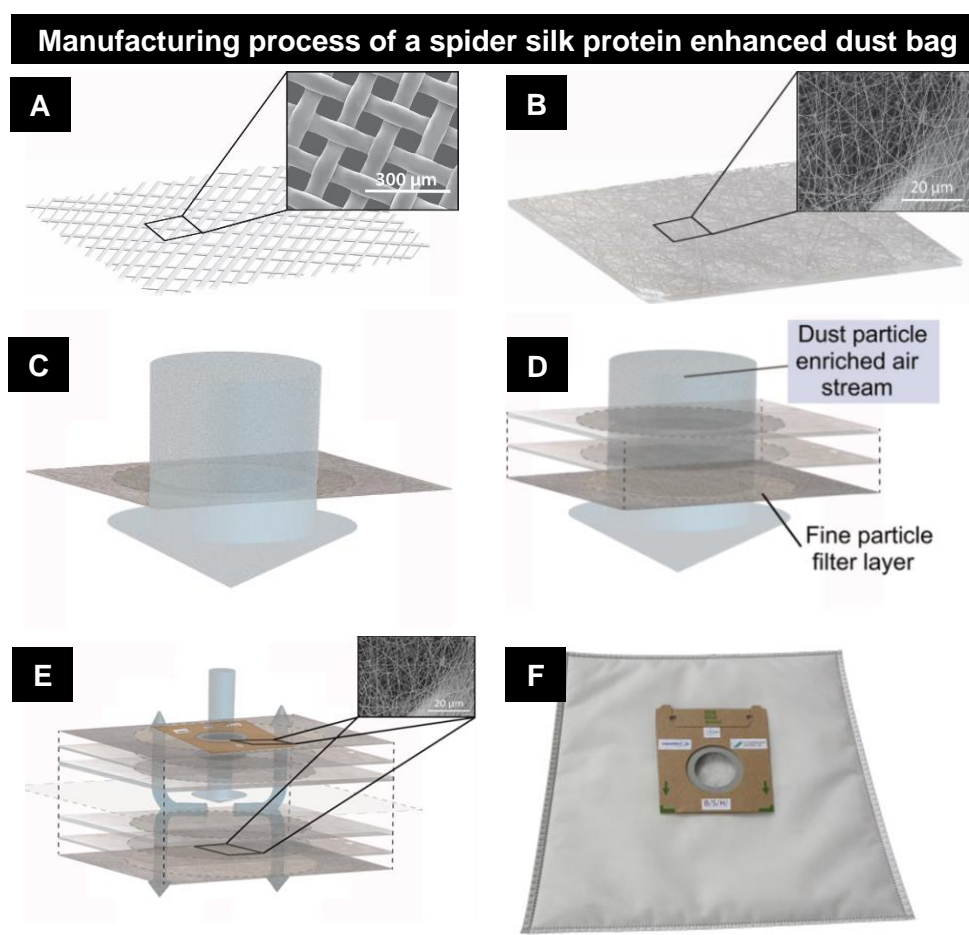


**Figure 3.11:** Spider silk protein fiber mesh fine particle layer and complete dust bag production process with A: polyamide support material with 90 μm gap width, B: deposited nonwoven mesh on the support layer and C: exemplary particle deposition filtration test of fine particle filter layer as well as D: scheme of the complete spider silk protein based filter setup and E: scheme of a complete dust bag (double mirrored stack of D) and F: photograph of E, modified from.<sup>[11]</sup>

The electro-spun uniform fiber mats were tested regarding their filtration efficiency (particle deposition, air permeability and pressure drop) as a single layered fine particle filter (Figure 3.11 C), as well as, combined with intermediate-sized dust and raw dust filter layers acting as a complete dust filter (Figure 3.11 D). Filtration efficiency tests were performed for a complete dust bag. The raw particle filter layer (>2 mm, polyester stacked fleece), combined with an intermediate filter layer (> 0.5 mm, polypropylene spun bond fleece) and the final layer based on eADF4(C16) spider silk nonwoven mesh enhanced PA support of 625 cm<sup>2</sup> at a surface coverage of 100 mg/m<sup>2</sup> (Figure 3.11 D, top to bottom). The nonwoven mesh was oriented towards the inside of the stack, maintaining its mechanical integrity throughout the filtration process.

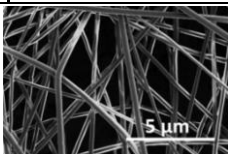
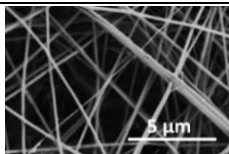
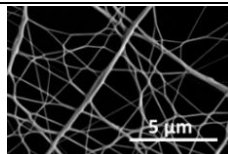
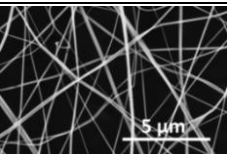
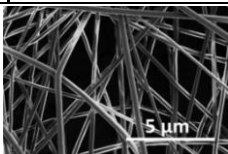
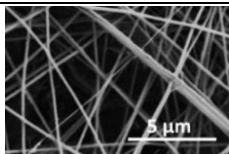
In a commercial standard vacuum cleaner equipped with filter bags, the dust particle stream is led into the core of the filter bag and further passes the upper and lower filter stacks (Figure 3.11 E). To build a novel spider silk protein mesh enhanced filter bag prototype, two identical filtration stacks were combined by orienting the raw particle filter layers towards each other. The fine particle filter layers formed the outer layer of the final setup with the nonwoven coated sides facing to the inside. Thus, placed in a vacuum cleaner with a proper dust bag socket, the air stream reached the bags core, passing first the raw particle filter, then through the intermediate particle filter, and finally through the spider silk covered PA woven mat (Figure 3.11 E). A hole was cut through the center of the upper stack, to act as the inlet and enabling air guidance to the core of the double stack. The edges of the layer stack were fixed using pulsed ultrasound welding and cut to a final size of 400 cm<sup>2</sup>. A paper-filter adaptor was attached to the inlet hole enabling the deployment in a conventional vacuum cleaner, as shown in the photograph (Figure 3.11 F).



## Fiber mesh comparison

Based on the two biopolymers, recombinant ChryC1 and eADF4(C16), and the synthetic polymers PEO and PLA, four different submicron fiber mats were produced and tested regarding their applicability as fine dust particle filters. Nonwoven meshes were spun from different dope concentrations (see 2.5), yielding fiber diameters from 80 nm to about 400 nm in the case of ChryC1, 95 nm to about 400 nm using eADF4(C16), about 250 nm for PLA and about 220 nm for PEO. Filtration efficiency measurements revealed a clear dependency of the particle deposition on material, fiber diameter, and coating thickness. The recombinant lacewing silk protein ChryC1, as well as, eADF4(C16) were both solved in HFIP and electrostatically spun using the optimal parameters to yield negatively charged spider silk protein (PI: 3.48) and moderately negatively charged lacewing silk protein (PI: 5.8) fiber meshes (Table 3.6). In contrast, polymeric PLA was dissolved in TCM and PEO was dissolved in water since HFIP was not dissolving these materials. Dope concentrations comprised 60 (A), 100 (B) and 140 g/L (C) of eADF4(C16) spider silk protein, as well as, 50 (A), 70 (B), and 90 g/L (C) in case of ChryC1 lacewing silk protein, 60 g/L of PLA and 35 g/L of PEO.

**Table 3.6:** Basic information of electro-spun nonwoven mats including materials, molecular weight, main fiber diameter, average pore size, surface charge at neutral pH and exemplary SEM images, modified from.<sup>[11]</sup>

| Material                            | PLA   | PEO   | ChryC1   |   | eADF4(C16)  |   |
|-------------------------------------|---|---|--|---|---|---|
| Molecular Weight $M$ [kDa]          | 39  | 400   | 84   |   | 48  |   |
| Fiber Diameter $\varnothing_F$ [nm] | 245 +/- 53  | 221 +/- 52  | A  | 80 ± 24   | A   | 95 ± 24   |
|                                     |   |   | B  | 205 ± 59  | B   | 239 ± 49  |
|                                     |   |   | C  | 401 ± 91  | C   | 402 ± 61  |
| Pore Size $\varnothing_P$ [μm]      | 7.3 +/- 2.2   | 4.7 +/- 2.2   | A  | 2.9 ± 0.9   | A   | 3.7 ± 1.4   |
|                                     |   |   | B  | 2.8 ± 0.8   | B   | 2.3 ± 0.9   |
|                                     |   |   | C  | 1.8 ± 0.7   | C   | 1.2 ± 0.6   |
| Surface charge at neutral pH        | neutral   | neutral   | negative   |   | negative  |   |
|                                     |  |  |  |  |  |  |

The produced fiber meshes from polymeric materials both exposed neutral surface net charges at neutral pH, whereas fiber mats spun from biopolymers exposed negative surface net charges.<sup>[202,229-231]</sup> In addition, fiber diameters in all meshes were found to be dependent on both the molecular weight of the used polymers and the dope concentration. The higher the molecular weight, the larger the fiber diameter becomes and hence the dope concentration had to be lowered to yield fibers with equal diameters. Whipping effects and repulsive forces during electrospinning affected polymer jets and lead to a chaotic fiber deposition resulting in coherent pores with inhomogeneous but distinct diameter distribution per layer and spinning set-up (PLA:  $\varnothing_p$ : 7.3 +/- 2.2  $\mu\text{m}$ , pore fraction: 97%; PEO:  $\varnothing_p$  : 4.7 +/- 2.2  $\mu\text{m}$ , pore fraction: 95.4%; ChryC1 A:  $\varnothing_p$ : 2.9 +/- 0.9  $\mu\text{m}$ , pore fraction: 96.7%, B:  $\varnothing_p$ : 2.8 +/- 0.8  $\mu\text{m}$ , pore fraction: 92,5%, C:  $\varnothing_p$  1.8 +/- 0.7  $\mu\text{m}$ , pore fraction: 80.8 %; eADF4(C16) A:  $\varnothing_p$ : 3.7 +/- 1.4  $\mu\text{m}$ , pore fraction: 97.4%, B:  $\varnothing_p$ : 2.3 +/- 0.9  $\mu\text{m}$ , pore fraction: 91.5 %, C:  $\varnothing_p$ : 1.2 +/- 0.6  $\mu\text{m}$ , pore fraction: 73.2%). Higher concentrated spinning dopes resulted in smaller pore sizes due to the decrease in viscosity. Whipping effects were consequently reduced.

## **Deposition rates of electrospun fiber meshes on PA support**

### **a) Fiber meshes made from PEO & PLA**

In case of PLA, the particle deposition rate reached sufficient values, approaching those of the standard dust bag, only at a surface coverage of 210  $\text{mg m}^{-2}$  (Figure 3.12 and Table 3.7). Pressure drop rates were intermediate with 116 - 193 Pa (see 2.7.6.2) and increasing with growing surface coverage values. In contrast, PEO nonwoven mats yielded reasonable particle deposition rates only at the highest tested surface coverage (210  $\text{mg/m}^2$ ), but especially for lower particle diameters deposition rates are considerably below the reference value (standard dust bag). Yet, PEO fiber meshes also yielded the lowest pressure drop rates in all tested materials.

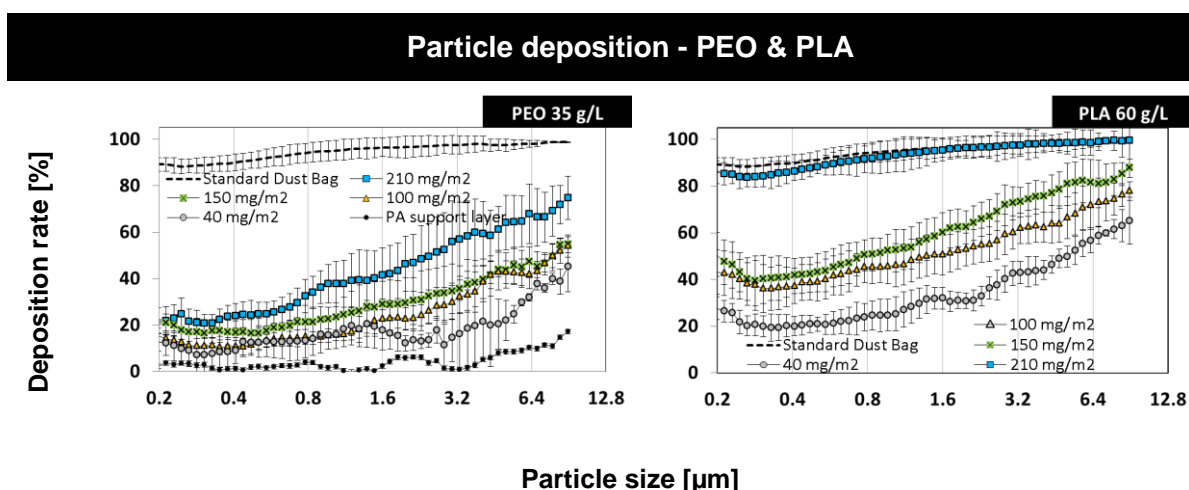


**Figure 3.12:** Deposition rates of poly(lactic acid) (PLA) and poly(ethylene oxide) (PEO) meshes with different grammage each on PA supports and of standard dust bag respectively using a A2 - Arizona fine test dust.

**Table 3.7:** Filter parameters and deposition rates of poly(lactic acid) (PLA) and poly(ethylene oxide) (PEO) meshes on PA supports using a A2 - Arizona fine test dust. Pressure drop differences  $\Delta p$  were determined between that of clean and dust filled filter layers.

| Parameter                                     |                        | PLA             |      |      |      | PEO  |      |      |      |
|---|------------------------|-----------------|------|------|------|------|------|------|------|
| Mean fiber diameter $d$ [nm]                  |                        | 200 < $x$ < 250 |      |      |      |      |      |      |      |
| Amount of layer material [mg/m <sup>2</sup> ] |                        | 40              | 100  | 150  | 210  | 40   | 100  | 150  | 210  |
| Layer thickness $LT$ [ $\mu$ m]               |                        | 99              | 247  | 371  | 519  | 63   | 158  | 237  | 332  |
| Number of fiber mesh layers                   |                        | 440             | 1100 | 1649 | 2308 | 281  | 703  | 1054 | 1475 |
| Air permeability [L/m <sup>2</sup> s]         |                        | 2761            | 2486 | 1671 | 1091 | 2790 | 2455 | 2077 | 1430 |
| Deposition Rate / Retention                   | Ret <sub>0.2</sub> [%] | 28              | 43   | 51   | 86   | 13   | 16   | 51   | 22   |
|   | Ret <sub>0.8</sub> [%] | 25              | 45   | 51   | 92   | 14   | 15   | 21   | 29   |
|   | Ret <sub>3.2</sub> [%] | 41              | 62   | 73   | 98   | 17   | 32   | 36   | 48   |
|   | Ret <sub>8.9</sub> [%] | 65              | 78   | 88   | 100  | 45   | 54   | 55   | 74   |
| $\Delta p$ [Pa]                               |                        | 116             | 127  | 129  | 193  | 23   | 30   | 34   | 40   |

## b) Fiber meshes made from ChryC1

Filter layers based on Lacewing-silk (ChryC1) showed good deposition rates but higher pressure drop rates compared to that of the two synthetic polymers. The correlation between fiber diameter and particle deposition was tested by ES dopes with different material concentrations yielding different fiber diameters. Small fiber diameters (50 - 150 nm) lead to low particle deposition rates, while large fiber diameters (400 - 450 nm), yielded higher deposition rates at the cost of an increasing pressure drop. The combined best performance was achieved at intermediate fiber diameter and a surface coverage of 210 mg/m<sup>2</sup> with intermediate fiber diameters (150 - 250 nm, 70 g/L) exceeding that of a standard dust bag at eminent pressure drop rate (Figure 3.13 and Table 3.8).

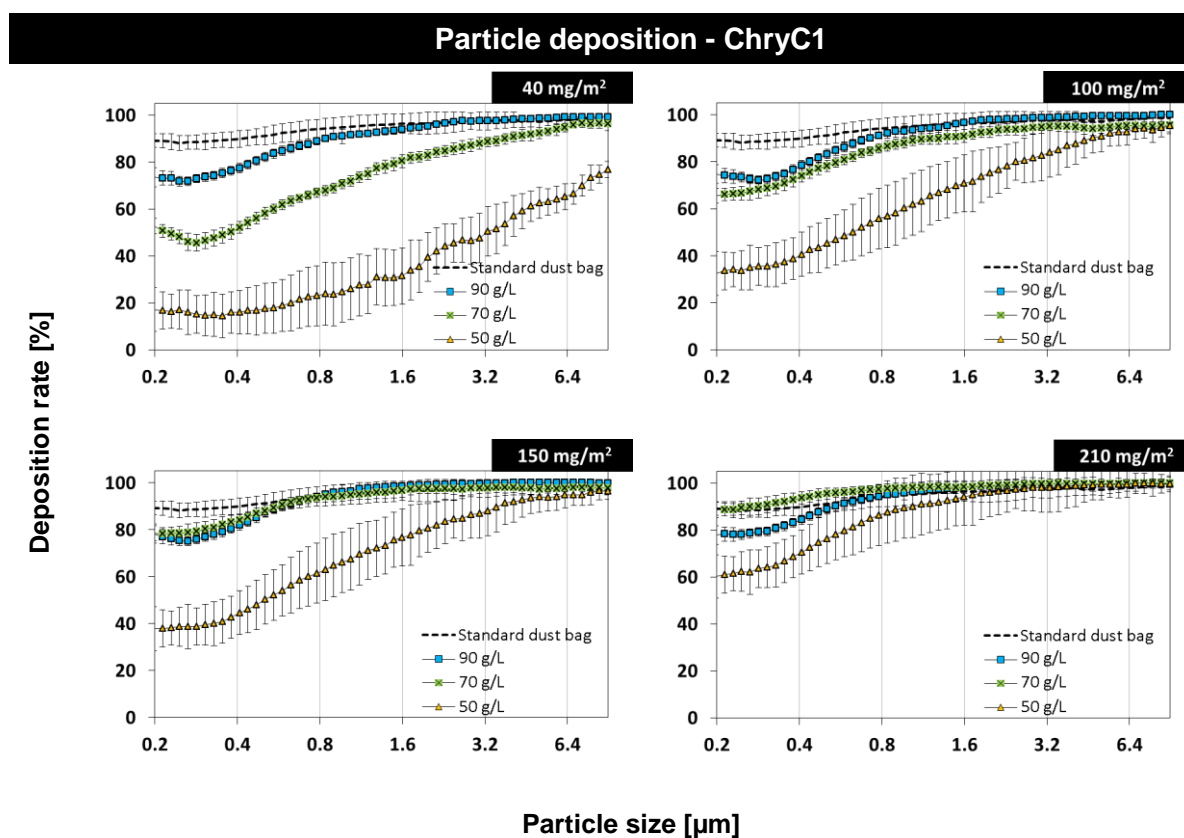


**Figure 3.13:** Deposition rates of lacewing silk protein (ChryC1) meshes (different grammage, as well as, dope concentrations) on PA supports in comparison to standard dust bags using A2 - Arizona fine test dust.

**Table 3.8:** Filter parameters and deposition rates of lacewing silk (ChryC1) meshes on PA supports using A2 - Arizona fine test dust. Pressure drop differences  $\Delta p$  were determined between that of clean and dust filled filter layers, modified from.<sup>[11]</sup>

| Parameter                                     |                        | ChryC1          |                |      |      |      |      |                 |     |      |     |     |                 |    |     |     |     |
|---|------------------------|-----------------|----------------|------|------|------|------|-----------------|-----|------|-----|-----|-----------------|----|-----|-----|-----|
| Mean fiber diameter $d$ [nm]                  |                        | A               | 50 < $x$ < 150 |      |      |      | B    | 150 < $x$ < 250 |     |      |     | C   | 350 < $x$ < 450 |    |     |     |     |
| Amount of layer material [mg/m <sup>2</sup> ] |                        | 40              | 100            | 150  | 210  | 40   | 100  | 150             | 210 | 40   | 100 | 150 | 210             | 40 | 100 | 150 | 210 |
| Layer thickness $LT$ [ $\mu$ m]               |                        | 90              | 224            | 337  | 471  | 38   | 94   | 142             | 198 | 13   | 32  | 48  | 68              |    |     |     |     |
| Number of fiber mesh layers                   |                        | 898             | 2244           | 3366 | 4713 | 168  | 419  | 629             | 880 | 30   | 75  | 113 | 159             |    |     |     |     |
| Air permeability [L/m <sup>2</sup> s]         |                        | 2583            | 1919           | 1742 | 1428 | 1710 | 1326 | 1107            | 877 | 1579 | 867 | 783 | 645             |    |     |     |     |
| Deposition Rate / Retention                   | Ret <sub>0.2</sub> [%] | 17              | 33             | 38   | 60   | 53   | 66   | 78              | 88  | 74   | 75  | 78  | 78              |    |     |     |     |
|   | Ret <sub>0.8</sub> [%] | 24              | 57             | 63   | 88   | 68   | 87   | 94              | 98  | 90   | 92  | 95  | 95              |    |     |     |     |
|   | Ret <sub>3.2</sub> [%] | 57              | 84             | 88   | 98   | 89   | 95   | 98              | 99  | 98   | 99  | 99  | 99              |    |     |     |     |
|   | Ret <sub>8.9</sub> [%] | 77              | 96             | 97   | 99   | 96   | 96   | 98              | 99  | 99   | 100 | 100 | 100             |    |     |     |     |
|   |                        | $\Delta p$ [Pa] |                |      |      |      |      |                 |     |      |     |     |                 |    |     |     |     |
|   |                        | 26              | 82             | 89   | 123  | 96   | 196  | 227             | 320 | 183  | 186 | 200 | 306             |    |     |     |     |

### c) Fiber meshes made from eADF4(C16)

Nonwoven meshes of spider silk eADF4(C16) showed an improved particle deposition at larger fiber diameters, but the pressure drop was seen to exceed the limit at those conditions.<sup>[29]</sup> Similar to the other tested materials, thin fibers (50 - 150 nm, 60 g/L) were not capable of sufficiently capturing the dust particles. Nonwoven fiber meshes made from eADF4(C16) showed the highest overall particle deposition of all materials tested at the cost of the highest pressure drop rates. Best combination of both parameters with good particle deposition rates, outcompeting that of standard dust bags, and acceptable pressure drop rates were detected using fiber diameters between 200 nm and 250 nm for intermediate (100 g/L) and highest (140 g/L) tested dope material concentration, as shown in Figure 3.14 and Table 3.9. This is consistent with previously reported results.<sup>[202]</sup>

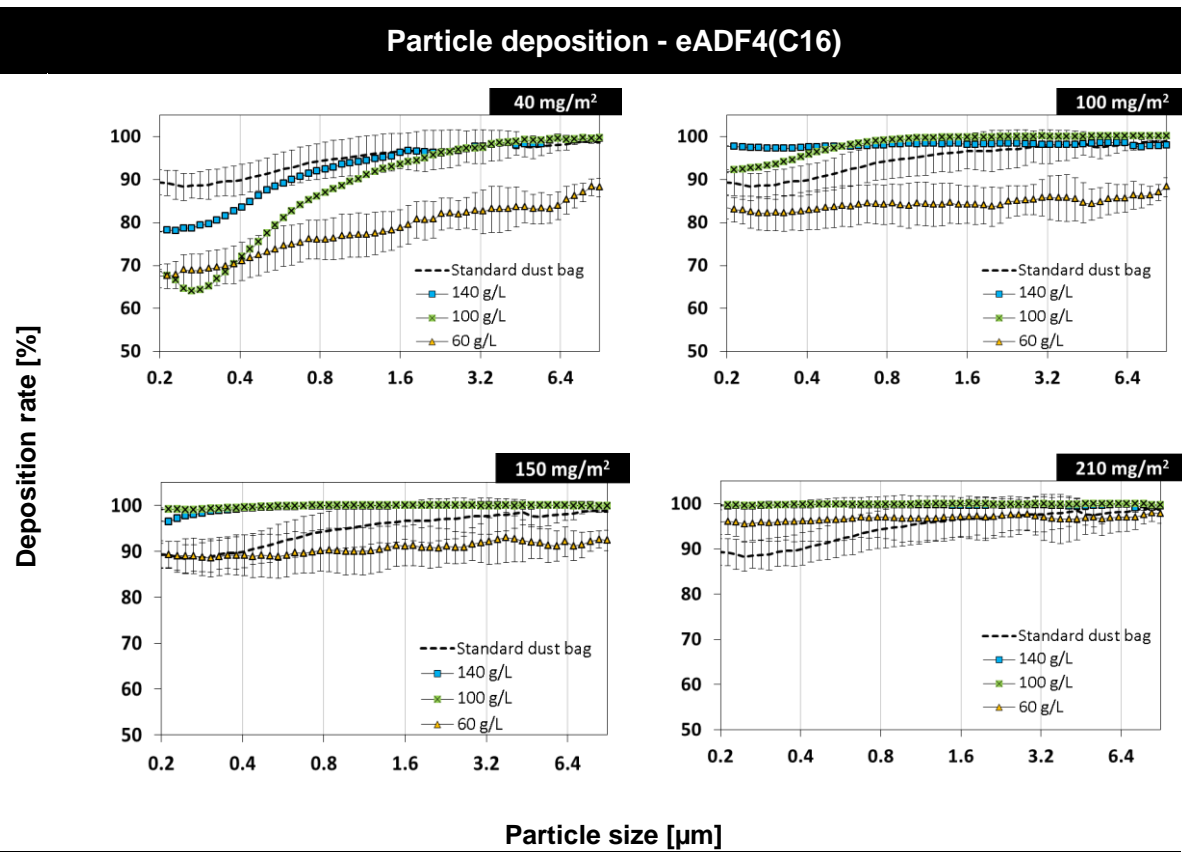


**Figure 3.14:** Deposition rates of spider silk protein eADF4(C16) meshes with different gram-mage, as well as, dope concentrations each on PA supports and of standard dust bag respectively using A2- Arizona fine test dust.

**Table 3.9:** Filter parameters and deposition rates of spider silk (eADF4(C16)) fiber meshes on PA supports using a A2 - Arizona fine test dust. Pressure drop differences  $\Delta p$  were determined between that of clean and dust filled filter layers, modified from.<sup>[11]</sup>

| Parameter                                     |                        | eADF4(C16)     |     |      |      |                 |     |     |     |                 |     |     |     |
|---|------------------------|----------------|-----|------|------|-----------------|-----|-----|-----|-----------------|-----|-----|-----|
|   |                        | A              |     |      |      | B               |     |     |     | C               |     |     |     |
| Mean fiber diameter $d$ [nm]                  |                        | 50 < $x$ < 150 |     |      |      | 150 < $x$ < 250 |     |     |     | 350 < $x$ < 450 |     |     |     |
| Amount of layer material [mg/m <sup>2</sup> ] |                        | 40             | 100 | 150  | 210  | 40              | 100 | 150 | 210 | 40              | 100 | 150 | 210 |
| Layer thickness $LT$ [μm]                     |                        | 113            | 282 | 424  | 593  | 31              | 78  | 117 | 163 | 8               | 21  | 31  | 44  |
| Number of fiber mesh layers                   |                        | 311            | 776 | 1165 | 1632 | 138             | 345 | 518 | 725 | 73              | 183 | 274 | 384 |
| Air permeability [L/m <sup>2</sup> s]         |                        | 1396           | 757 | 492  | 352  | 1274            | 579 | 349 | 238 | 639             | 425 | 213 | 130 |
| Deposition Rate / Retention                   | Ret <sub>0.2</sub> [%] | 83             | 89  | 96   | 69   | 69              | 92  | 99  | 100 | 78              | 98  | 97  | 100 |
|   | Ret <sub>0.8</sub> [%] | 84             | 90  | 96   | 86   | 86              | 99  | 100 | 100 | 92              | 98  | 98  | 100 |
|   | Ret <sub>3.2</sub> [%] | 86             | 92  | 97   | 97   | 97              | 100 | 100 | 100 | 98              | 99  | 99  | 99  |
|   | Ret <sub>8.9</sub> [%] | 88             | 92  | 98   | 99   | 99              | 100 | 100 | 100 | 99              | 100 | 100 | 100 |
| <b><math>\Delta p</math> [Pa]</b>             |                        |                |     |      |      |                 |     |     |     |                 |     |     |     |
|   |                        | 109            | 163 | 198  | 295  | 128             | 241 | 286 | 453 | 239             | 370 | 535 | 869 |

#### d) Particle deposition tests using a complete dust bag equipped with a spider silk protein based fine particle filter layer

The best performing setup (eADF4(C16), 100g/L, 150-250nm, 100g/m<sup>2</sup>) on PA mesh support was selected and implemented in a filter bag acting as a fine dust filter layer (see above). Particle deposition measurements revealed an outstanding filtration capability in this set-up, outperforming a standard dust bag (Figure 3.15).

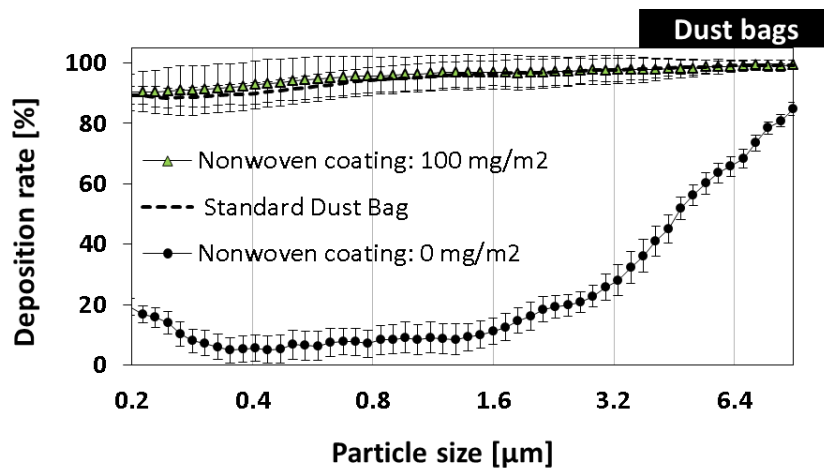


**Figure 3.15:** Deposition rates of spider silk protein of spider silk (eADF4(C16)) fiber meshes on PA support implemented in a prototype dust bag in comparison of a prototype dust bag with PA support and without silk protein mesh fine dust filtration layer, as well as, a standard dust bag respectively using an A2 - Arizona fine test dust.

This set-up yielded a decreased pressure drop, as well as, a better particle deposition throughout the whole particle range when compared to the commercial dust bag (Table 3.10). The silk protein nonwoven layer clearly is the most important part of this set-up regarding particle deposition, as depicted in Figure 3.15.



**Table 3.10:** Filter parameters and deposition rates of spider silk (eADF4(C16)) fiber meshes on PA support implemented in a test dust bag (Figure 3 A) compared to that of the conventional filter using a A2-Arizona fine dust test. Pressure drop differences  $\Delta p$  were determined between that of clean and dust filled filter layers.

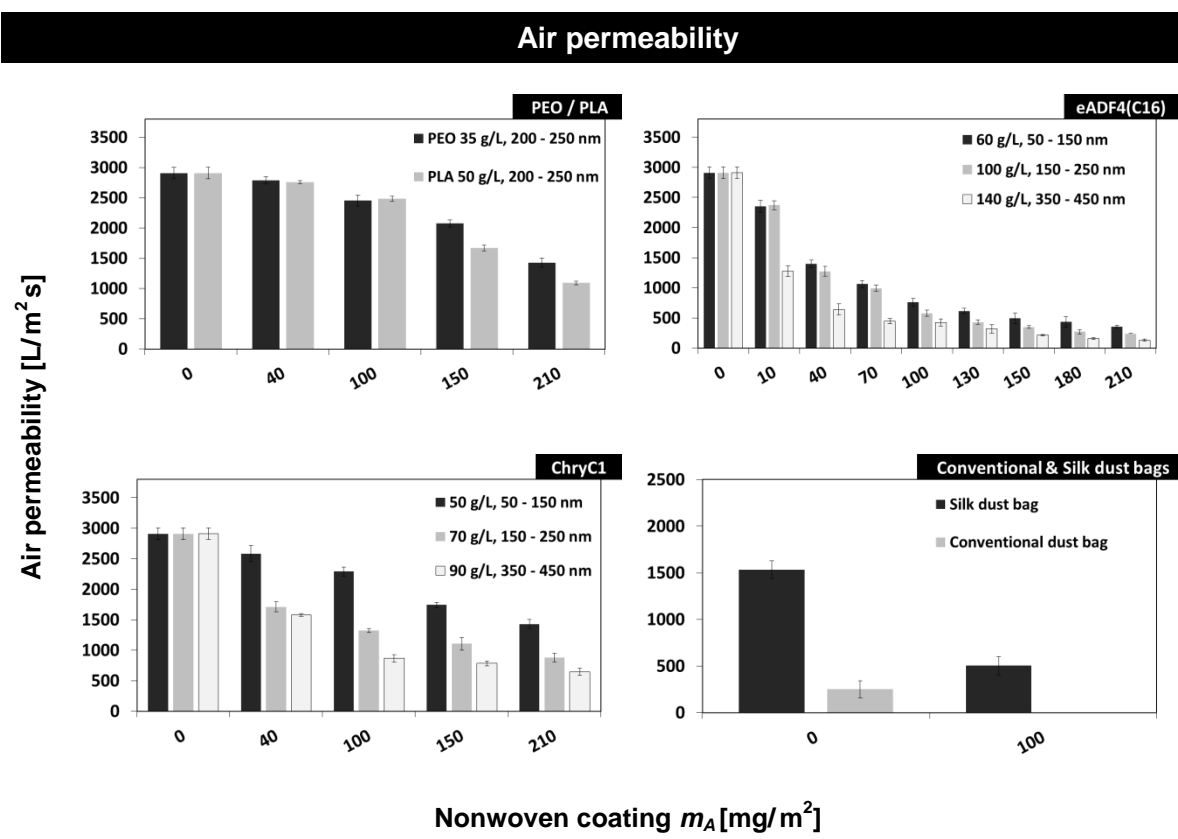
| Parameter                                     |                        | Conventional dust bag | eADF4(C16) spider silk protein dust bag |
|---|------------------------|-----------------------|---|
| Mean fiber diameter $d$ [nm]                  |                        |                       | 150 < $x$ < 250                         |
| Amount of layer material [mg/m <sup>2</sup> ] |                        |                       | 100                                     |
| Layer thickness $LT$ [μm]                     |                        |                       | 78                                      |
| Number of fiber mesh layers                   |                        |                       | 345                                     |
| Air permeability [L/m <sup>2</sup> s]         |                        | 250                   | 503                                     |
| Deposition rate / retention                   | Ret <sub>0.2</sub> [%] | 89                    | 90                                      |
|   | Ret <sub>0.8</sub> [%] | 95                    | 96                                      |
|   | Ret <sub>3.2</sub> [%] | 98                    | 98                                      |
|   | Ret <sub>8.9</sub> [%] | 99                    | 100                                     |
| $\Delta p$ [Pa]                               |                        | 193                   | 115                                     |

### Air permeability tests of electrospun nonwoven fiber meshes on PA support

At fiber diameters of 200 nm-250 nm, nonwoven PEO fiber mats showed good air permeability up to highest polymer surface coverage (Table 3.11). A similar result is obtained for PLA nonwoven meshes. Though, for higher nonwoven mesh grammages air permeability was below that of PEO meshes. Spider silk fiber meshes extended spinning duration, and thus a higher surface material coverage, resulted in an exponential decrease of air permeability, whereas largest fiber diameters showed the upmost decreasing influence. For the setup with 100-250 nm diameter of eADF4(C16) fibers, a minimal air permeability of 500 L/m<sup>2</sup>s was reached at 100 mg/m<sup>2</sup> surface fiber mesh coating. Regarding lacewing silk protein ChryC1, fiber mesh diameters of 50-150 nm yielded a linear decrease in air permeability at increasing amount of layer material.

Compared to spider silk protein, intermediate (100-250 nm) and large (350-450 nm) fiber diameters led to exponentially dropping air permeability rates at equal surface fiber mesh coverage. Though, higher values could be analyzed. The dust bag prototype showed rather high air permeability (about 1500 L/m<sup>2</sup>s) without a nonwoven fiber mesh layer and good air permeability (about 500 L/m<sup>2</sup>s) compared to single fine dust filter layer (250 L/m<sup>2</sup>s).

**Table 3.11:** Air permeability of different dust filter systems on PA mesh support, modified from.<sup>[11]</sup>



### Quality factor analysis of a complete dust bag equipped with a spider silk protein based fine particle filter layer in comparison to a commercial dust bag

The quality factor (QF) represents an important parameter for evaluation of filter materials by describing the particle filtration efficiency in relation to the pressure loss, and

therefore the energy uptake. This factor was first introduced by Hinds, 1998.<sup>[232]</sup> Since the original formula contains the penetration value of dust particles not determined herein, the equation was modified according to the used set-up. The quality factor QF of a filter was determined from ten independent efficiency values for the conventional, as well as, the spider silk filter set-up and calculated by Equation 3.5 with particle deposition efficiency PD and pressure drop  $\Delta p$ .<sup>[233]</sup>

$$QF = \ln[(PD)^{-1}] \Delta p^{-1} \quad (3.5)$$

The particle filtration QF of a conventional dust bag with  $x$  representing the particle diameter and a linear regression was lower than the respective quality factor of the filter with a spider silk coated PA support layer (Figure 3.16) and showed a linear regression according to Equation 3.6.

$$R_{QF,comm.bag} = 0.003x + 0.008 \quad (3.6)$$

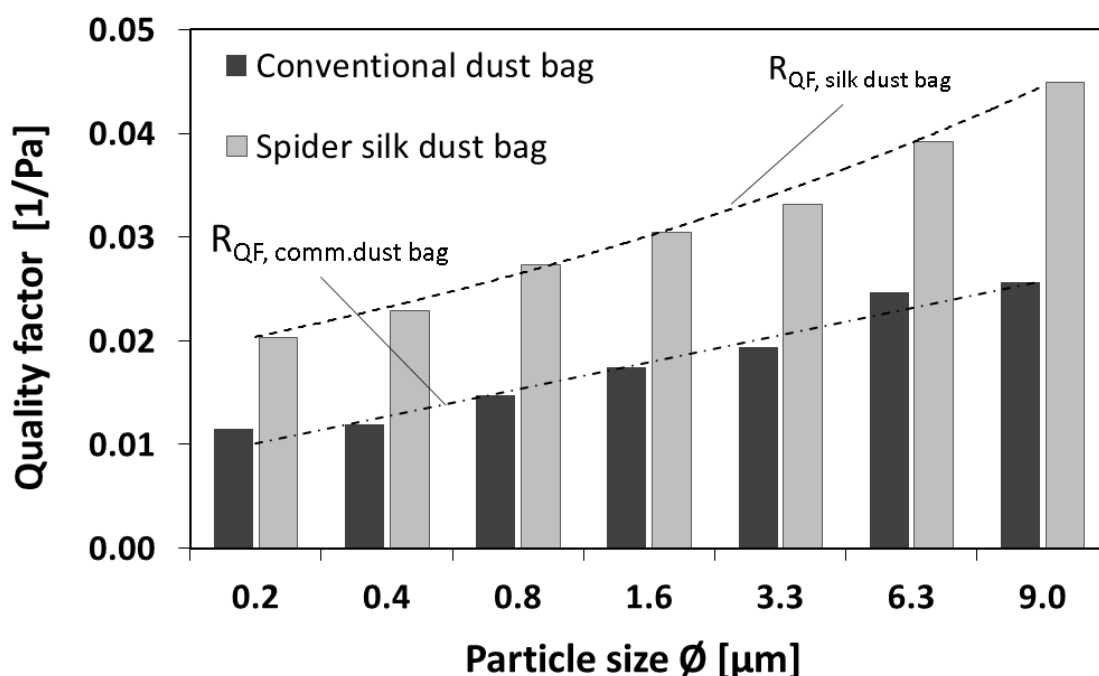


**Figure 3.16:** Quality factor of a spider silk-containing filter set-up in comparison to that of a conventional one at different particle size and the pressure drop, modified from.<sup>[11]</sup>

The total filter quality of the spider silk enhanced filter was nearly doubled over the whole particle size range and increased exponentially. The regression of the silk dust bag QF was approximated by Equation 3.7.

$$R_{QF,silk\ dust\ bag} = 0.02e^{0.13x} \quad (3.7)$$

### **3.2.3 Centrifuge electrospinning parameter analysis for large scale nonwoven mesh production**

Since the centrifuge electrospinning method and setup used in this work were novel and specialized for this task, the parameters for each dope had to be identified. Starting from the preliminarily discovered ideal electric field strengths for electrospinning, the additional parameters were analyzed to complete the set-up.

#### **3.2.3.1 Characterization of voltage and rotational speed**

In centrifugal electrospinning the driving force is a combination of the electrostatic field and the centrifugal force, induced by the rotational speed of the center bell. Hence, three-dimensional graphs were used to compare the fiber mesh quality at different spinning parameters. The evaluation of best fitting spinning parameters comprised data sets with an optically judged fiber mesh quality (1: worst to 7: best), see Figure 3.17) and combination of rotational speed and voltage (Figure 3.18).

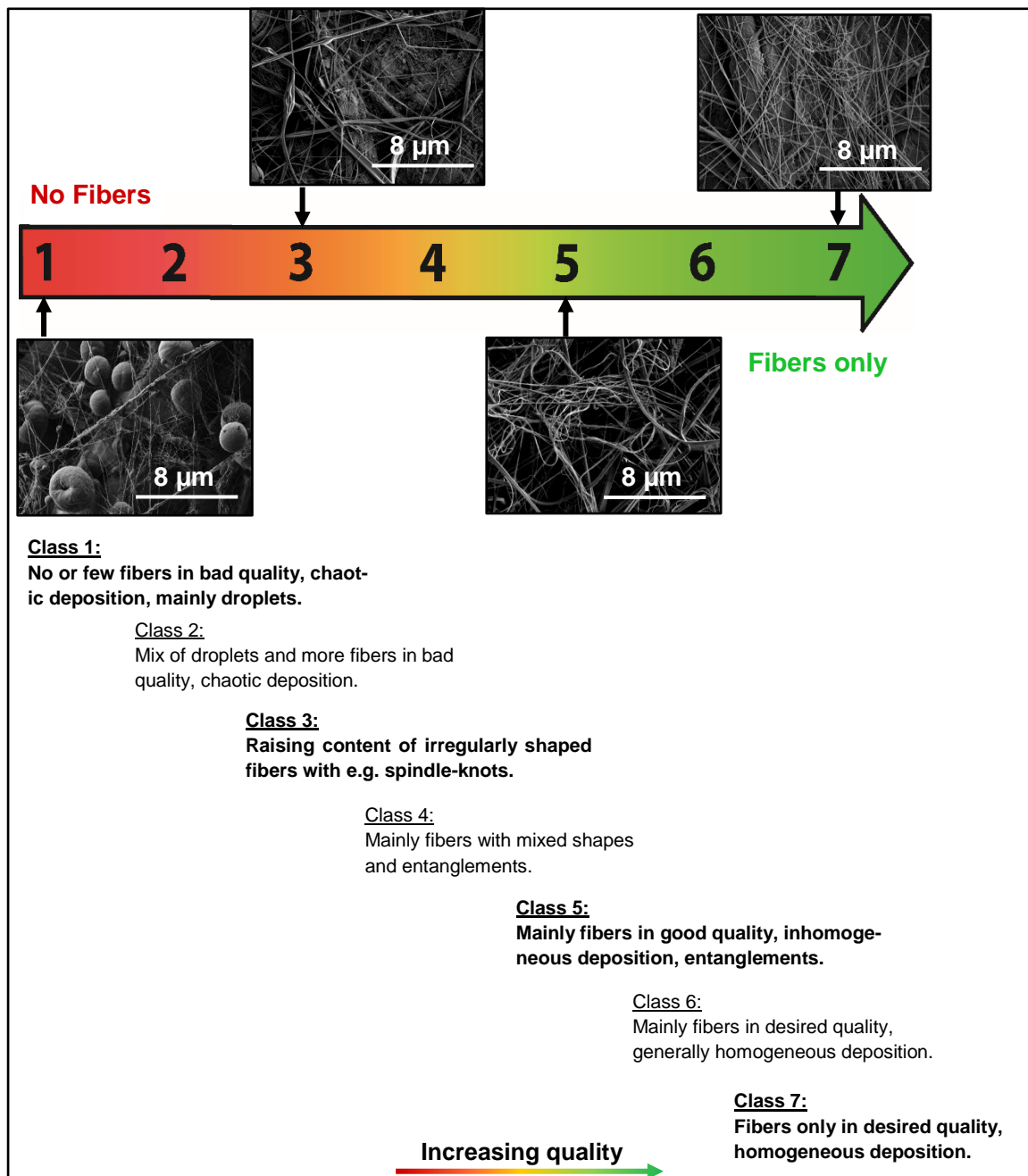


**Figure 3.17:** Explanation and exemplary images of evaluation (quality) classes of centrifuge electro-spun fiber mats.

Aqueous PEO spinning dopes could be spun well at both high rotational speed and voltage, whereas lower combinations thereof yielded insufficient results (50krpm, 90kV). In contrast, PLA dope solutions were sufficiently spun under the whole range of applicable parameter combinations with best results obtained at low rotational speed and the highest voltage (20krpm, 90kV). The fiber meshes spun from spider silk protein (eADF4(C16)) showed optimal quality at low rotational speed and intermediate voltage. Consequently, for further tests the combination of 10krpm and 50kV was applied.

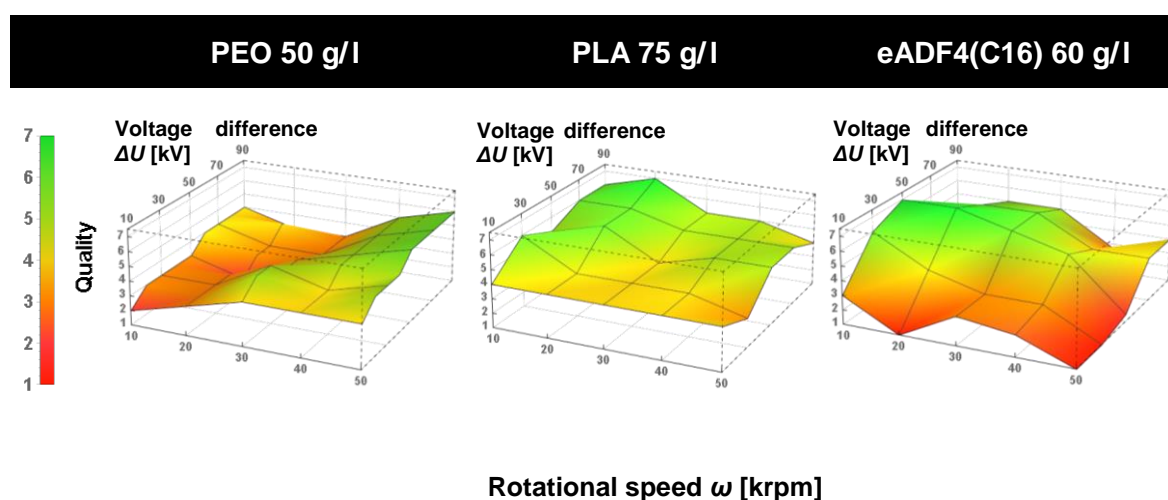
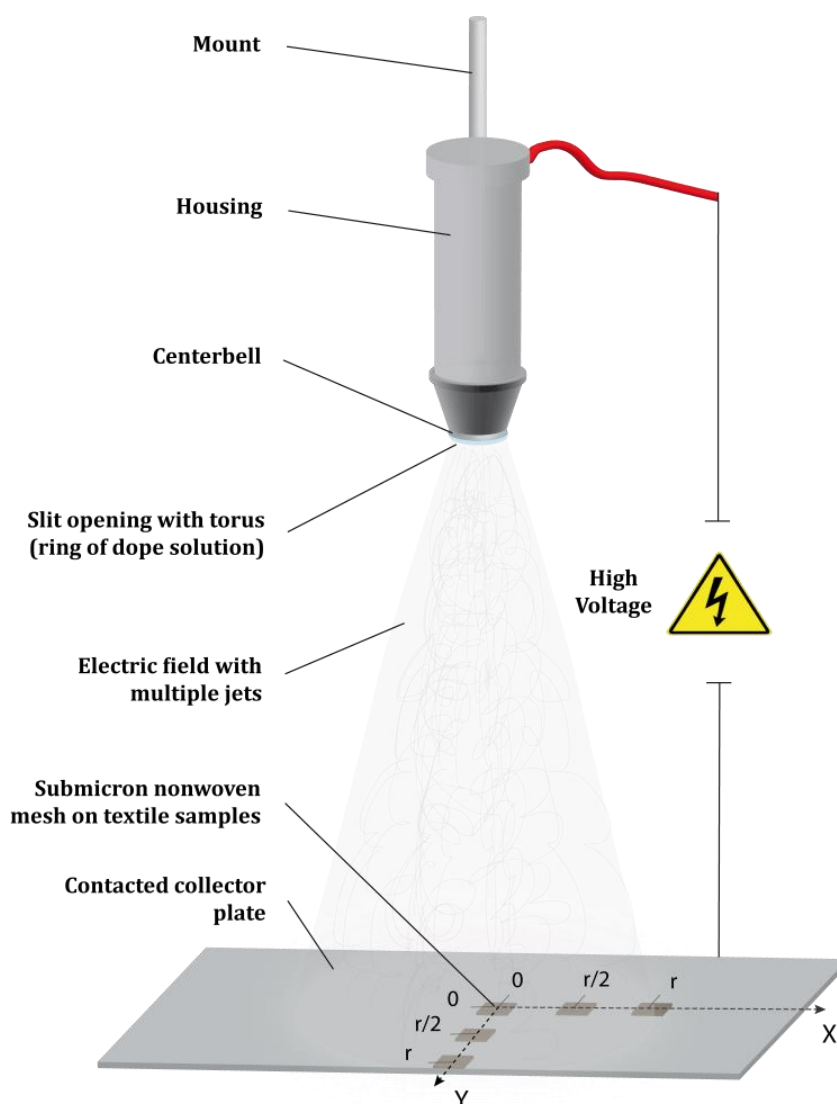


**Figure 3.18:** Three dimensional quality plots of centrifuge electro-spun nonwoven meshes using the materials PEO, PLA and eADF4(C16) at a voltage difference  $\Delta U$  [kV] and rotational speed  $\omega$  [krpm]; quality is rated from 1 (red, worst result, no fibers) to 7 (bright green, best result, dense and closed homogeneous fiber mesh).

### 3.2.3.2 Electrode distance for centrifugal electrospinning of nonwoven meshes (Spinning height)

In case of centrifugal electrospinning, the electrostatic field strength was tested similarly to that of electrospinning. Since the rotational motion of the spinning head creates a constant nonwoven deposition area independent of the collector distance from the center bell, the deposition radius could not be taken into consideration as a parameter. The spinning quality was set as a measure in dependence of the axial distance from the deposition area-center on the collector plate (Figure 3.19).

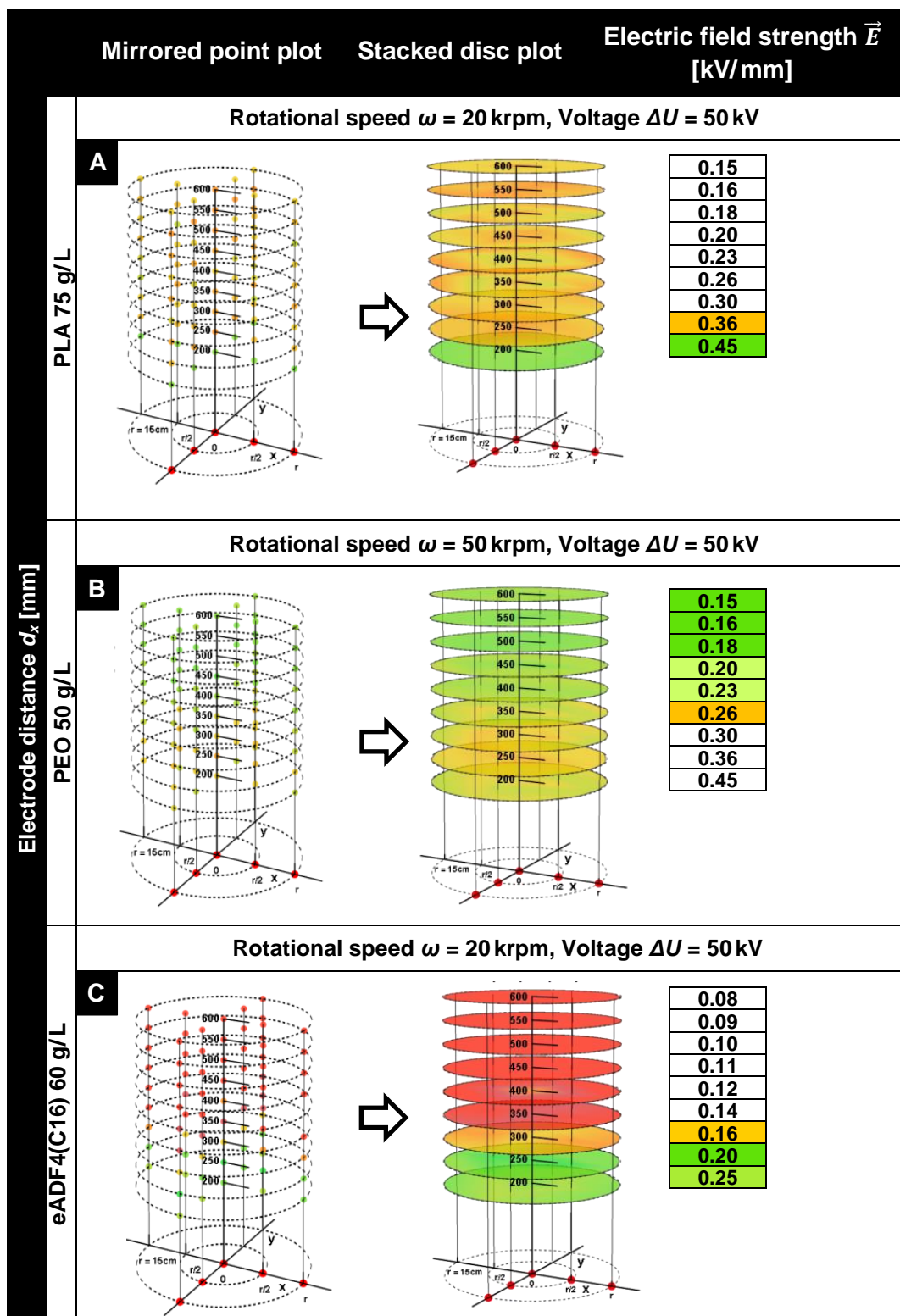
Therefore, 5 samples each were placed on the collector electrode at the center point  $(0, 0)$ ,  $(r/2, 0)$  and  $(r, 0)$  to evaluate the vertical spinning direction and  $(0, r/2)$  and  $(0, r)$  to evaluate the horizontal one. To reduce the dataset, it was assumed that the horizontal and vertical results could be considered as alike at same distances  $(r, r/2)$  starting from the center point, and therefore could be mirrored.



**Figure 3.19:** Schematic collection of centrifugal electrospinning samples for disk extrapolation and electrode distance evaluation, three samples were placed into vertical, as well as, horizontal direction starting from the center of the deposition area.

As shown for PLA in Figure 3.20 A, the resulting spots on one plane (electrode distance) were extrapolated to sectors of rings and autocompleted to colored discs. Here, the resulting mesh quality is directly displayed in the disks by gradually changing colors from 7 (bright green, best mesh results) to 1 (red, no fibers obtained, worst results). The colored stacked disc plot in case of PLA, centrifuge electrospun by using a dope solution with a material concentration of 75 g/L, displays an ideal collector distance of 200 mm and rapidly dropping fiber mesh qualities at increasing collector distances. Herein, the ideal collector distance was focused in a small range. The resulting electric field strength of 0.45 kV/mm represented the highest values in all tests. In contrast to that, the aqueous PEO spinning dope (50 g/L) was spun with satisfying results over the whole range of applicable collector distances (Figure 3.20 B). Despite this, best results were obtained at about 500 mm and resulting electric field strength of 0.18 kV/mm. Centrifugal electrospinning of recombinant spider silk protein eADF4(C16) resulted in a narrow range of applicable field strengths to produce a fiber mesh (Figure 3.20 C-E). Results obtained from centrifuge electrospinning dope with consistent parameters, but different voltage differences clearly illustrated the ideal electric field strength of 0.2 kV/mm for eADF4(C16) dopes.





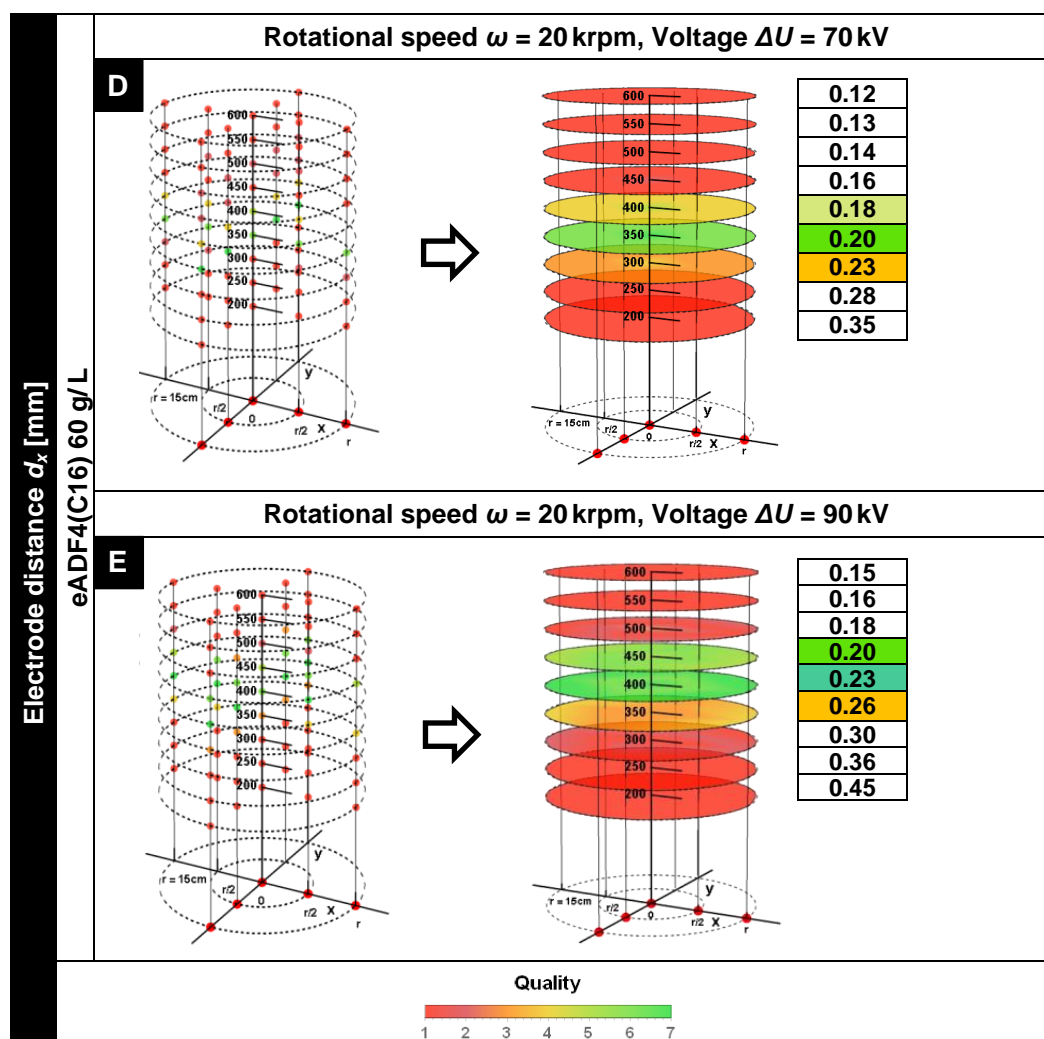


**Figure 3.20:** Colored disk stack height comparison of centrifuge electrospun PLA (A) and PEO (B) at optimal spinning parameters, as well as, of eADF4(C16) (60g/L) at voltage differences 50kV (C), 70kV (D) and 90kV (C) and resulting electric field strengths at constant rotating velocities of 20 krpm.

### 3.3 Influences of E- and CE-spinning on the resulting fiber mesh quality

Fiber quality, in terms of fiber dimension and mechanics, are the utmost important quality indices for the evaluation of the used parameter set-up. Fiber diameter, morphology and secondary structure of the spun nonwoven fiber mesh coatings were analyzed and evaluated in this context.

### 3.3.1 Comparison of resulting fiber diameter in classical and centrifuge electrospinning

Alternating dope concentrations in classical (ES) and centrifugal (CES) electrospinning yielded varying fiber diameters and differently shaped fiber mats. The fiber diameter obtained from both classical and centrifuge electrospinning processes were influenced differently by the spinning dope concentration. The different materials were each spun at optimized conditions for ES (see Table 3.5) and CES (PLA: 0.75 g/L, 0.45 kV/mm, 20 krpm; PEO: 0.5 g/L, 0.18 kV/mm, 50 krpm; eADF4(C16): 60 g/L, 0.2 kV/mm, 20 krpm). For electrospun PEO, a maximal fiber diameter of about 500 nm at 50 g/L dope concentration was found. The diameter decreased about 50 - 100 nm with a dope concentration reduction of 5 g/L. Yet, the minimal achievable fiber diameter was found to be 100 - 200 nm at 25 g/L (Figure 3.21 PLA). In contrast to that, CES of PEO was possible with dope concentrations of 50 and 75 g/L only, resulting in fiber diameter between 100 and 200 nm (Figure 3.21 PEO). A severe impact of dope concentration was observed on the resulting fiber diameter for highly volatile solutions of PLA in TCM using ES. A broad range of applicable dope concentrations from 60 to 220 g/L led to a linear increase of fiber diameter from 200 nm to 5  $\mu$ m. Only the lowest spinnable PLA dope concentration led to satisfying fiber diameter (about 200 nm). Moreover, CES of lowest concentrated dope solutions (25 g/L) led to fiber diameters below 100 nm (nano-fibers), whereas a linear increase in dope concentrations up to 75 g/L both lead to maximal fiber diameters of about 200 nm. In the case of CES eADF4(C16) the average fiber diameter of about 150 nm was independent of the applied dope concentration (60 - 140 g/L). In comparison, ES of eADF4(C16) lead to fiber diameters of 100 - 1000 nm exponentially increasing with dope concentrations between 60 - 180 g/L. The lacewing protein ChryC1 was spun only using ES in the concentration range of 50 - 90 g/L resulting in linearly increasing fiber diameters from 100 to 400 nm, compared to ES of eADF4(C16) (Figure 3.21 and Figure 3.9) using the lowest possible dope concentration.

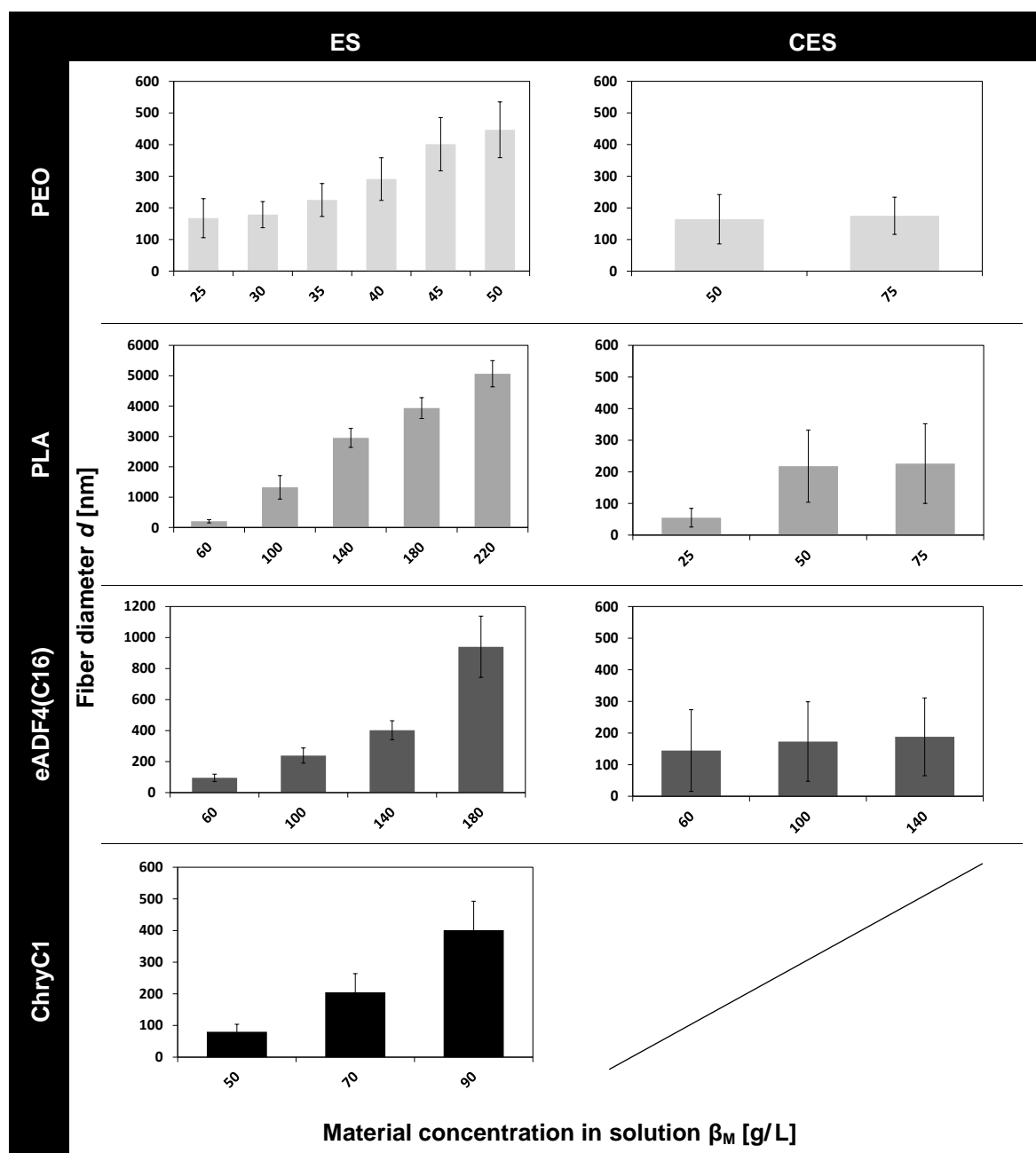


**Figure 3.21:** Fiber diameter comparison for classical and centrifuge electrospinning of all materials at all tested different dope concentrations, spun at best obtained conditions for ES (see Table 3.5) and CES (see Figure 3.20).

Both classical and centrifuge electrospinning methods could be used for successful production of submicron nonwoven meshes from PEO, PLA, ChryC1 and eADF4(C16) (Figure 3.22).

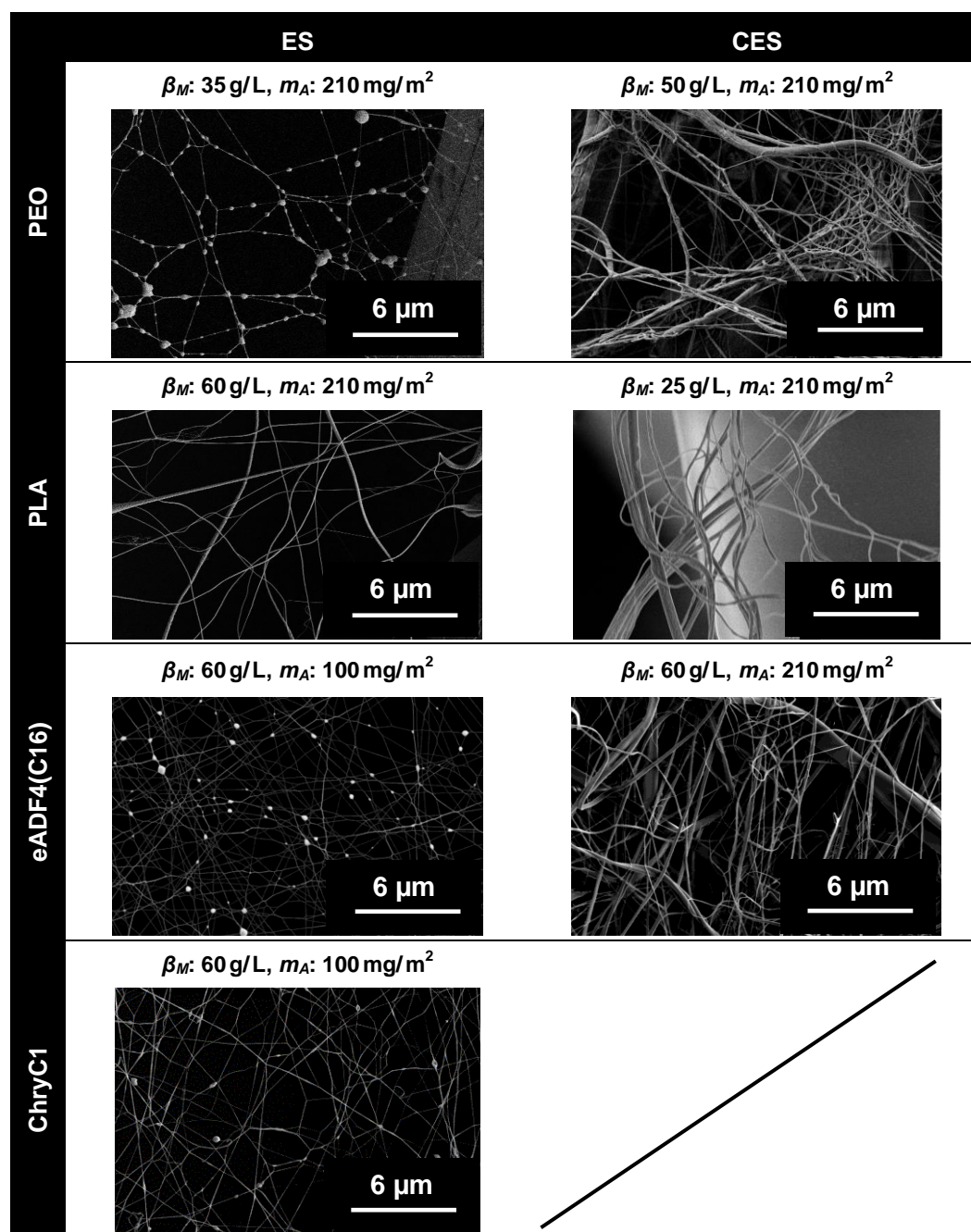


**Figure 3.22:** SEM pictures of fiber meshes of all tested raw materials and dope concentrations yielding comparable nonwoven fiber meshes with same diameters for each material processed with ES and CES.

Electrospinning of PEO resulted in a beaded fiber morphology, whereas centrifugal electrospinning led to fibers with a smooth surface and broad diameter distribution. In case of PLA, both methods yielded smooth fibers, but E-spun fibers appeared more homogeneous in regards to fiber diameters. Electrospinning of recombinant proteins yielded

smooth homogeneous fibers with small diameters, which were randomly, but insignificantly beaded in terms of eADF4(C16). Centrifuge electrospinning was carried out with eADF4(C16) only and yielded smooth and multifold fibers with increased diameter, but less heterogeneously when compared to centrifuge electrospun synthetic polymers.

### 3.3.2 Influence of ES and CES on the secondary structure of spider silk fibers

Transformation of a protein's random coils or  $\alpha$ -helices into more compact  $\beta$ -sheets, strengthens the protein fiber integrity and raises resistance in a humid environment.<sup>[234]</sup> Posttreatment by ethanol vapor was analyzed using FTIR, followed by subsequent Fourier self-deconvolution (FSD).<sup>[235]</sup> The influence of this treatment could be quantified by analysis of the amide I band (Figure 3.23).

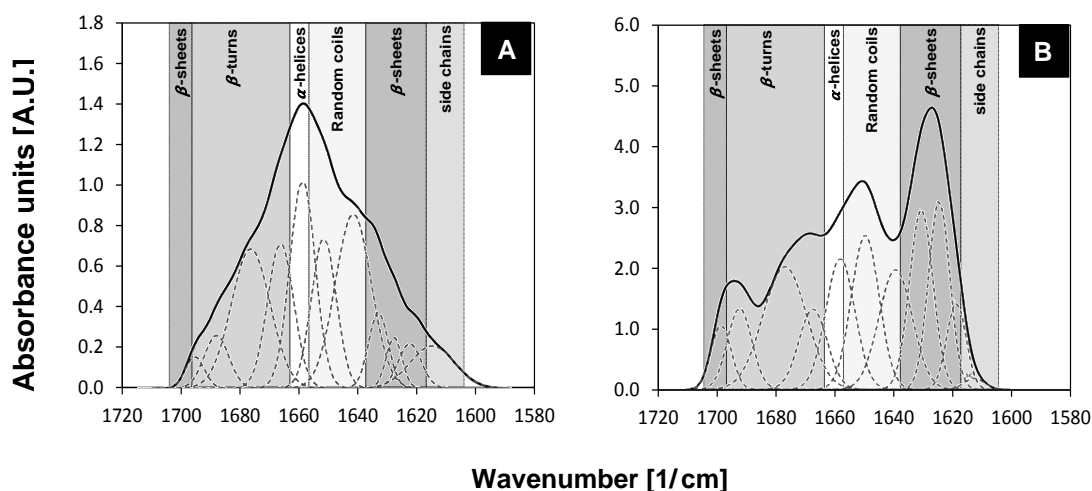


**Figure 3.23:** Fourier self-deconvoluted amide I band of an untreated (A) and a post-treated (B) spider silk nonwoven mesh. The solid line displays the absorbance band resulting from the single contribution peaks (dotted lines) as derived after deconvolution. The assignment of the respective curves was based on the published values from Hu et al.<sup>[218]</sup>

In as-spun fibers, this band was mainly composed of peaks related to turns, as well as,  $\alpha$ -helical and unstructured regions resulting in a maximum at 1660 1/cm. After posttreatment, the maximum shifted to 1620 1/cm with increased  $\beta$ -sheet content as analyzed by FSD.

The structural content is displayed in Figure 3.24. As-spun silk protein nonwoven fibers exhibited a high content of alpha helical and random coil structures. This was determined to be about 50% in total after ES. The low amount of  $\beta$ -sheet structures (about 12%) increased to over 30% by posttreatment at the expense of alpha helical (about 12%) and random coil structures (about 18%). Side chains and turns remained similar in both steps. In contrast, nonwoven meshes produced via CESD revealed 20% of  $\beta$ -sheet structures directly after spinning and comprised about 12% of alpha helical structures. The  $\beta$ -sheet structures were increased to over 30% after posttreatment, which might be considered to be the achievable maximum.

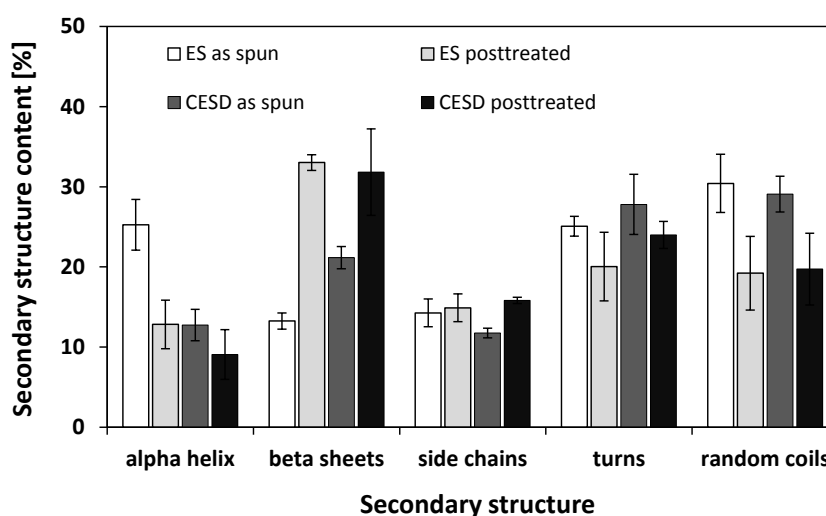


**Figure 3.24:** Secondary structure content of classical and centrifuge electrospun eADF4(C16) fiber meshes as spun and after ethanol vapor treatment,  $n = 3$ .

The percentage of fibers, containing aligned structures, was additionally analyzed using birefringence in polarized light microscopy (Figure 3.25). Bright field microscopy revealed fiber meshes of comparable structure and morphology.

In polarized light, electrospun fiber meshes show a low degree of reflection, indicating reduced amount of anisotropy, whereas as-spun fiber meshes produced via CES, as well as, post treated ES and CES fiber meshes exhibited a high degree of birefringence. Centrifugal electrospinning induced the build-up of anisotropic structures even before post-treatment.

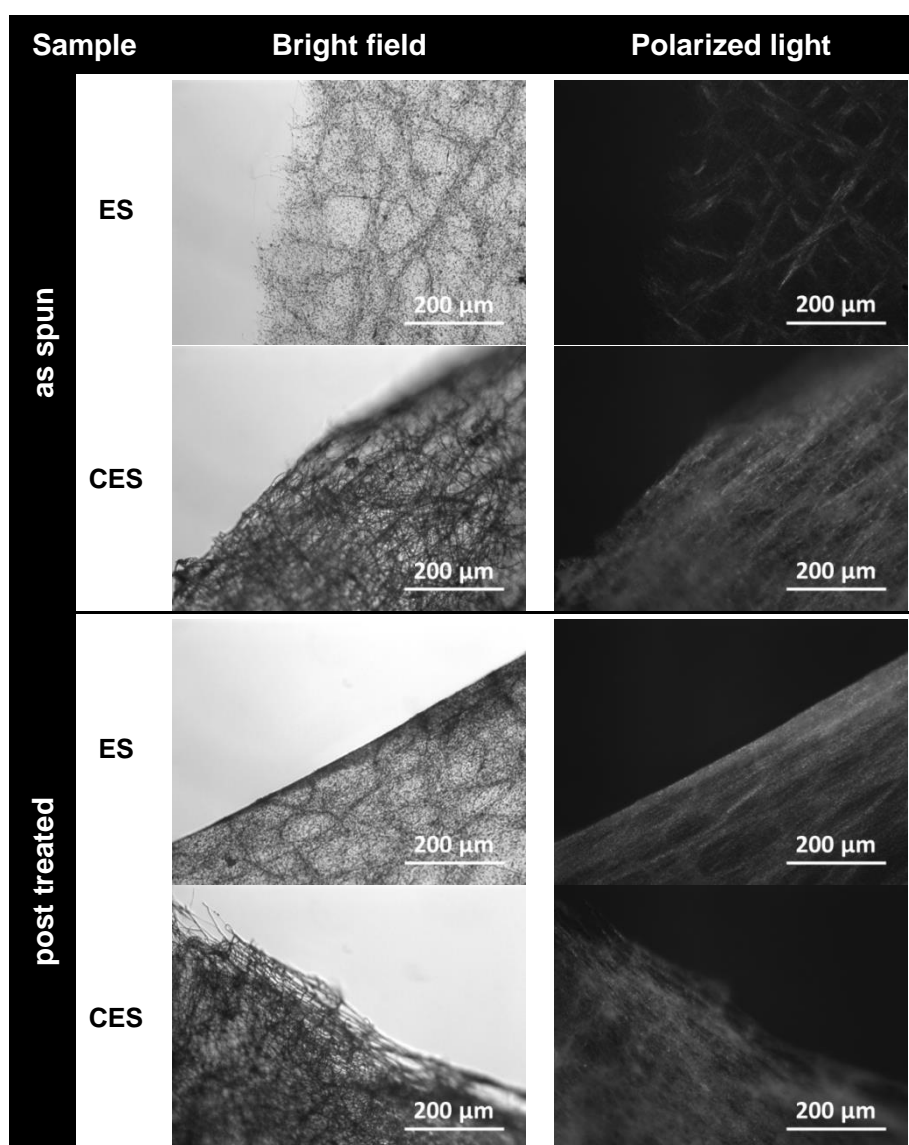


**Figure 3.25:** Optical images of ES and CES-spun eADF4(C16) fiber meshes as-spun and after ethanol vapor treatment with bright field (left) and polarized light microscopy (right).



## 4 Discussion

Silk proteins are extraordinarily versatile and may be processed into different morphologies, encouraging researchers and engineers to experiment with different material combinations, shapes and processes to make use of the known mechanical and physico-chemical properties for novel approaches.

In this work two entirely different processing methods were used, a foam coating for protective purposes and a submicron fiber nonwoven mesh coating for the implementation in dust particle filter bags. Both methods and applications were investigated concerning their main processing parameters.

### 4.1 Coating of industrially produced fibers using spider silk proteins

The products to be coated were standard natural and polymeric fibers and their advanced form, provided as woven and fabrics. Although low concentration aqueous solutions are standard in research and industry, standard coating procedures, such as foulard processes and spray coating had to be discarded for aqueous spider silk protein solutions, since the high amount of required silk solutions showed high material and energy costs. Therefore, a foam coating approach was investigated.

First, the stability of the foaming solution was investigated.<sup>[236]</sup> Furthermore, the foaming of low concentrated aqueous silk solutions, possible beneficial additives and the processing parameters, such as air volume stream, air pressure and rotational shear forces was analyzed. The parameter set-up yielded a maximum amount of temporarily stable foam, which could be soaked into the fibers and fabrics and then be collapsed in a controlled manner under slight vacuum.

It was found that the surface roughness of the underlying single fibers had a strong impact on the percentage of absorbed silk protein. The rub fastness behavior was analyzed using a specially designed test which was inspired by the known capstan test.<sup>[236,237]</sup>

Coating stability was subsequently investigated with water and ethanol, revealing stable coatings. Finally, the rub fastness of coated complete furniture textiles was analyzed using the pilling abrasion test with different material mixtures, as well as, coating steps under increasing numbers of revolutions. It was found that all textiles showed improved behavior at low strain (small number of revolutions), as well as, high strain (large number of revolutions) dependent on the fiber material. Whereas, natural material yarns showed a large strain resistance even without coating, pilling tendency of coated polymer yarn fabrics could be reduced by up to 3 categories (about 200%) rendering the coating highly efficient.

#### **4.1.1 Influence of shear forces and surfactant deployment on foam production**

To achieve stable foams it was crucial to obtain small bubble diameters as described by Cooke and Hirt.<sup>[238]</sup> The main processing parameters were adequately adjusted at room temperature, such as the aeration in form of the utilized air flow rate and air pressure, as well as, the shear stress in the applied form of the propeller's rotations per minute. Smaller bubbles with larger specific surface-area-to-volume ratios showed reduced tendencies to collapse.<sup>[239]</sup>

As described by Wenzel et al., foam bubble diameters decreased under high shear in motion.<sup>[240]</sup> Similar results were published by Parikh.<sup>[241]</sup> Since a propelling unit was used in this work and no tubular set-up, increased shearing was applied by rotational forces. It could be confirmed that maximized shear rates and therefore revolutions per minute increase the blow ratio. It is likely that this effect continues for even higher shear rates, but in the presented setup 1000 rpm was the highest applicable rotational speed. In terms of the aeration, both intermediate flow rate and pressure were beneficial. This effect seems antithetic to common sense, since foam generation in simple devices, such as syphons, depends mainly on high pressure. The set-up is not closed, and therefore, the pressure is not maintained inside the liquid volume. Created air bubbles pass through the medium and accumulate at the surface. Trapping these new bubbles in the foamed medium highly depends on the shear rate as shown by Drenckhan and Saint Jalmes.<sup>[242]</sup> Politova et al. described the bubble size in a foam created in a planetary mixer.<sup>[243]</sup>

The air entrapment in the foam is limited, and therefore its volume-growth is limited. Also, the air entrapment and air volume ratio is relative to the gained bubble sizes.

Transferred to the presented setup, these findings clearly affirmed the results. The employed propeller construction and maximal applied rotational speed result in a limited shear force. When more air is taken into the system and the velocity bubble creation is larger than that of bubbles bursting on the surface (Figure 4.1 A), the bubbles accumulate inside the foam or at the surface. As soon as the inner pressure of these bubbles exceeds the membrane surface tension, these bubbles burst. The emerging pressure force may even destroy fractions of the desired foam as a result (Figure 4.1 B). Reducing this effect by using special foaming agents and detergents in combination with setting up optimal working parameters is of utmost importance to yield a homogeneous silk protein coating distribution in stable foam with high integrity as well as a small bubble structure (Figure 4.1 C).

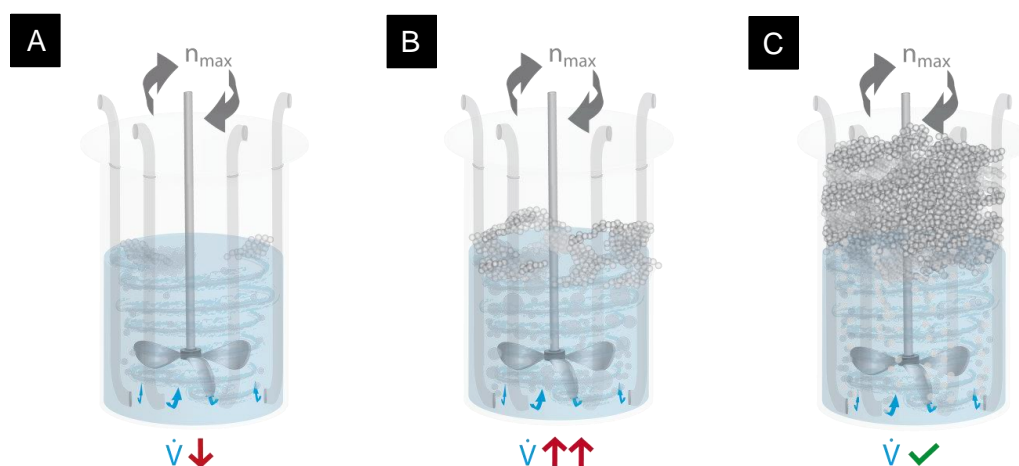


**Figure 4.1:** Schematic illustration of laboratory scale foaming process with an air flow rate, yielding no foam (A), exceeding air flow, air bubble aggregation and collapsing foam (B) and ideal air flow rate and accumulating foam (C).

The surfactant fulfills two main purposes. First, it enables the foamability itself by reducing the aqueous surface tension. On the surface of water-based liquids, water molecules

and the molecule cluster (Figure 4.3 A) arrange in a way that attractive forces are oriented to the inside. Therefore, the molecules on the surface are excessively contracted. Surfactant molecules may accumulate on the liquid's surface and envelop the water molecules, reducing this tension significantly. Subsequently, air bubbles also might be entrapped in such agglomerated water-surfactant conjunctions, increasing essentially the systems foamability.

The second important effect of the surfactant is the stabilization of the silk protein molecules. Aqueous solutions of spider silk proteins are produced via dialysis. Dissolved in solution eADF4(C16) molecules are unfolded. Disturbing factors such as shear forces or the thermal energy by stirring friction enforce misfolding and aggregation. As reported by Gleuwitz, the surfactant also stabilizes the silk protein molecules in solution and prevents agglomeration.<sup>[236]</sup> The produced surfactant concentration herein displays a minimum value attuned to the utilized protein concentration. Below this value, precipitation of silk protein molecules is reported. Even though, a higher surfactant concentration is not aimed for, since a well-distributed silk protein concentration in the created foam is desired and an exceeding amount of surfactant molecules would block the silk. An exceeding employment of surfactant also increases the likelihood of producing silk protein free bubbles (Figure 4.3 B) and a subsequent inhomogeneous foam coating. The employed surfactant is a branched non-ionic iso-tridecyl-alcohol, displayed in Figure 4.2.<sup>[244]</sup> The hydrophilic negatively charged hydroxyl group likely interacts with the positively charged amino terminal group of eADF4(C16) silk protein, as well as, with the polar H-Groups of the water molecules. The hydrophobic carbohydrate chains of the surfactant molecule might either interact with the hydrophobic parts of the silk molecule chains, which are not protected, or stick to the outside, yielding a micelle-like structure.

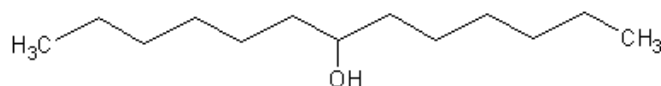


**Figure 4.2:** Ultravon Jun surfactant main ingredient, Iso-tridecyl-alcohol.

The ideal foam bubble (Figure 4.3 C) carries a membrane of surfactant enveloped silk protein - water conjugations on its surface. Ideally a wet silk protein film with surfactant is

deposited on the textile fiber surface when the bubble collapses. Consequently, by the applied vacuum the flexible wet film is still able to penetrate deeper into the yarn structure. After drying, the film hardens and acts as protective layer.

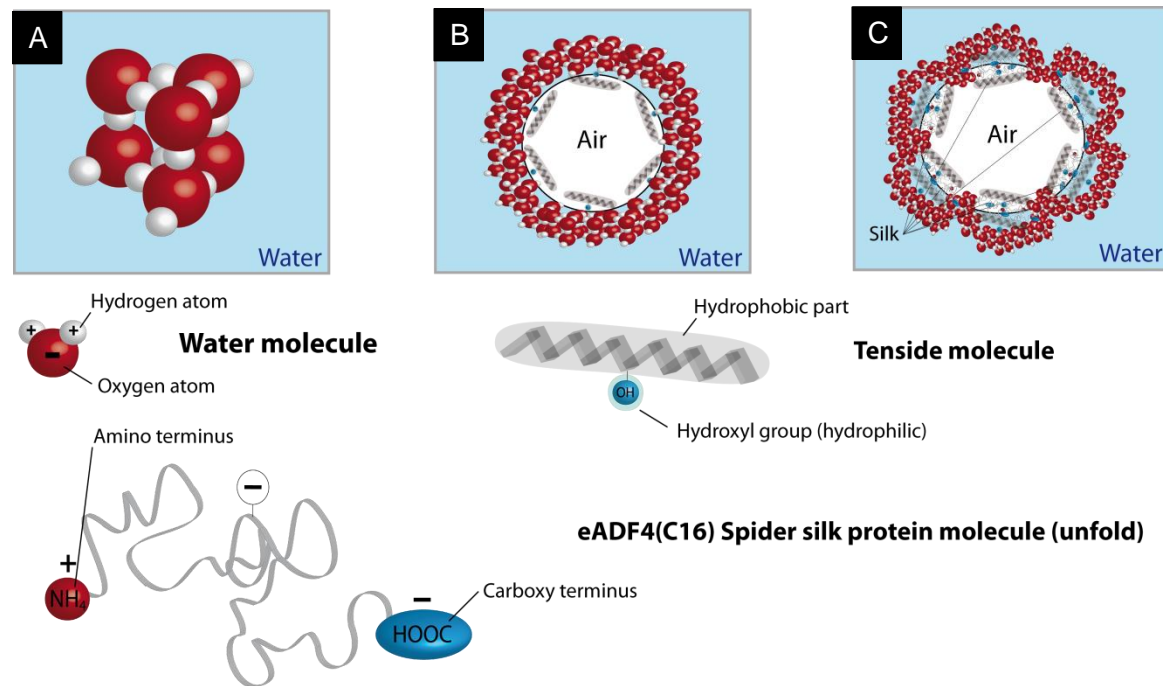


**Figure 4.3:** Schematic illustration of a water (6) molecule cluster (A), a foam bubble with water cluster-surfactant (iso-tridecyl-alcohol) conjugations (B), and an ideal bubble (C) carrying a membrane of surfactant enveloped silk protein - water conjugations on its surface.

#### 4.1.2 Adhesion behavior of spider silk proteins on different yarn fiber materials

Protective layers around any material strongly depend on the adhesion of the layer materials on the surface. Since the utilized template materials show no exposed surface charges, ionic interactions, as well as, cohesion effects can be discarded.

Since no other chemical linker or coupling agents are used, physical adhesion is the primary stabilizing effect of silk molecules on the fiber surface morphology. In this context, the surface roughness of the underlying yarn materials has the highest impact.

As optically analyzed, the natural fibers show inherent surface imperfections. The silk protein film on the natural (N) fabric was uniform, homogeneous and covered cavities, as well as, voids in the surface. The rayon fibers feature OH-groups, which support the adsorption of polar molecules in the presence of aqueous solutions. In this context the smoothening effect is higher than in case of poly(ethylene terephthalate). The latter inherits a negative surface charge, likely to develop electrostatic repulsion of the also negatively charged eADF4(C16) molecules. In contrast to that, the coating was good on polymeric textile P2. Most polymeric fibers are produced via melt spinning, yielding a very smooth surface. PAN fibers on the contrary, which are present in the polymeric fabrics at over 56 %, are produced via either dry-jet wet spinning or classic wet spinning. The latter is often preferred in industry because of the significantly higher production efficiency, but results in filaments with longitudinal grooves as reported by Wang et al.<sup>[245]</sup> Morris et al., reduced this effect by thorough adjustment of spinning parameters, such as the coagulation bath temperature.<sup>[246]</sup> Although these grooves are undesirable in some applications, the grooved surface morphology of the employed PAN fibers significantly facilitated the foam coating in this work. The smooth surface of PET enforced faster delamination subsequent to initial fractures and abrasion due to friction.

#### **4.1.3 Stabilizing and protective effects of spider silk protein foam coatings**

The vulnerability to abrasive friction and the resulting yarn fraying, as well as, pilling behavior of furniture textiles was determined to be significantly reduced on three different fabrics by a newly established spider silk protein foam coating method. Pilling of fabrics is based on single yarns torn out of their matrix. This can either happen due to ripping or when individual fibers slip over each other, as described by Hearl.<sup>[247]</sup> Since the standard testing counterpart material reassembles everyday cotton cloth with a structured fiber surface and textile woven roughness, the basic friction level is already increased. The protective coating had two effects on the textiles. First, the protein foam coating led to fibrous bridges between the yarn filaments. That reduced the ripping out of those filaments and prevented the consequent pilling. These contact points were found on all three fabrics. The second protective effect was the presence of homogeneous films, which covered the fibers and filled the gaps between them, to protect entire yarns.

Voids and imperfections were filled and smoothed on the fiber surface. Subsequently, the friction was reduced between test fabric and coated textile. Both effects decelerated the destruction for all fabrics considerably. A second coating cycle raised the absorbed amount of silk, and therefore, the film thickness on all samples. Yet, no significant additional improvement of the textiles abrasion resistance could be found.

Mainly, the fiber surface roughness and the adhesion of the film on the fiber surface, as well as, the fabric texturization influenced the protective effect. Structured fiber materials show more friction, and the silk coating has a stronger impact thereon. The better the adhesion between film and fiber, the more of the protective coating is ablated before delamination occurs. Therefore, the initial ripping out of single fibers from the surrounding matrix is reduced. The partially natural textile fabric showed a low tendency to pill throughout all revolutions in the uncoated state. The linen fabric consists to 53 % of smooth rayon and PET fibers. Therefore, pilling is reduced by a severe reduction of friction. The ring yarn weaving technology additionally stabilizes the yarn integrity and offers higher resistance to mechanical stress.<sup>[247]</sup>

Both polymeric fabrics featured rather smoothly PAN and PET fibers. Yet, Polymeric fabric P1 showed a high initial texturization. Additionally, it is produced by combed yarn weaving and a simple wet-stretching posttreatment. Altogether, these characteristics lead to an increased pilling abrasion without coating. These processing steps ensure a higher amount of exposed textile fibers on the fabric surface in order to feature a soft and warm touch.<sup>[248,249]</sup> The tendency to pill therefore is increased as well. The amount of pills was undesirably high. Upon silk coating, the pilling was remarkably reduced, in case of fabric P1 at long-term strain (5000 rounds) up to about 200 %. Specifically, the fibrous contact points stabilized the total fabric integrity, prevented single fibers from ripping out of their matrix, and therefore delayed the abrasion induced pilling. Additionally, the film-like coating temporarily reduced the attacking surface of the testing standard cloth and consequently the emerging friction. Evidently, the initial destruction of the fabric P1 was caused by pilling of PET fibers. A similar behavior was found in the case of the second polymeric fabric P2. This fabric was produced using a ring yarn weaving and a final steam pressing treatment, yielding a compact fabric morphology and reduced surface texturization. Thus, this fabric is more compact and stable by default. Even without a protective coating, the initial destruction requires higher strain, and therefore, this fabric shows less destruction throughout all numbers of revolutions, compared to fabric P1.

Though, the abrasion resistance increased in equal measure regarding short-, intermediate- and especially on long-term resistance, supporting the made assumptions as a result of the silk protein foam coating. It is highly probable that the protective effects are even increasable by improvement of the adhesion of silk coating on PET fibers, since these PET fibers are present in all three tested fabric types in substantial amounts. This can either be achieved by texturizing the fiber surface during production or chemically modifying the PET and silk molecules with linking groups. The employment of a PET-subversion with positive or neutral surface net charge could also significantly increase the coating efficiency, and its impact upon abrasion induced yarn fraying and fiber pilling. Transfer of foam production and textile coatings from laboratory to industrial-scale.

The successful development of a protective spider silk protein foam coating, consisting of a foaming solution, as well as, the foaming parameters and the application immediately suggests the transfer to industrial scales. Since wet processing methods are standardized in furniture textile production, the same is true for conveyer belts, means of stretching and treatment, as well as, drying chambers and collection methods. Mainly foam production and application have to be adapted to large-scale processes.

Foaming devices for the production of increased volumes of foam are barely commercially available. Only a few devices were patented as generic foaming devices.<sup>[250]</sup> Customized approaches are prominent because of the manifold foam ingredients and their required production parameters, as well as, the application forms in combination with the comparably rare employment of such devices. The diverse foaming methods (stirring, gas purging, whipping, shaking, etc.) require a concrete adaption of the foam-producing device to the distinct process.<sup>[242]</sup> In this context, industrial applications with mechanical foam creation appear potentially achievable upon stirring basis, higher possible numbers of revolution and therefore higher amounts of foamed medium. The found optimum of agitation versus fumigation should be satisfied to yield maximum foam percentages. Yet, it is highly advisable to intensely investigate the foaming behavior and durability of spider silk protein foaming solutions, in the presence of higher numbers of propelling revolutions, and therefore, stirring than the maximal applicable numbers of the laboratory set-up in this work.

The foam application was performed using a rotating vacuum drum. Such applications are technically used for the cleaning of slurry (rotary vacuum drum filter) or the transpor-



tation of fragile elements.<sup>[185,251]</sup> Since the pores in the mantle of such hollow vacuum drums are smaller than the minimum diameter of the bulk material, they are perfectly suited for the coating of textiles. The implementation into a textile process line requires not much effort, since the single elements only comprise of a doctor blade with a collecting tank with the length of the vacuum drum, the drum itself, which should be supported by two axially mounted bearings and connected to a vacuum generating device, and a supportive structure. The textile is transported by conveyer rolls and led over the drum with the inner side on the drum surface, describing a parabolic form in cross section. At the lowest point of this parabola a doctor blade is situated in a close distance to the textile and loaded with foam towards the textile transport direction. The foam is cut in a desired height, applied to the textile surface and disrupted by the applied vacuum. Thereby, the foam is absorbed by the textile volume. Excessing fluid is carried further into the drum and led into the foaming device to be recycled. Yet, the positive aspects of fluid recycling and re-foaming are not indefinitely applicable as reported by Glewitz.<sup>[236]</sup> The induced shear stress upon foaming and vacuum application combined with pumping processes lead to aggregation on one hand, and to the destruction and fragmentation of spider silk proteins in the foam solution on the other hand, after more than two cycles. Those effects may either lead to silk aggregate participation and a subsequent face separation, rendering the foaming solution useless, or to severely reduced textile pilling resistance upon foam coatings with eADF4(C16).

## **4.2 Fiber production based on spider silk proteins**

The silk protein-based production of submicron fibers was implemented by electrospinning. Dust particle air filters were produced and fiber diameters, as well as, varying amounts of coating material, and submicron fiber mesh layer thicknesses were tested (Chapter 3.2.2.3). The batch production of submicron filter layers using conventional electrospinning hampers the processing time severely. Additionally, the secondary structure of silk protein fiber meshes requires posttreatment to increase the crystalline secondary structure content and to prevent the fiber dissolution by moisture.<sup>[99,252,253]</sup> Centrifuge electrospinning led to an increased spinning efficiency by multiplication of spinning jets, and therefore, severely decreased the overall time consumption. Due to a fixed and static template positioning system, the spinning procedure was still in batch mode. The secondary structure of centrifuge electrospun silk fibers showed a significantly increased content of crystalline structures (Chapter 3.3.2, Figure 3.24 and Figure 3.25).

In a final step, the best performing submicron fiber mesh was placed in a complete filter set-up and tested concerning its performance. The particle deposition in combination with the air permeability resulted in a filtration quality factor, outperforming a standard dust bag (Chapter 3.2.2.3).

### **4.2.1 Differences in the dope materials and their rheological effects and concentration ranges**

Electrospinning has been investigated for decades, and even though the underlying parameters are strongly dependent on many factors, they are well established for each system and application. The more complex the production setup, the more parameters may influence the spinning process. In consequence, they have to be understood and neutralized or muted. Many parameters influence electrospinning and have to be adjusted thoroughly. The molecular weight of the polymer, the solvent, the dope concentration and dynamic dope viscosity, the relative humidity, the temperature and the voltage difference are the most crucial parameters.

Especially the solvent should be chosen carefully, since it has an important impact on whipping effects of polymer jets during spinning, which lead to a chaotic fiber deposition resulting in anisotropic pores with inhomogeneous, but distinct diameters per layer and spinning set-up.

Whilst the relative humidity and the temperature may be kept constant, the dope is pre-defined and the viscosity and dope concentration have to be analyzed initially. The PEO with 400 kg/mol, exhibits a steep incline concerning the dynamic viscosity at increasing concentrations, when dissolved in water with a high surface tension and low vapor pressure. The long-chained molecules reach through several levels of the shear induced flowing liquid layers and have an exponential impact on the viscosity at higher concentrations. On the contrary, PLA is dissolved in highly volatile trichloromethan and becomes more inviscid. Additionally, the shorter molecules bridge fewer numbers of liquid layers and have smaller impact on the viscosity with increasing concentration. The resulting fiber diameters from both materials showed a similar progression tendency. Packed in a tightest possible way, the diameters of both fiber types are similar.

Silk fibers have distinct primary and secondary structures. Silk proteins eADF4(C16) and ChryC1 have been dissolved in highly volatile HFIP, with lower vapor pressure than TCM. During the spinning process, as the fibers are formed, shear forces partially induce  $\beta$ -sheets. As the fibers are stretched, those regions provide mechanical resistance, and the breaking energy of silk fibers is increased. In case a higher spinning distance is applied, an increased flight time, fiber stretching and therefore smaller fiber diameters could be achieved compared to the employment of polymer spinning dopes.

### 4.2.2 The field strength as guiding spinning parameter for upscaling purposes

The most important dynamic parameters for electrospinning were found to be the potential difference  $\Delta U$  [kV] and the collector distance (spinning height)  $d_x$  [mm]. The correlation of both could be displayed as the quotient  $\Delta U/d_x$ , which results in a static form of the field strength  $\vec{E}$  [kV/mm]. The values were determined for electrospinning as displayed in Table 4.1.

**Table 4.1:** Electrostatic field strength of all tested dope materials at best spinning results for classical and centrifuge electrospinning and their factor after transfer.

|   | Electrostatic field strength, $\vec{E}$ [kV/mm] |      |            |        |
|---|---|------|------------|--------|
|   | PEO   | PLA  | eADF4(C16) | ChryC1 |
| <b>Electrospinning (ES)</b>             | 0.08  | 0.10 | 0.12       | 0.13   |
| <b>Centrifuge Electrospinning (CES)</b> | 0.16  | 0.36 | 0.20       | -      |
| <b>Factor (ES/CES)</b>                  | 2.00  | 3.60 | 1.67       | -      |

The electrostatic field strengths applied to achieve optimal fiber quality are in a close range, suggesting a similar spinning behavior due to the same solvent and similar dynamic viscosities, as well as, molecular weights. The polymeric dopes show reduced values for their electrostatic field strengths. The aqueous dope solution of PEO requires an enhanced flight time, and therefore, increased spinning distance to let the fibers harden and evaporate the water. Higher values for the voltage do not support spinning since the increased attractive forces disrupt the fiber jets from the cone before their sufficient hardening. As a result, the necessary field strength is also low. For PLA, the collector distance and flight time were reduced but still higher than for PEO, but also the potential difference had to be reduced. Higher voltages would result in a drying of the Taylor cone and subsequent clogging of the cannula, cancelling the spinning process.

Direct transfer of the spinning process and parameters to centrifuge electrospinning was not possible, since the rotational speed of the centrifuge had an additional influence. Three-dimensional screenings revealed the working ranges for each dope. The direct adjustment of the collector distances yielded inadequate fiber qualities, recalculated from the found electrostatic field strengths. Subsequent height-screenings revealed clear tendencies concerning the increase factor. For silk protein in HFIP and aqueous PEO dope solution the factor was about 2. The centrifugal force on the emerging fiber jets, as well as, the guiding air, both evoke lateral forces. They subsequently require increased attractive forces in the collector's direction. Thereupon, if the acceleration of the fibers towards the collector is too low, the rotational movement of the center bell twists the emerging jets to yarn-like structures and no nonwoven mesh is deposited. Especially for aqueous PEO dope solution the additional shear forces and energy intake have beneficial effects on the spinning result, leading to less beading and more uniform fibers. In the case of PLA, dissolved in TCM, the necessary field strength for optimal results in centrifuge electrospinning was even higher. The highly volatile solvent is affected by the rotational movement and the shielding air stream. The emerging jets need to be exceedingly accelerated before drying out at the center bell. Lowest possible collector distances with increased potential differences result in a field strength transfer factor of 3. Additionally, the doubled and tripled field strengths had a positive impact on the fiber diameter since, increased attractive forces accelerate the fiber stretching and smaller diameters might be obtained.

### 4.2.3 Effects of silk protein nanofiber nonwovens on particle deposition

The most important factors regarding submicron fiber meshes are their diameter for filtration purposes and particle deposition, the gaps between them and the gap consistency, as well as, surface morphology. Wendorff et al. named 3 main molecular processes, presented by Hinds, contributing to filtering effects: Interception, impaction and particle diffusion as displayed in Figure 4.4.<sup>[232,254]</sup> An airstream, led through a filtration fiber mesh, follows a path around the single fibers. Each of these stream lines (blue arrow in Figure 4.4 A-D) carries dust particles of different sizes and charges.

Particles, following the streamlines around the submicron fibers might be caught on the surface when passing in a distance below the particle diameter (Interception, Figure 4.4 A). For very high air flow velocities, impaction might occur if particles are tossed out of the streamlines and caught on the fiber surface (Figure 4.4 B). This effect is irrelevant for particles below 200 nm. As a third effect, diffusive motion is performed by small particles, leaving their stream lines and traveling chaotically until deposition (Figure 4.4 C). Nonwoven meshes made from eADF4(C16) feature negative charges.<sup>[255]</sup> During filtration electrostatic forces occur, enhancing the deposition of positively charged particles (Figure 4.4 D). Furthermore, silk proteins might be chemically modified to feature desired properties. This was done in the case of positively charged eADF4( $\kappa$ 16), which might be employed to deposit negatively charged dust particles.<sup>[256]</sup> Co-spinning of both materials could severely amplify the overall particle deposition capability.

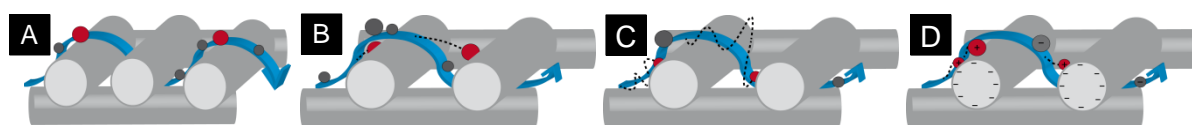


**Figure 4.4:** Schematic illustration of possible molecular particle deposition effects in air filtration processes: interception (A), impaction (B), diffusion (C), extended by electrostatic interaction (D), with the illustrated air stream (blue arrow) carrying dust particles (gray), that are caught on the fiber surface (red), modified from stated sources<sup>[232]</sup> and<sup>[254]</sup>.

In this work, particle deposition measurements were carried out with a dust-stream face-velocity of 25 cm/s and particle diameters ranging from 0.2 - 8.9  $\mu\text{m}$  (Figure 4.5, gray field). For these parameter combinations the main molecular filtration effects, besides the named electrostatic interaction, are interception and particle diffusion for dust particles between 200 nm and 2  $\mu\text{m}$ . Particles larger than 1  $\mu\text{m}$  are mainly filtered by interception on the fiber surface. Above the particle size of 2  $\mu\text{m}$ , gravity also plays a role in particle deposition.

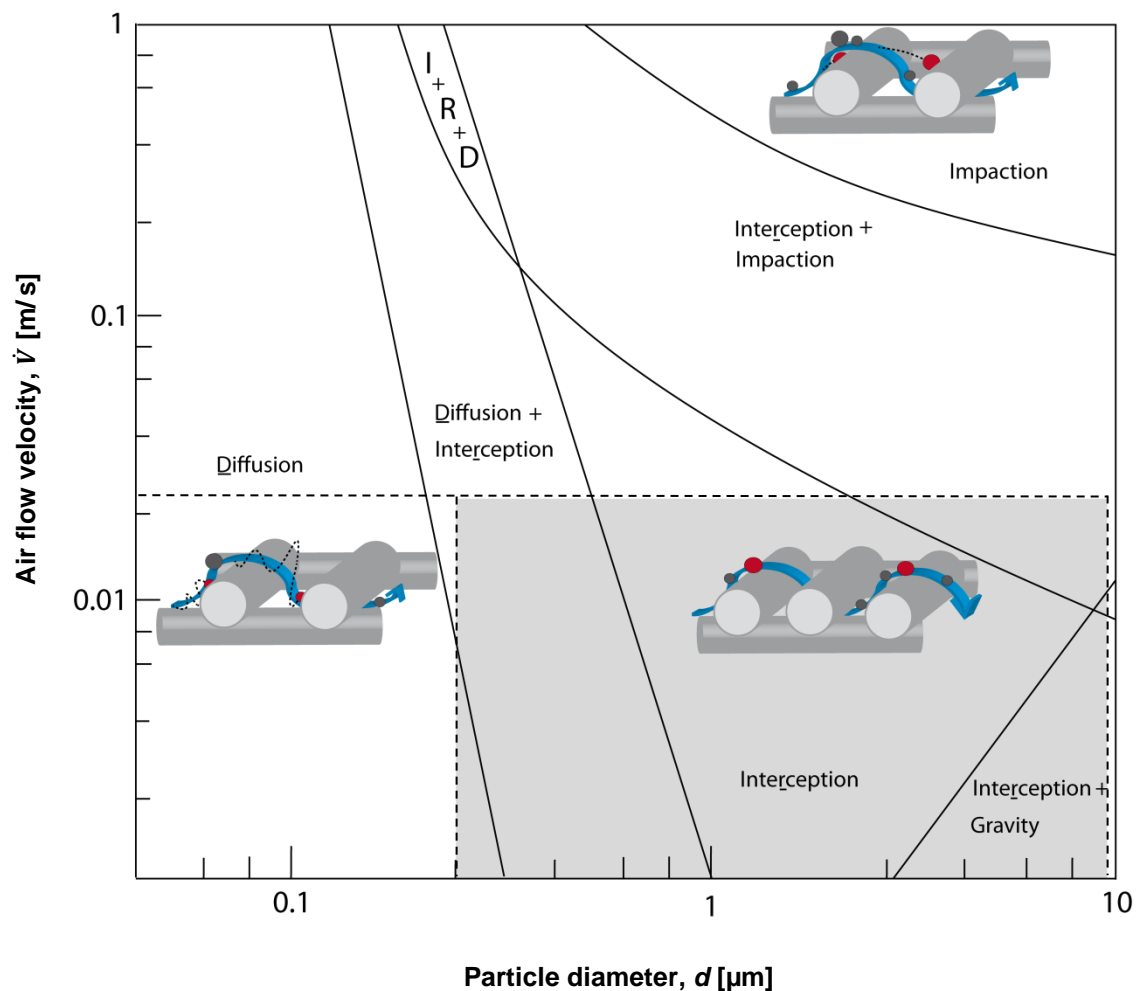


**Figure 4.5:** Schematic overview of molecular particle filtration effects in nonwoven meshes in dependence of airflow velocity,  $\dot{V}$  and particle diameter,  $d$  featuring diffusive motions, interception, impaction and gravity effects, modified from sources <sup>[232]</sup> and <sup>[254]</sup>.

Small diameter fiber-meshes feature an increased specific surface area. In theory, this feature should enhance the deposition capacity of thin fibers, since particles have a higher tendency to experience interception.

Yet, smaller fibers also feature a decreased volume and tend to congregate to larger fiber bundles. Provided, that the same surface area is covered with the equal amount of material, vacancies occur in between those bundles. The deposited inhomogeneous fiber meshes hence exhibit larger gaps in between fiber bundles, unlike the more homogeneous meshes from fibers with larger diameters without gaps. Those voids allow small particles to pass through more easily due to an increased pressure drop in these areas. This theory could be confirmed with the performance of silk-based filters featuring small-diameter fibers.<sup>[11]</sup> Yet, the employment of dense nonwoven meshes also enhances the formation of a filter cake which blocks the air stream yielding higher pressure drop rates thus confirming inefficiency concerning energy consumption. The diffusive filtration of nonwoven mesh coatings yielded the highest particle deposition rates in addition to the interception capabilities of submicron fibers with intermediate-sized diameters ( $200 \text{ nm} < x < 250 \text{ nm}$ ) and a moderate layer thickness ( $100 \text{ mg/m}^2$ ). To set up a complete dust bag, standard filtration materials were combined with nonwoven fiber meshes on PA support.

Nonwoven mats of silk proteins as-spun exhibit predominantly  $\alpha$ -helical and random coil secondary structure rendering the submicron fibers sensitive to moisture. These structures are dissolved even by air humidity. The posttreatment of the fiber mats with ethanol, followed by water vapor, induces and maximizes the  $\beta$ -sheet secondary structure content. The well-established initiation of crystalline structures stabilizes the fibers, enhancing their mechanical stability and preventing their environmental condition-induced destruction, as reported in previous studies.<sup>[202,228]</sup> A special side effect of the necessary posttreatment and also a beneficial feature of silk protein submicron fibers is a partial resolving of the protein fibers at their surface. Subsequently, the procedure is causing a re-solidification, which strengthens the fiber-networks by physical crosslinks. Additionally, this effect enhances filtration capabilities since fiber slipping is minimized and pores remain constant in size.<sup>[11,202]</sup>



### 4.3 Upscaling potential of nonwoven coatings by centrifugal electrospinning

The biggest drawback of electrospinning is the low output of standard devices in the production of high performance silk protein submicron fiber nonwoven dust particle filter mats. Even modern multi-jet approaches only offer limited acceleration of the process. By contrast, the centrifuge spinning device employed in this work features a torus build-up with a multitude of possible jets, with a clear advantage regarding jet count per area. Therefore, the spinning efficiency is higher and the dope throughput is highly increased. In applications, the spinning efficiency could be increased by a factor of 600.

To stabilize the produced spider silk nonwoven fiber mats, posttreatment is crucial.<sup>[257-262]</sup> Centrifuge electrospinning showed increased  $\beta$ -sheet structure content as spun. In CES, the emerging lateral forces, as well as, the counter-measures induce additional shear stress on the fibers. As a consequence, those submicron fibers are poststretched. It was found in previous studies that shear forces lead to the formation of crystalline  $\beta$ -sheet structures in natural spinning process.<sup>[263,264]</sup> Other studies reported the induction of such structures on spider silk protein fibers upon post stretching.<sup>[252,261]</sup> It is likely that the additional shear stress during centrifuge electrospinning acts as in-flight poststretching to induce crystalline structures. Yet, the content of about 20% is insufficient to render the fiber mats water stable. Therefore, a shielded inline post-treatment chamber, located ahead of a collection system is recommended to further accelerate continuous spider silk nonwoven spinning process and therefore enable an upscaling.

---

## 5 Summary

Sustainable and environmentally friendly alternatives to crude oil based materials are nowadays extensively investigated. Biopolymers, such as spider silk, have been employed by humans as an alternative ever since, and are additionally known for their good mechanical stability. The greatest drawback of spider silk is the lack of availability. During the last decades the reverse decoding of protein structures into designed gene sequences enabled the development of recombinant production of silk proteins such as *Araneus diadematus* dragline silk protein (eADF4(C16)) or *Chrysoperla carnea* egg stalk protein (ChryC1).

The focus of this work was the development of two processing methods for spider silk proteins and the evaluation of their upscaling potential. The first application was an environmentally friendly and water-based protective spider silk protein foam coating for furniture textiles to reduce abrasive textile destruction derived from pilling. Parameters were investigated to achieve stable and uniform aqueous foams, and spider silk foaming dopes were analyzed. Subsequently, a novel foam coating was developed. Three different fabrics were foam-coated with recombinant spider silk protein (eADF4(C16)) and analyzed regarding their vulnerability to friction and resulting yarn fraying, as well as pilling. One fabric mainly contained the natural materials cotton and rayon. The two other polymeric fabrics comprised PES and PA. Primarily homogeneous and stable coatings were applied to single yarns, which were then analyzed regarding yarn fraying. Subsequently, complex fabrics were coated and they revealed an increase in durability and a decrease in pilling tendency upon abrasive friction analyzes.<sup>[247]</sup> A film-like fiber surface coating and smoothing in combination with fibrous contact points reduced the friction and ripping out of single filaments, preventing the consequent pilling and prolonging the lifetime of the furniture fabric. In the presence of the silk coating a clear correlation between lowered yarn fraying and pilling tendency was determined. For all three tested fabrics these effects were significantly reduced, and upon silk foam coating the fabric quality was doubled in short as well as long-term abrasion tests.

The second part of this work aimed at the production of electro-spun submicron nonwoven fiber mats. Four different submicron fiber mats were tested and compared regarding their applicability as fine dust particle filter meshes, including the synthetic polymers PEO and PLA and two biopolymers, namely recombinant silk protein ChryC1 and eADF4(C16). In a first approach, nonwoven fiber meshes with different fiber diameters were successfully electro-spun on a commercially available PA support-woven. A clear dependency could be determined regarding the filtration efficiency fiber diameter and coating thickness.

Centrifuge electrospinning was employed for the production of submicron nonwoven fiber meshes on PA mesh material to test the potential for large-scale production. The most critical step was the proper adjustment of the electrospinning process's spinning conditions to the novel method, as well as, the adjustment of its spinning parameters. Process-related spinning parameters introduce additional shear forces into the fibers. Those yielded fiber diameters below 100 nm and an increased content of crystalline  $\beta$ -sheet structures as spun. The inherent random coil secondary structure content rendered centrifuge spun spider silk nonwoven fibers water soluble. Hence, additional post-treatment was required. Electro-spun spider silk meshes were the best material tested concerning particle deposition, air permeability and pressure drop. Additionally, the negative surface net charge of eADF4(C16) submicron fibers contributed to the better performance of spider silk nonwoven meshes. A new silk-containing filter set-up was developed as a prototype providing a significantly higher filtration quality factor than a conventional filter bag. As calculated in previous studies, the use of such spider silk-containing dust bags could save 9 kg of CO<sub>2</sub>-equivalents per domestic home and per year in an industrial country such as Germany.<sup>[265]</sup> The results of both approaches highlight the promising upscaling potential of spider silk applications.

## 6 Zusammenfassung

In der Forschung werden derzeit nachhaltige und umweltfreundliche Ersatzstoffe zu Rohöl-basierten Materialien untersucht. Biopolymere werden von der Menschheit seit jeher als Alternative verwendet, von denen insbesondere (Spinnen-) Seiden für ihre hervorragenden mechanischen Eigenschaften bekannt sind. Der größte Nachteil von Spinnenseide ist allerdings ihre geringe Verfügbarkeit. Während der vergangenen Jahrzehnte ermöglichte die reverse Translation von Proteinsequenzen in designte Gensequenzen die Entwicklung der rekombinanten Produktion von Seidenproteinen, wie das *Araneus diadematus* Abseilfadenprotein (eADF4(C16)) oder das *Chrysoperla carnea* Eierstielprotein (ChryC1).

Der Fokus dieser Arbeit lag auf der Entwicklung zweier neuartiger Prozessierungsmethoden für Spinnenseidenproteine. Die erste Anwendung bestand aus einer umweltfreundlichen und wasserbasierten Schutzbeschichtung aus Spinnenseidenprotein-Schaum für Möbelbezugsstoffe zur Reduktion von abrasiver Textilerstörung durch Pilling bzw. Knötchenbildung. Die Parameter zur Herstellung stabiler und gleichmäßiger Schäume wurden untersucht. Weiterhin wurden die zur Schaumherstellung benötigten Spinnenseidenlösungen analysiert. In der Folge wurde eine neuartige Schaumbeschichtungsmethode entwickelt. Drei verschiedene Textilien wurden mit rekombinantem Spinnenseidenprotein (eADF4(C16)) beschichtet und bezüglich ihrer Anfälligkeit auf Reibung und dem resultierenden Ausfransen von Einzelfasern analysiert. Darunter befand sich ein Textil, welches hauptsächlich aus den Materialien Baumwolle und Viskose aufgebaut ist, sowie zwei PES und PA enthaltende Polymer-basierte Stoffe. Zunächst wurden einzelne Garnfasern mit homogenen und stabilen Beschichtungen versehen, welche anschließend auf die Anfälligkeit bezüglich des Ausfransens hin untersucht wurden. Nachfolgend wurden komplexe Textilien beschichtet, wodurch ein Anstieg in der Haltbarkeit und eine Reduktion der Pilling-Anfälligkeit gegenüber abrasiver Reibung erreicht werden konnte.

Eine filmartige Beschichtung und Glättung der Textilfaseroberflächen verringerte die Reibung und das Herausreißen von Einzelfasern, wodurch das daraus resultierende Pilling verhindert und die Lebensdauer des Möbelbezugsstoffs verlängert werden konnte. In Kombination mit der Seidenbeschichtung konnte eine klare Abhängigkeit zwischen der verringerten Ausfransung der Textilgarne und der Pilling-Anfälligkeit der Textilien festgestellt werden. Diese negativen Effekte wurden im Fall aller drei untersuchten Textilien stark reduziert. Aufgrund der Seiden-Schaumbeschichtung konnte letztlich die Textilqualität bei Kurz- und Langzeitbelastung verdoppelt werden.

Die zweite Anwendung, welche in dieser Arbeit untersucht wurde, zielte auf die Produktion von elektrogesponnenen Fasermatten für die Feinstaubfiltration ab. Dafür wurden vier verschiedene sub-mikro Fasermatten untersucht und bezüglich deren Effizienz im Einsatz als Feinstaubfilterauflagen verglichen. Sie basierten auf den synthetischen Polymeren PEO und PLA, sowie den beiden Seidenproteinen ChryC1 und eADF4(C16). Zunächst wurden Fasermatten mit unterschiedlichen Faserdurchmessern erfolgreich auf kommerziell erhältliches PA-Gewebe, welches als Stabilisationsunterlage und Träger verwendet wurde, elektro-gesponnen. Es konnte eine klare Abhängigkeit der Filtrationseffizienz von den eingesetzten Materialien, der Beschichtungsdicke, sowie den Faserdurchmessern festgestellt werden. Florfliegen- und Spinnenseidenfasermatten übertrafen die Leistungsfähigkeit derer, welche aus polymeren Materialien hergestellt wurden. Die Seidenfasermatten wurden mit Wasser- und Ethanol Dampf nachbehandelt, um kristalline  $\beta$ -Faltblatt Strukturen zu induzieren und die Wasserlöslichkeit der Fasermatten zu reduzieren. Weiterhin verstärkte die Nachbehandlung die mechanische Stabilität und die Partikelabscheidung der Filtermatten.

Ein Zentrifugen-Elektrospinnverfahren mit dem Potenzial zur Hochskalierung wurde zur Produktion von sub-mikro Fasermatten auf PA-Gewebe verwendet. Der entscheidendste Schritt war hierbei die entsprechende Anpassung und Übertragung der Spinnparameter- und Bedingungen vom Elektrospinnprozess auf die neue Methode. Prozessparameter tragen während des Spinnvorgangs zusätzliche Scherkräfte in die Fasern ein, wodurch Zentrifugen-elektro-gesponnene Fasern mit Durchmessern unter 100 nm und einem gesteigerten Anteil an  $\beta$ -Faltblattstrukturen entstanden.

Aufgrund der hervorragenden Partikelabscheidung, der Luftdurchlässigkeit und des geringen Druckabfalls waren elektrogewebene Spinnenseidenfasermatten am besten für die Verwendung als Filtermaterialien geeignet. Zusätzlich trug die negative Oberflächenladung der eADF4(C16) sub-mikro Fasern zur gesteigerten Filterleistung der Spinnenseidenfasermatten bei. Es wurde ein neuartiger Filterbeutelprototyp, mit einer Feinstaubfilterlage aus Spinnenseide hergestellt, welcher einen signifikant höheren Filterqualitätsfaktor aufwies als ein konventioneller Filterbeutel. Wie bereits in früheren Studien berechnet wurde, könnte die Verwendung solcher Seiden-beinhaltenen Staubbeutel in Industrieländern wie Deutschland 9 kg von CO<sub>2</sub> Äquivalenten pro Haushalt und Jahr einsparen.<sup>[265]</sup>

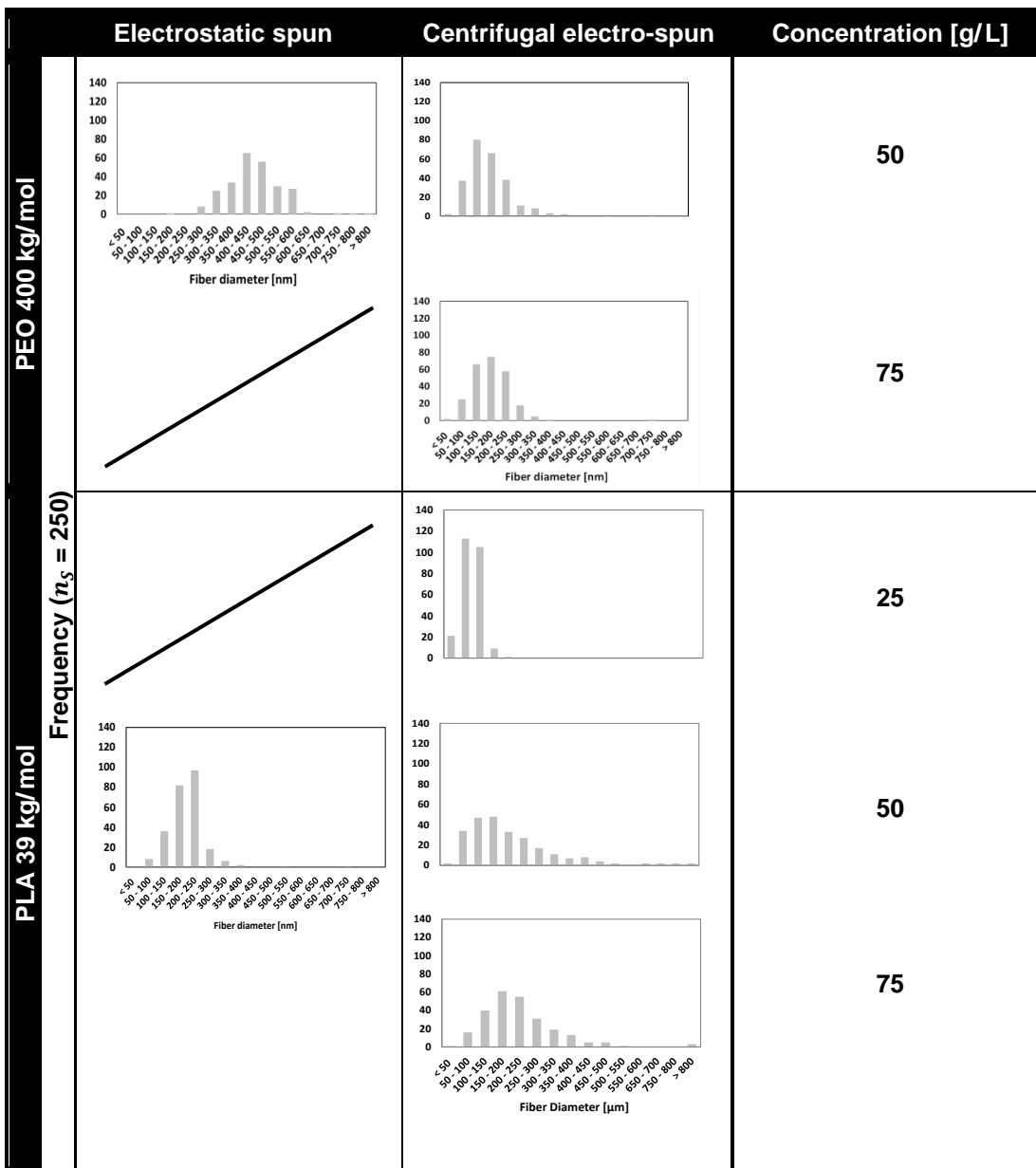


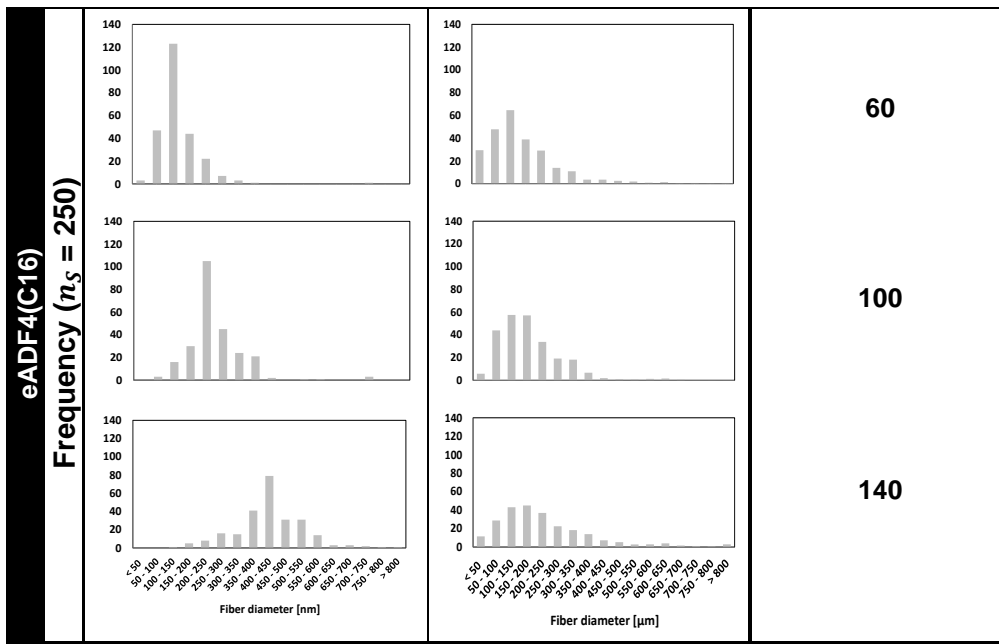


7 Appendix

Supportive Information

Fiber diameter histogram analysis





---

## References

- [1] **Namazi, H.:** Polymers in our daily life. *Bioimpacts* 7(2), 73-74 (2017).
- [2] **Feldman, D., and Barbalata, A.:** Synthetic Polymers: Technology, Properties, Applications. *Springer Netherlands: Rotterdam* (1996).
- [3] **Kamigaito, M.:** Precision Polymerization of Plant-Derived Vinyl Monomers for Novel Bio-Based Polymers. *Presentation*, Nagoya University (2018).
- [4] **Kalnins, M. M., Conde Braña, M. T., and Gedde, U. W.:** Treatment of polyethylene and polypropylene with chlorosulphonic acid to study the surface morphology. *Polymer Testing* 11(2), 139-150 (1992).
- [5] **Kostov, K. G., et al.:** Study of polypropylene surface modification by air dielectric barrier discharge operated at two different frequencies. *Surface and Coatings Technology* 234(1), 60-66 (2013).
- [6] **Kaneko, H., Minegishi, T., and Domen, K.:** Recent Progress in the Surface Modification of Photoelectrodes toward Efficient and Stable Overall Water Splitting. *Chemistry – A European Journal* 24(22), 5697-5706 (2018).
- [7] **Klumpp, A., Hoffmeister, J., and Schulze, V.:** Mechanical Surface Treatments. *ICSP-12*. Institute of Applied Materials (IAM -WK), Karlsruhe Institute of Technology, Germany:Goslar (2014).
- [8] **Schulze, V.:** Modern Mechanical Surface Treatment: States, Stability, Effects. *John Wiley & Sons Ltd.: Hoboken* (2006).
- [9] **Koleske, J. V.:** Mechanical Properties of Solid Coatings in *Encyclopedia of Analytical Chemistry*. John Wiley & Sons Ltd.: Charleston (2006).
- [10] **Parmaj, O. S., and Teli, M. D.:** Textile Coating. *Presentation*, Institute of chemical technology: Mumbai (2016).
- [11] **Jokisch, S., Neuenfeldt, M., and Scheibel, T.:** Silk-Based Fine Dust Filters for Air Filtration. *Advanced Sustainable Systems* 1(10), 1700079 (2017).
- [12] **Sen, A. K.:** Coated textiles : principles and applications. *CRC Press: Boca Raton* (2008).
- [13] **Capponi, M., et al.:** Foam Technology in Textile Processing. *Review of Progress in Coloration and Related Topics* 12(1), 48-57 (1982).
- [14] **Prud'homme, R. K., and Khan, S. A.:** Foams : theory, measurements, and applications. *Marcel Dekker. New York* (1996).
- [15] **Glowania, M., et al.:** Foulard with internal squeeze rollers for coating of coarse mashed textiles with high-viscosity coating compounds. *Melliand international textile reports* 89(10), E115 (2008).
- [16] **Kalliala, E., and Talvenmaa, P.:** Environmental profile of textile wet processing in Finland. *Journal of Cleaner Production* 8(2), 143-154 (2000).

- [17] **Sen, A. K.:** Coated Textiles: Principles and Applications, Second Edition. *CRC Press London: Boca Raton* (2008).
- [18] **Swedish Chemicals Agency:** Occurrence and use of highly fluorinated substances and alternatives. *Report from a government assignment: 112* (2015).
- [19] **Blum, A.:** Flame retardance & six classes of harmful chemicals - How science can impact policy & purchasing. *Presentation, University of California, Berkeley - Green science policy institute* (2018).
- [20] **Bergemann, E. P., Opre, J. E., and Henneberry, M.:** Environmentally friendly solvent. *US6096699A, US application*, (1999).
- [21] **Rosi Reddy, K., et al.:** New environmentally friendly solvent free synthesis of dihydropyrimidinones catalysed by N-butyl-N,N-dimethyl- $\alpha$ -phenylethylammonium bromide. *Tetrahedron Letters* 44(44), 8173-8175 (2003).
- [22] **Gopalakrishnan, M., et al.:** New environmentally-friendly solvent-free synthesis of imines using calcium oxide under microwave irradiation. *Research on Chemical Intermediates* 33(6), 541-548 (2007).
- [23] **Song, J. H., et al.:** Biodegradable and compostable alternatives to conventional plastics. *Philosophical transactions of the Royal Society of London. Series B, Biological sciences* 364(1526), 2127-2139 (2009).
- [24] **Genaidy, A., et al.:** Health effects of exposure to carbon nanofibers: Systematic review, critical appraisal, meta analysis and research to practice perspectives. *Science of the Total Environment* 407(12), 3686-3701 (2009).
- [25] **Encyclopaedia Britannica, Inc.:** Filtration. <https://www.britannica.com/science/filtration-chemistry>, accessed: Nov 27 (2017).
- [26] High efficiency filters and filter media for removing particles from air — Part 1: Classification, performance, testing and marking. *ISO 29463-1 16* (2017).
- [27] **Peplow, M.:** The plastics revolution: how chemists are pushing polymers to new limits. *Nature* 536(7616), 266-8 (2016).
- [28] **Morlet, A., et al.:** The New Plastic Economy: Rethinking the future of plastics. *World Economic Forum, Ellen MacArthur Foundation, McKinsey & Co.* (2016).
- [29] **Elias, H.-G.:** An introduction to polymer science. *VCH Weinheim: Cambridge* (1997).
- [30] **Mark, J. E.:** Physical Properties of Polymers Handbook. *Springer: New York* (2007).
- [31] **Moldoveanu, S. C.:** Chapter 6 Polymers with saturated carbon chain backbone in *Techniques and Instrumentation in Analytical Chemistry*. Elsevier: (2005).
- [32] **McKetta, J. J.:** Encyclopedia of Chemical Processing and Design: Volume 30 - Methanol from Coal: Cost Projections to Motors: Electric. *Taylor & Francis: New York* (1989).
- [33] **Matabola, K., et al.:** Single polymer composites: A review. *Journal of Materials Science* 44(23), 6213-6222 (2009).

- [34] **Nicholson, L. M., et al.:** How Molecular Structure Affects Mechanical Properties of an Advanced Polymer. (1999).
- [35] **sunfire GmbH:** Erste Kommerzielle Blue Crude-Produktion Entsteht in Norwegen. <http://www.sunfire.de/de/unternehmen/presse/detail/erste-kommerzielle-blue-crude-produktion-entsteht-in-norwegen>, accessed: Mar 1 (2017).
- [36] **Buddrus, J.:** Grundlagen der Organischen Chemie. *de Gruyter. Berlin* (2011).
- [37] **Pötsch, W. P., Fischer, A., and Mueller, W.:** Lexikon bedeutender Chemiker. *Verlag Harri Deutsch: Frankfurt a.M.* (1988).
- [38] **Advameg, Inc.:** Polyesters. <http://www.chemistryexplained.com/PI-Pr/Polyesters.html>, accessed: Mar 1 (2018).
- [39] **Bornak, R.:** Different Methods of PET Production and Its Economy. *European Journal of Scientific Research* 107(1), 1-10 (2013).
- [40] **Kricheldorf, H.:** Polycondensation: History and New Results. *Springer. Berlin Heidelberg* (2013).
- [41] **Dammer, O.:** Lexikon der angewandten Chemie. *Verlag des Bibliographischen Instituts: Leipzig* (1882).
- [42] **Kendrion Kuhnke Automation GmbH:** Chemische Beständigkeit von Kunststoffen [https://kuhnke.kendrion.com/attachment/ICS/ics\\_pdf\\_brochure/ics\\_pdf\\_chemische-bestaendigkeit-2015\\_de.pdf](https://kuhnke.kendrion.com/attachment/ICS/ics_pdf_brochure/ics_pdf_chemische-bestaendigkeit-2015_de.pdf), accessed: Mar, 1 (2015).
- [43] **de Ilarduya, A. M., and Muñoz-Guerra, S.:** Chemical Structure and Microstructure of Poly(alkylene terephthalate)s, their Copolyesters, and their Blends as Studied by NMR. *Macromolecular Chemistry and Physics* 215(22), 2138-2160 (2014).
- [44] **Bunsell, A. R.:** Handbook of Properties of Textile and Technical Fibres. *Elsevier Science:* (2018).
- [45] **Encyclopaedia Britannica, Inc. :** Polyacrylonitrile. <https://www.britannica.com/science/polyacrylonitrile>, accessed: Mar 1 (2014).
- [46] **Wiley-VCH:** Ullmann's Polymers and Plastics *John Wiley & Sons: Hoboken* (2016).
- [47] **Bailey, F. E.:** Poly(ethylene oxide). *Academic Press: New York* (1976).
- [48] **Jang, H.-J., Shin, C. Y., and Kim, K.-B.:** Safety Evaluation of Polyethylene Glycol (PEG) Compounds for Cosmetic Use. *Toxicological Research* 31(2), 105-136 (2015).
- [49] **Solomon, M. M.:** Anti-foam emulsions. *US2829112A*, US application, Sep 22 (1955).
- [50] **Working, P. K., et al.:** Safety of Poly(ethylene glycol) and Poly(ethylene glycol) Derivatives in *Poly(ethylene glycol)*. American Chemical Society: (1997).
- [51] **Hacker, M. C., and Mikos, A. G.:** Principles of Regenerative Medicine (Second edition) - Synthetic Polymers. *Academic Press: San Diego* (2011).
- [52] **Schiller, L. R., et al.:** Osmotic effects of polyethylene glycol. *Gastroenterology* 94(4), 933-941 (1988).

- [53] **Walker, W. J. J., Reed, J. S., and Verma, S. K.:** Polyethylene Glycol Binders for Advanced Ceramics in *A Collection of Papers on Engineering Aspects of Fabrication of Ceramics: Ceramic Engineering and Science Proceedings*. Vol. 14, (2008).
- [54] **Kolattukudy, P. E.:** Polyesters in higher plants. *Adv Biochem Eng Biotechnol.* 71(1), 1-49 (2001).
- [55] **Aravamudhan, A., et al.:** Chapter 4 - Natural Polymers: Polysaccharides and Their Derivatives for Biomedical Applications in *Natural and Synthetic Biomedical Polymers*. Elsevier: Oxford (2014).
- [56] **Gupta, B. S.:** Biotextiles as Medical Implants: Manufacture, types and properties of biotextiles for medical applications. *Woodhead Publishing: Cambridge* (2013).
- [57] **Hearle, J. W. S.:** Textile Fibers: A Comparative Overview A2 - Buschow, K.H. Jürgen in *Encyclopedia of Materials: Science and Technology (Second Edition)*. Elsevier: Oxford (2001).
- [58] **Turbak, A. F.:** Solvent Spun Rayon, Modified Cellulose Fibers and Derivatives in *ACS Symposium Series*. Vol. 58, (1977).
- [59] **Lauder, R.:** Chondroitin sulphate: A complex molecule with potential impacts on a wide range of biological systems. *Complementary therapies in medicine* 17(1), 56-62 (2009).
- [60] **Du, J., and Eddington, N.:** Determination of the Chondroitin Sulfate Disaccharides in Dog and Horse Plasma by HPLC Using Chondroitinase Digestion, Precolumn Derivatization, and Fluorescence Detection. *Analytical Biochemistry* 306(2), 252-258 (2002).
- [61] **Volpi, N.:** Oral absorption and bioavailability of ichthyic origin chondroitin sulfate in healthy male volunteers. *Osteoarthritis and Cartilage* 11(6), 433-441 (2003).
- [62] **Mhurchu, C. N., et al.:** Effect of chitosan on weight loss in overweight and obese individuals: a systematic review of randomized controlled trials. *Obesity Reviews* 6(1), 35-42 (2005).
- [63] **Felt, O., Buri, P., and Gurny, R.:** Chitosan: A Unique Polysaccharide for Drug Delivery. *Drug Development and Industrial Pharmacy* 24(11), 979-993 (1998).
- [64] **Patel, M. P., Patel, R. R., and Patel, J. K.:** Chitosan Mediated Targeted Drug Delivery System: A Review. *Journal of pharmacy & pharmaceutical sciences* 13(4), 536-557 (2010).
- [65] **European Committee for Standardization:** Plastics - Recommendation for terminology and characterisation of biopolymers and bioplastics *Technical Committee CEN/TC 249: 12* (2010).
- [66] **Sin, L. T., Rahmat, A., and Rahman, W. A. W. A.:** Polylactic Acid: PLA Biopolymer Technology and Applications. *William Andrew: Norwich* (2012).
- [67] **Castro-Aguirre, E., et al.:** Poly(lactic acid)—Mass production, processing, industrial applications, and end of life. *Advanced Drug Delivery Reviews* 107(Supplement C), 333-366 (2016).
- [68] **Polymer Solutions:** Polymers and Cosmetics. <https://www.polymersolutions.com/blog/polymers-and-cosmetics/>, accessed: Oct 25 (2014).

- [69] **Aravamudhan, A., et al.:** Chapter 4 – Natural Polymers: Polysaccharides and Their Derivatives for Biomedical Applications in *Natural and Synthetic Biomedical Polymers*. Elsevier Inc.: Oxford (2014).
- [70] **Plackett, D., and Vázquez, A.:** 7 - Natural polymer sources in *Green Composites*. Woodhead Publishing: Cambridge (2004).
- [71] **Burg, K.:** Chapter 6 - Poly( $\alpha$ -ester)s in *Natural and Synthetic Biomedical Polymers*. Elsevier: Oxford (2014).
- [72] **Riley, A.:** 12 - Basics of polymer chemistry for packaging materials in *Packaging Technology*. Woodhead Publishing: (2012).
- [73] **Barrett, A., and Lepitre, B.:** Bioplastic News. *Presentation*, Bioplastic News (2013).
- [74] **Hill, R. G.:** 10 - Biomedical polymers in *Biomaterials, Artificial Organs and Tissue Engineering*. Woodhead Publishing: (2005).
- [75] **Craig, C. L.:** Spiderwebs and Silk: Tracing Evolution From Molecules to Genes to Phenotypes. *Oxford University Press: Oxford* (2003).
- [76] **Wood, P. A., and Gabbutt, P. D.:** Silken chambers built by adult pseudoscorpions in laboratory culture. *Bulletin of the British Arachnological Society* 4(4), 285-293 (1979).
- [77] **Whitehead, W. F., and Rempel, J. G.:** A study of the musculature of the black widow spider, *Latrodectus mactans* (Fabr.). *Canadian Journal of Zoology* 37(6), 831-870 (1959).
- [78] **Peters, R.:** Vergleichende Untersuchungen über Bau und Funktion der Spinnwarzen und Spinnwarzenmuskulatur einiger Araneen. *Zool. Beitr.* 13(5, 48, 50), 29-119 (1967).
- [79] **Hilbrant, M.:** Development and Evolution of the Spider Silk Producing System. *Dissertation*, Universität zu Köln (2008).
- [80] **Benjamin, S. P., and Zschokke, S.:** Webs of theridiid spiders: construction, structure and evolution. *Biological Journal of the Linnean Society* 78(3), 293-305 (2003).
- [81] **Morewood, W., Hoover, K., and Sellmer, J. C.:** Predation by *Achaearanea tepidariorum* (Araneae: Theridiidae) on *Anoplophora glabripennis* (Coleoptera: Cerambycidae). *Great Lakes Entomologist* 36(1-2), 31-34 (2003).
- [82] **Zschokke, S., and Fritz, V.:** Web construction patterns in a range of orb-weaving spiders (Araneae). *European Journal of Entomology* 92(3), 523-541 (1995).
- [83] **Kovoor, J.:** L'appareil séricigène dans les genres *Nephila* Leach et *Nephilengys* Koch: anatomie microscopique, histochimie, affinités avec d'autres Araneidae. *Revue Arachnologique* 7(8), 15-34 (1986).
- [84] **Herold Heike, M., and Scheibel, T.:** Applicability of biotechnologically produced insect silks. *Zeitschrift für Naturforschung C* 72(9-10), 365 (2017).
- [85] **Omenetto, F. G., and Kaplan, D. L.:** New Opportunities for an Ancient Material. *Science (New York, N.Y.)* 329(5991), 528-531 (2010).

- [86] **Heim, M., Romer, L., and Scheibel, T.:** Hierarchical structures made of proteins. The complex architecture of spider webs and their constituent silk proteins. *Chemical Society Reviews* 39(1), 156-164 (2010).
- [87] **Hardy, J. G., Romer, L. M., and Scheibel, T. R.:** Polymeric materials based on silk proteins. *Polymer* 49(20), 4309-4327 (2008).
- [88] **Gosline, J. M., et al.:** The mechanical design of spider silks: from fibroin sequence to mechanical function. *The Journal of experimental biology* 202(23), 3295-303 (1999).
- [89] **Weisman, S., et al.:** Fifty years later: The sequence, structure and function of lacewing cross-beta silk. *Journal of structural biology* 168(3), 467-475 (2009).
- [90] **Bauer, F., et al.:** Dependence of mechanical properties of lacewing egg stalks on relative humidity. *Biomacromolecules* 13(11), 3730-5 (2012).
- [91] **Allmeling, C., Reimers, K., and Vogt, P. M.:** Wonder material of Nature - Spider silk in plastic surgery. *Chemie in Unserer Zeit* 41(6), 428-434 (2007).
- [92] **Modanu, M., et al.:** Sibling cannibalism in a web-building spider: Effects of density and shared environment. *Behavioural Processes* 106(1), 12-16 (2014).
- [93] **Huemmerich, D., Slotta, U., and Scheibel, T.:** Processing and modification of films made from recombinant spider silk proteins. *Applied Physics a-Materials Science & Processing* 82(2), 219-222 (2006).
- [94] **Heim, M., Keerl, D., and Scheibel, T.:** Spider Silk: From Soluble Protein to Extraordinary Fiber. *Angewandte Chemie-International Edition* 48(20), 3584-3596 (2009).
- [95] **Heidebrecht, A., and Scheibel, T.:** Recombinant Production of Spider Silk Proteins. *Advances in Applied Microbiology, Vol 82* 82(115-153 (2013).
- [96] **Vendrely, C., and Scheibel, T.:** Biotechnological production of spider-silk proteins enables new applications. *Macromolecular Bioscience* 7(4), 401-9 (2007).
- [97] **Neuenfeldt, M., and Scheibel, T.:** Sequence Identification, Recombinant Production, and Analysis of the Self-Assembly of Egg Stalk Silk Proteins from Lacewing *Chrysoperla carnea*. *Biomolecules* 7(2), 43 (2017).
- [98] **Bauer, F.:** Development of an artificial silk protein on the basis of a lacewing egg stalk protein. *Dissertation, Universität Bayreuth* (2013).
- [99] **Vollrath, F., and Knight, D. P.:** Liquid crystalline spinning of spider silk. *Nature* 410(1), 541 (2001).
- [100] **Iizuka, E.:** Silk Thread - Mechanism of Spinning and Its Mechanical-Properties. *Applied Polymer Symposia* 41, 173-185 (1985).
- [101] **Sutherland, T. D., et al.:** Insect Silk: One Name, Many Materials. *Annual Review of Entomology* 55(1), 171-188 (2010).
- [102] **Weisman, S., et al.:** An Unlikely Silk: The Composite Material of Green Lacewing Cocoons. *Biomacromolecules* 9(11), 3065-3069 (2008).



- [103] **Rudall, K. M., and Kenchington, W.:** Arthropod Silks: The Problem of Fibrous Proteins in Animal Tissues. *Annual Review of Entomology* 16(1), 73-96 (1971).
- [104] **Pennsylvania State University, Department of Energy and Mineral Engineering:** Are we running out of oil? <https://www.e-education.psu.edu/eme801/node/486>, accessed: Nov 15 (2018).
- [105] **Pellegrino, M.:** Grand challenges in polymer chemistry: energy, environment, health. *Frontiers in chemistry* 1(1), 31 (2013).
- [106] **Pillay, V., et al.:** A review of polymeric refabrication techniques to modify polymer properties for biomedical and drug delivery applications. *AAPS PharmSciTech* 14(2), 692-711 (2013).
- [107] **Sherazi, T.:** Graft Polymerization in *Encyclopedia of Membranes*. Springer: Berlin Heidelberg (2015).
- [108] **Brady, J., et al.:** Chapter 7 - Polymer Properties and Characterization in *Developing Solid Oral Dosage Forms (Second Edition)*. Academic Press: Boston (2017).
- [109] **Ramnarace, R., and Dalton, H. R.:** 36 - Gastrointestinal drugs in *Side Effects of Drugs Annual*. Elsevier: Amsterdam (2010).
- [110] **Elias, H.-G.:** Makromoleküle: Anwendungen von Polymeren. *Wiley*. (2009).
- [111] **Falbe, J., and Regitz, M.:** RÖMPP Lexikon Chemie, 10. Auflage, 1996-1999: Band 6: T - Z. *Georg Thieme Verlag: Stuttgart* (2014).
- [112] **Matamá, T., and Cavaco-Paulo, A.:** 5 - Enzymatic modification of polyacrylonitrile and cellulose acetate fibres for textile and other applications in *Advances in Textile Biotechnology*. Woodhead Publishing: Cambridge (2010).
- [113] **Colorado State University** Polymers are everywhere. [https://www.teachengineering.org/lessons/view/csu\\_polymer\\_lesson01](https://www.teachengineering.org/lessons/view/csu_polymer_lesson01), accessed: Aug 5 (2017).
- [114] **Brandau, O.:** 2 - Material Basics in *Stretch Blow Molding (Second Edition)*. William Andrew Publishing: Oxford (2012).
- [115] **Gelfand Center:** Natural vs Synthetic Polymers. <https://www.cmu.edu/gelfand/education/k12-teachers/polymers/natural-synthetic-polymers/>, accessed: Jul 11 (2016).
- [116] **Engels, H. W., et al.:** Rubber, 4. Chemicals and Additives in *Ullmann's Encyclopedia of Industrial Chemistry*. Wiley-VCH Verlag GmbH & Co. KGaA: Weinheim (2004).
- [117] **Goodyear, C.:** Improvement in India-Rubber Fabrics. US application, 1844 (1844).
- [118] **Venkatesan, J., Lowe, B., and Kim, S. K.:** 3 - Bone tissue engineering using functional marine biomaterials in *Functional Marine Biomaterials*. Woodhead Publishing: Cambridge (2015).
- [119] **Cheema, U., Ananta, M., and Mudera, V.:** Collagen: Applications of a Natural Polymer. in *Regenerative Medicine and Tissue Engineering - Cells and Biomaterials*. Vol. 1, (2011).

- [120] **Jiang, T., et al.:** Chapter 5 - Chitosan as a Biomaterial: Structure, Properties, and Applications in Tissue Engineering and Drug Delivery in *Natural and Synthetic Biomedical Polymers*. Elsevier: Oxford (2014).
- [121] **Patra, A. K., and Pattanayak, A. K.:** 16 - Novel varieties of denim fabrics in *Denim*. Woodhead Publishing: Cambridge (2015).
- [122] **Heidebrecht, A., et al.:** Biomimetic Fibers Made of Recombinant Spidroins with the Same Toughness as Natural Spider Silk. *Advanced Materials* 27(13), 2189-2194 (2015).
- [123] **Spiess, K., et al.:** Impact of initial solvent on thermal stability and mechanical properties of recombinant spider silk films. *Journal of Materials Chemistry* 21(35), 13594-13604 (2011).
- [124] **Zeplin, P. H., et al.:** Spider Silk Coatings as a Bioshield to Reduce Periprosthetic Fibrous Capsule Formation. *Advanced Functional Materials* 24(18), 2658-2666 (2014).
- [125] **Doblhofer, E., et al.:** Structural Insights into Water-Based Spider Silk Protein-Nanoclay Composites with Excellent Gas and Water Vapor Barrier Properties. *ACS Applied Materials & Interfaces* 8(38), 25535-43 (2016).
- [126] **Weisman, S., et al.:** Fifty years later: the sequence, structure and function of lacewing cross-beta silk. *Journal of structural biology* 168(3), 467-75 (2009).
- [127] **Bauer, F., and Scheibel, T.:** Artificial egg stalks made of a recombinantly produced lacewing silk protein. *Angewandte Chemie* 51(26), 6521-4 (2012).
- [128] **Lintz, E. S., and Scheibel, T. R.:** Dragline, Egg Stalk and Byssus: A Comparison of Outstanding Protein Fibers and Their Potential for Developing New Materials. *Advanced Functional Materials* 23(36), 4467-4482 (2013).
- [129] **Golser, A. V., and Scheibel, T. R.:** Biotechnological production of the mussel byssus derived collagen preColD. *Rsc Advances* 7(61), 38273-38278 (2017).
- [130] **Weisman, S., et al.:** Honeybee silk: Recombinant protein production, assembly and fiber spinning. *Biomaterials* 31(9), 2695-2700 (2010).
- [131] **Bourzac, K., and Schäfer, K.:** Auf Spidersmans Spuren. *Technology Review* 2017, <https://www.heise.de/tr/artikel/Auf-Spidermans-Spuren-3687571.html> (2018).
- [132] **Gries, T., Veit, D., and Wulfhorst, B.:** Textile Technology: An Introduction. *Carl Hanser Verlag GmbH & Company KG: München* (2015).
- [133] **Pasquini, N.:** Polypropylene Handbook. *Carl Hanser Verlag GmbH & Company KG: München* (2005).
- [134] **Raghavan, B., Soto, H., and Lozano, K.:** Fabrication of Melt Spun Polypropylene Nanofibers by Forc spinning. *Journal of Engineered Fibers and Fabrics* 8(1), 155892501300800106 (2013).
- [135] **Bansal, R. C., and Donnet, J. B.:** 16 - Pyrolytic Formation of High-performance Carbon Fibres in *Comprehensive Polymer Science and Supplements*. Pergamon: Amsterdam (1989).
- [136] **Vogler, H.:** Wettstreit um die Polyamidfasern. *Chemie in Unserer Zeit* 47(1), 62-63 (2013).

- [137] **Karger-Kocsis, J.:** Polypropylene. *Springer Netherlands: Amsterdam* (1999).
- [138] **Nadella, H. P., et al.:** Melt spinning of isotactic polypropylene: Structure development and relationship to mechanical properties. *Journal of Applied Polymer Science* 21(11), 3003-3022 (1977).
- [139] **Lu, F. M., and Spruiell, J. E.:** The influence of resin characteristics on the high speed melt spinning of isotactic polypropylene. II. On-line studies of diameter, birefringence, and temperature profiles. *Journal of Applied Polymer Science* 34(4), 1541-1556 (1987).
- [140] **Brazinsky, I., Williams, A. G., and LaNieve, H. L.:** The dry spinning process: Comparison of theory with experiment. *Polymer Engineering & Science* 15(12), 834-841 (1975).
- [141] **Web Studio IIT Madras, NPTEL:** Introduction to solution spinning. <http://nptel.ac.in/courses/116102010/18#>, accessed: Jan 13 (2013).
- [142] **Fang, X., et al.:** Gel spinning of UHMWPE fibers with polybutene as a new spin solvent. *Polymer Engineering & Science* 56(6), 697-706 (2016).
- [143] **Ward, I. M., Coates, P. D., and Dumoulin, M. M.:** Solid Phase Processing of Polymers. *Carl Hanser Verlag GmbH & Co. KG*: (2000).
- [144] **Tanner, D., Fitzgerald, J. A., and Phillips, B. R.:** The Kevlar Story—an Advanced Materials Case Study. *Angewandte Chemie International Edition in English* 28(5), 649-654 (1989).
- [145] **Picken, S. J.:** Applications of Liquid Crystal Polymers: Part 1: Fibre Spinning. *Liquid Crystals Today* 6(1), 12-15 (1996).
- [146] **Hammami, M. A., Krifa, M., and Harzallah, O.:** Centrifugal force spinning of PA6 nanofibers – processability and morphology of solution-spun fibers. *The Journal of The Textile Institute* 105(6), 637-647 (2014).
- [147] **Rouette, H. K.:** Handbuch Textilveredlung. *Deutscher Fachverlag: Frankfurt am Main* (2006).
- [148] **Fang, Y., et al.:** A comparative parameter study: Controlling fiber diameter and diameter distribution in centrifugal spinning of photocurable monomers. *Polymer* 88(1), 102-111 (2016).
- [149] **Zhang, Z., and Sun, J.:** Research on the development of the centrifugal spinning. *MATEC Web Conf.* 95(07003), 01-04 (2017).
- [150] **Hou, T., et al.:** Highly porous fibers prepared by centrifugal spinning. *Materials & Design* 114(1), 303-311 (2017).
- [151] **Nava, R., et al.:** Centrifugal Spinning: An Alternative for Large Scale Production of Silicon–Carbon Composite Nanofibers for Lithium Ion Battery Anodes. *ACS Applied Materials & Interfaces* 8(43), 29365-29372 (2016).
- [152] **Coulomb, C. A.:** Premier mémoire sur l'électricité et le magnétisme. *Histoire de l'Académie Royale des Sciences. Imprimerie Royale* 1(1), 569–577 (1785).

- [153] **Coulomb, C. A.:** Second mémoire sur l'électricité et le magnétisme. *Histoire de l'Académie Royale des Sciences. Imprimerie Royale* 1(1), 578–611 (1785).
- [154] **Malin, S., and Barraclough, D.:** Gilbert's De Magnete: An Early Study of Magnetism and Electricity. *Eos* 81(21), 233-241 (2000).
- [155] **Cooley, J. F.:** Apparatus for electrically dispersing fluids. *US692631A*, US application, (1902).
- [156] **Thompson, C. J., et al.:** Effects of parameters on nanofiber diameter determined from electrospinning model. *Polymer* 48(23), 6913-6922 (2007).
- [157] **Rutledge, G. C., and Fridrikh, S. V.:** Formation of fibers by electrospinning. *Advanced Drug Delivery Reviews* 59(14), 1384-1391 (2007).
- [158] **King, S. G., Stolojan, V., and Silva, S. R. P.:** Large area uniform electrospun polymer nanofibres by balancing of the electrostatic field. *Reactive and Functional Polymers* 129(1), 89-94 (2018).
- [159] **Ramakrishna, S., et al.:** Tip to Collector Distance *ElectrospinTec* 2018, [http://electrospin.tech.com/tip-to-collector.html#.XQ-QV\\_7gqUk](http://electrospin.tech.com/tip-to-collector.html#.XQ-QV_7gqUk) (2016).
- [160] **Ramakrishna, S.:** An Introduction to Electrospinning and Nanofibers. *World Scientific: Singapur* (2005).
- [161] **Lagaron, J. M., et al.:** 3 - Biomedical applications of electrospinning, innovations, and products in *Electrospun Materials for Tissue Engineering and Biomedical Applications*. Woodhead Publishing: (2017).
- [162] **Wang, L., and Ryan, A. J.:** 1 - Introduction to electrospinning in *Electrospinning for Tissue Regeneration*. Woodhead Publishing: Cambridge (2011).
- [163] **Taylor, S. G.:** Electrically driven jets. *Proceedings of the Royal Society of London. A. Mathematical and Physical Sciences* 313(1515), 453-475 (1969).
- [164] **Reznik, S. N., et al.:** Transient and steady shapes of droplets attached to a surface in a strong electric field. *Journal of Fluid Mechanics* 516(1), 349-377 (2004).
- [165] **Yarin, A. L., Koombhongse, S., and Reneker, D. H.:** Taylor cone and jetting from liquid droplets in electrospinning of nanofibers. *Journal of Applied Physics* 90(9), 4836-4846 (2001).
- [166] **Reneker, D. H., and Yarin, A. L.:** Electrospinning jets and polymer nanofibers. *Polymer* 49(10), 2387-2425 (2008).
- [167] **Stachewicz, U., et al.:** Surface free energy analysis of electrospun fibers based on Rayleigh-Plateau/Weber instabilities. *European Polymer Journal* 91(1), 368-375 (2017).
- [168] **H., M. M., et al.:** Electrospinning and electrically forced jets. I. Stability theory. *Physics of Fluids* 13(8), 2201-2220 (2001).
- [169] **Huebner, A. L., and Chu, H. N.:** Instability and breakup of charged liquid jets. *Journal of Fluid Mechanics* 49(2), 361-372 (1971).

- [170] **Mougawaz, S.:** Formelsammlung Elektrik. <http://www.gymnasium-horkesgath.de/physik/formel/formel.htm>, accessed: Dec 1 (2013).
- [171] **Cruzan, J.:** Electric charge (q). <http://xaktly.com/ElectricCharge.html>, accessed: Jul 20 (2018).
- [172] **Walczak, Z. K.:** Processes of Fiber Formation: 1st Edition. *Elsevier Science: Amsterdam* (2002).
- [173] **Fine, J., and De Tora, S. A.:** Method of producing fibrous structure. *US4223101A*, US application, Sep 16, 1980 (1980).
- [174] **Formhals, A.:** Process and apparatus for preparing artificial threads. *US1975504A*, US application, Oct 2, 1934 (1929).
- [175] **Formhals, A.:** Method and apparatus for the production of fibers. *US2116942A*, USA application, Mai 10, 1938 (1934).
- [176] **Norton, C. L.:** Method of and apparatus for producing fibrous or filamentary material *US2048651A*, US application, Jul 21, 1936 (1933).
- [177] **Berling, E.:** Gas mixture analyzer. *US3350918A*, US application, Nov 07, 1967 (1964).
- [178] **Lacasse, K., and Baumann, W.:** Textile Chemicals: Environmental Data and Facts. *Springer: Berlin Heidelberg* (2012).
- [179] **Gulrajani, M. L., et al.:** Advances in the Dyeing and Finishing of Technical Textiles. *Woodhead Publishing: Cambridge* (2013).
- [180] **Heermann, P.:** Technologie der Textilveredelung, 2nd Vol. *Springer: Berlin Heidelberg* (2013).
- [181] **Kiessling, A., and Matthes, M.:** Textil-Fachwörterbuch. *Schiele & Schön: Berlin* (1993).
- [182] **Behery, H. M.:** Effect of Mechanical and Physical Properties on Fabric Hand. *Taylor & Francis: London* (2005).
- [183] **Okamoto, M., and Yoshida, S.:** Suede-like raised woven fabric and process for the preparation thereof. *US4103054A*, US application, Jun 17, 1976 (1977).
- [184] **Syduzzaman, M., Touhiduzzaman, M., and Rashid, K.:** Effects of Raising and Sueding on the Physical and Mechanical Properties of Dyed Knitted Fabric. *Journal of Textile Science & Engineering* 6(1), 1000228 (2015).
- [185] **Horrocks, A. R., and Anand, S. C.:** Handbook of Technical Textiles - Volume 2: Technical Textile Applications. *CRC Press: Boca Raton* (2000).
- [186] **Ding, X., and Harris, T. A. L.:** Review on penetration and transport phenomena in porous media during slot die coating. *Journal of Polymer Science Part B: Polymer Physics* 55(22), 1669-1680 (2017).
- [187] **Giessmann, A.:** Coating Substrates and Textiles: A Practical Guide to Coating and Laminating Technologies. *Springer: Berlin Heidelberg* (2012).
- [188] **Booth, G. L.:** Coating Equipment and Processes. *Lockwood Publishing Ltd.: Nottingham* (1970).

- [189] **Soroka, W.:** Illustrated Glossary of Packaging Terminology. *Institute of Packaging Professionals: Reston* (2008).
- [190] **Co., S. S.:** Automatic & Air Atomizing Spray Nozzles - Spray Controllers & Spray Manifolds. *Online Article, Cyco Group* (2018).
- [191] **Jones, I., and Stylios, G. K.:** Joining Textiles: Principles and Applications. *Elsevier Science: Amsterdam* (2013).
- [192] **Adanur, S.:** Wellington Sears Handbook of Industrial Textiles. *Taylor & Francis: Milton Park* (1995).
- [193] **Kenry, L., and T., C.:** Nanofiber technology: current status and emerging developments. *Progress in Polymer Science* 70(1), 1-17 (2017).
- [194] **Varagnolo, S., et al.:** Highly sticky surfaces made by electrospun polymer nanofibers. *Rsc Advances* 7(10), 5836-5842 (2017).
- [195] **Wang, X., et al.:** Electrospun nanofibrous materials: a versatile medium for effective oil/water separation. *Materials Today* 19(7), 403-414 (2016).
- [196] **Killi, N., Gundloori, R., and Paul, L.:** Antibacterial Non-woven Nanofibers of Curcumin Acrylate Oligomers. *New Journal of Chemistry* 39(6), 4464-4470 (2015).
- [197] **Kratochvil, M. J., et al.:** Nonwoven Polymer Nanofiber Coatings That Inhibit Quorum Sensing in *Staphylococcus aureus*: Toward New Nonbactericidal Approaches to Infection Control. *ACS Infectious Diseases* 3(4), 271-280 (2017).
- [198] **Zhang, Y., et al.:** Recent Development of Polymer Nanofibers for Biomedical and Biotechnological Applications. *Journal of Materials Science Materials in Medicine* 16(1), 933-946 (2005).
- [199] **Hassanzadeh, P., et al.:** Chitin Nanofiber Micropatterned Flexible Substrates for Tissue Engineering. *Journal of materials chemistry B* 1(34), (2013).
- [200] **Hamada, H., and Mitsuhashi, M.:** Effect of cellulose nanofibers as a coating agent for woven and nonwoven fabrics. *Nordic Pulp&Paper* 31(2), 255-260 (2016).
- [201] **Kucukali, O. M., Nergis, F. B., and Candan, C.:** Design of electrospun polyacrylonitrile nanofiber-coated nonwoven structure for sound absorption. *Polymers for Advanced Technologies* 29(4), 1255-1260 (2018).
- [202] **Lang, G., Jokisch, S., and Scheibel, T.:** Air filter devices including nonwoven meshes of electrospun recombinant spider silk proteins. *Journal of visualized experiments: JoVE* 75(1), e50492 (2013).
- [203] **Scheibel, T.:** Spider silks: recombinant synthesis, assembly, spinning, and engineering of synthetic proteins. *Microbial Cell Factories* 3(1), 14 (2004).
- [204] **Scheibel, T.:** Silk—a biomaterial with several facets. *Applied Physics A* 82(2), 191-192 (2006).
- [205] **Slotta, U., Spieß, K., and Scheibel, T.:** Spider Silk in *The Functional Fold*. Pan Stanford: New York (2012).

- [206] **Lang, G., Herold, H. M., and Scheibel, T.:** Properties of Engineered and Fabricated Silks in *Fibrous Proteins: Structures and Mechanisms*. Springer International Publishing: Cham (2017).
- [207] **Lammel, A., et al.:** Recombinant spider silk particles as drug delivery vehicles. *Biomaterials* 32(8), 2233-2240 (2011).
- [208] **Hardy, J. G., Leal-Egaña, A., and Scheibel, T. R.:** Engineered Spider Silk Protein-Based Composites for Drug Delivery. *Macromolecular Bioscience* 13(10), 1431-1437 (2013).
- [209] **Elsner, M. B., et al.:** Enhanced cellular uptake of engineered spider silk particles. *Biomaterial Science* 3(543), 543-551 (2014).
- [210] **DeSimone, E., et al.:** Biofabrication of 3D constructs: fabrication technologies and spider silk proteins as bioinks. *Pure and Applied Chemistry* 87(8), 737-749 (2015).
- [211] **Hardy, J. G., et al.:** Biomineralization of Engineered Spider Silk Protein-Based Composite Materials for Bone Tissue Engineering. *Materials* 9(7), 1-13 (2016).
- [212] **Schacht, K., Vogt, J., and Scheibel, T.:** Foams Made of Engineered Recombinant Spider Silk Proteins as 3D Scaffolds for Cell Growth. *ACS Biomaterials Science & Engineering* 2(4), 517-525 (2016).
- [213] **Schierling, M. B., Doblhofer, E., and Scheibel, T.:** Cellular uptake of drug loaded spider silk particles. *Biomater. Sci.* 4(10), 1515-1523 (2016).
- [214] **Lucke, M., et al.:** Engineered hybrid spider silk particles as delivery system for peptide vaccines. *Biomaterials* 172(21 Apr. 2018), 105-115 (2018).
- [215] **International Organization for Standardization:** Textiles - Universal system for designating linear density (Tex System). *ISO 1144: 2016-09* (2000).
- [216] **Jokisch, S., and Scheibel, T.:** Spider silk foam coating of fabric. *Pure and Applied Chemistry* 89(12), 1769-1776 (2017).
- [217] **Huemmerich, D., et al.:** Primary structure elements of spider dragline silks and their contribution to protein solubility. *Biochemistry* 43(42), 13604-13612 (2004).
- [218] **Hu, X., Kaplan, D., and Cebe, P.:** Determining Beta-Sheet Crystallinity in Fibrous Proteins by Thermal Analysis and Infrared Spectroscopy. *Macromolecules* 39(18), 6161-6170 (2006).
- [219] **ASTM International:** Standard Test Method for Coefficient of Friction, Yarn to Solid Material. *ASTM D3108-07: 2007* (2007).
- [220] **ASTM International:** Standard Test Method for Coefficient of Friction, Yarn to Yarn. *ASTM D3412-01: 2001* (2001).
- [221] **Gupta, B. S.:** Frictional Properties of Textile Materials in *Surface Characteristics of Fibers and Textiles*. Marcel Dekker Inc.: Basel (2001).
- [222] **Yuvaraj, D., and Nayar, R. C.:** A simple yarn hairiness measurement setup using image processing techniques. *Indian Journal of Fibre & Textile Research* 37(4), 331-336 (2012).

- [223] **Deutsches Institut für Normung e.V.:** Bestimmung der Neigung von textilen Flächengebilden zur Flusenbildung auf der Oberfläche und der Pillneigung – Teil 2: Modifiziertes Martindale-Verfahren in Textilien. *EN ISO 12945-2: 2000-11* (2000).
- [224] **Gries, T., and Klopp, K.:** Füge- und Oberflächentechnologien für Textilien - Verfahren und Anwendungen. *Springer: Berlin Heidelberg* (2007).
- [225] **Schramm, G. A., and Haake, G.:** A Practical Approach to Rheology and Rheometry. *Haake: Lilienthal* (1994).
- [226] **Mezger, T. G.:** Das Rheologie Handbuch: Für Anwender von Rotations- und Oszillations-Rheometern (Farbe und Lack Edition). *Vincentz Network: Hannover* (2012).
- [227] **Potter, J. F., and Brown, W. L.:** Method and apparatus for foam treating pile fabrics. *US5219620A*, US application, Jun 15 (1993).
- [228] **Lang, G.:** Herstellung und Charakterisierung von Fasern aus rekombinanten Spinnenseidenproteinen und deren potentielle Applikationen. *Dissertation*, University Bayreuth (2015).
- [229] **Lang, G., et al.:** Mechanical Testing of Engineered Spider Silk Filaments Provides Insights into Molecular Features on a Mesoscale. *ACS Applied Materials & Interfaces* 9(1), 892-900 (2017).
- [230] **Zhang, X. H., Reagan, M. R., and Kaplan, D. L.:** Electrospun silk biomaterial scaffolds for regenerative medicine. *Advanced Drug Delivery Reviews* 61(12), 988-1006 (2009).
- [231] **Casasola, R., et al.:** Electrospun poly lactic acid (PLA) fibres: Effect of different solvent systems on fibre morphology and diameter. *Polymer* 55(18), 4728-4737 (2014).
- [232] **Hinds, W. C.:** Aerosol technology: properties, behavior, and measurement of airborne particles. *Wiley: New York* (1999).
- [233] **Yun, K. M., et al.:** Nanoparticle filtration by electrospun polymer fibers. *Chemical Engineering Science* 62(17), 4751-4759 (2007).
- [234] **Leal-Egana, A., et al.:** Interactions of Fibroblasts with Different Morphologies Made of an Engineered Spider Silk Protein. *Advanced Engineering Materials* 14(3), B67-B75 (2012).
- [235] **Spieß, K., Lammel, A., and Scheibel, T.:** Recombinant Spider Silk Proteins for Applications in Biomaterials. *Macromolecular Bioscience* 10(9), 998-1007 (2010).
- [236] **Gleuwitz, R.:** Textile Ausrüstung mit rekombinanter Spinnenseide. *Diplomarbeit*, Universität Bayreuth (2013).
- [237] **Blau, P. J.:** Friction Science and Technology: From Concepts to Applications, Second Edition. *CRC Press: Boca Raton* (2008).
- [238] **Cooke, T. F., and Hirt, D. E.:** 9 - Foam Wet Processing in the Textile Industry in *Foams: Theory: Measurements: Applications*. Routledge: Abingdon (2017).
- [239] **Walstra, P.:** Principles of Foam Formation and Stability in *Foams: physics, chemistry and structure*. Springer: Berlin Heidelberg (1989).



- [240] **Wenzel, H. G. J., Stelson, T. E., and Brungraber, R. J.:** Flow of High Expansion Foam in Pipes. *Journal of the Engineering Mechanics Division* 93(6), 153-166 (1967).
- [241] **Parikh, D.:** Experimental Study of Pressure Drop and Bubble Size in a Laboratory Scale Compressed Air Foam Generation System. *Masters Thesis*, Colorado School of Mines (2017).
- [242] **Drenckhan, W., and Saint-Jalmes, A.:** The science of foaming. *Advances in Colloid and Interface Science* 222(1), 228-259 (2015).
- [243] **Politova, N., et al.:** Self-regulation of foam volume and bubble size during foaming via shear mixing. *Colloids and Surfaces A: Physicochemical and Engineering Aspects* 539(1), 18-28 (2018).
- [244] **GmbH, H. T. E. G.:** Sicherheitsdatenblatt Ultravon Jun. *VCI/TEGEWA*, Langweid, 9 (2011).
- [245] **Wang, Y., et al.:** Formation of Surface Morphology in Polyacrylonitrile (PAN) Fibers during Wet-Spinning. *Journal of Engineered Fibers and Fabrics* 13(2), 155892501801300208 (2018).
- [246] **Morris, E. A., Weisenberger, M. C., and Rice, G. W.:** Properties of PAN Fibers Solution Spun into a Chilled Coagulation Bath at High Solvent Compositions. *Fibers* 3(4), 560 (2015).
- [247] **Hearle, J. W. S.:** Theoretical analysis of the mechanics of twisted staple fiber yarns. *Textile Research Journal* 35(12), 1060-1071 (1965).
- [248] **Power2SME Private Limited:** Combed Yarn. <https://www.power2sme.com/products/details/Yarn/Cotton/Combed%20Yarn>, accessed: Mar 26 (2012).
- [249] **Akter, N.:** Effects of Combed Yarn on Wet Knitted Finished Fabric Quality. *International Journal of Engineering & Technology* 11(6), 93-97 (2011).
- [250] **Hurst, A. J.:** Mechanical foaming device. *US2849215A*, US application, Aug 09, 1956 (1958).
- [251] **Kent, J. A.:** Kent and Riegel's Handbook of Industrial Chemistry and Biotechnology. *Springer: Berlin Heidelberg* (2010).
- [252] **Heidebrecht, A.:** Production and Characterization of Artificial Spider Silk Fibers with the Same Toughness as Natural Dragline Silk Fibers. *Dissertation*, Universität Bayreuth (2016).
- [253] **Koepfel, A., and Holland, C.:** Progress and Trends in Artificial Silk Spinning: A Systematic Review. *ACS Biomaterials Science & Engineering* 3(3), 226-237 (2017).
- [254] **Wendorff, J. H., Agarwal, S., and Greiner, A.:** Electrospinning : materials, processing, and applications. *Wiley-VCH: Weinheim, Germany* (2012).
- [255] **Lammel, A., et al.:** Silk Particles For Controlled And Sustained Delivery Of Compounds. *EP2506837A2*, Worldwide application, Nov 30 (2010).
- [256] **Helfricht, N., et al.:** Colloidal Properties of Recombinant Spider Silk Protein Particles. *The Journal of Physical Chemistry C* 120(32), 18015-18027 (2016).
- [257] **Kim, S. H., et al.:** Silk Fibroin Nanofiber. Electrospinning, Properties, and Structure. *The Society of Polymer Science* 35(1), 185 (2003).

- [258] **Rockwood, D. N., et al.:** Materials fabrication from *Bombyx mori* silk fibroin. *Nature Protocols* 6(1), 1612 (2011).
- [259] **Dyakonov, T., et al.:** Design and characterization of a silk-fibroin-based drug delivery platform using naproxen as a model drug. *Journal of Drug Delivery* 2012(490514), 10 (2012).
- [260] **Nazarov, R., Jin, H. J., and Kaplan, D. L.:** Porous 3-D scaffolds from regenerated silk fibroin. *Biomacromolecules* 5(3), 718-26 (2004).
- [261] **An, B., et al.:** Inducing  $\beta$ -sheets formation in synthetic spider silk fibers by aqueous post-spin stretching. *Biomacromolecules* 12(6), 2375-2381 (2011).
- [262] **Menezes, G. M., et al.:** Nanoscale investigations of synthetic spider silk fibers modified by physical and chemical processes. *Polymer Journal* 45(1), 997-1006 (2013).
- [263] **Eisoldt, L., Smith, A., and Scheibel, T.:** Decoding the secrets of spider silk. *Materials Today* 14(3), 80-86 (2011).
- [264] **Blamires, S. J., et al.:** Multiscale mechanisms of nutritionally induced property variation in spider silks. *PloS one* 13(2), e0192005 (2018).
- [265] **Lauterbach, A. Y., and Scheibel, T.:** Life cycle assessment of spider silk nonwoven meshes in an air filtration device. *Green Materials* 3(1), 15-24 (2015).

## Danksagung

An dieser Stelle möchte ich all jenen danken, die zum erfolgreichen Abschluss dieser Arbeit beigetragen haben. Zur gebührenden Anerkennung der entgegengebrachten Unterstützung und der Hilfe aller beteiligten Personen reichen Worte und der Umfang dieser Seiten eigentlich nicht aus. Dennoch möchte ich versuchen die wichtigsten Personen im Folgenden aufzuführen.

In höchstem Maße danke ich meinem Betreuer und Doktorvater Professor Dr. Thomas Scheibel für die Möglichkeit, an diesem spannenden und zukunftsweisenden Thema zu arbeiten und für das in mich gesetzte Vertrauen bei der Umsetzung verschiedenster Projekte. Ich bin dankbar für die Handlungsfreiheiten, welche mir bei wissenschaftlichen Experimenten, sowie der technischen Umsetzungen unkonventioneller Ideen zuteilwurden. Ebenfalls ein großer Dank gebührt euch „Fibers“ (meinen Kollegen), speziell Heike Herold, Martin Neuenfeldt, Joschka Bauer, Christopher Thamm, Kristin Schacht, Christian Haynl und natürlich meinen Bürokollegen Gregor Lang, Aniela Heidebrecht, Melanie Schiebel und David Keerl, sowie Adrian Golser. Ihr standet mir stets mit Rat und Tat zur Seite und hattet immer einen Lösungsansatz bei schwierigen Experimenten oder Ideen für gemeinsame Projekte. Nicht zuletzt wurde durch euch so mancher zähe Tag in der LT mit auflockernden Gesprächen und Aktivitäten versüßt.

Susanne Schramm, Andrea Bodner und Sabrina Raum danke ich für die ausdauernde Unterstützung beim Kampf gegen fehlende Dokumente und bürokratische Hürden. Ein herzliches Dankeschön gebührt Fabian Müller für die vielen Bemühungen und für seinen unermüdlichen Einsatz bei der gemeinsamen Initialisierung der Zentrifugenelektrospinnanlage. Insbesondere danke ich auch Andreas Schmidt, Johannes Diehl, Claudia Stemmann und Dr. Hendrik Bargel für die zahlreichen Stunden am Rasterelektronenmikroskop und die viele Geduld bei der Suche nach den besten Einstellungen, sowie die unzähligen Tipps und Ratschläge bei der oftmals hochambitionierten Laborarbeit. Ebenso bedanke ich mich bei Alexander Kern und Prof. Dr. Hans-Werner Schmidt (Makromolekulare Chemie I, Universität Bayreuth) für die Umsetzung der Partikelabscheidungsfiltermessungen.

Ich danke herzlich Dr. Martin Hummenik für den wissenschaftlichen Dialog und die fortwährende Unterstützung, sowie für die inhaltlichen Korrekturen und Verbesserungsvorschläge dieser Arbeit. Mein Dank gebührt weiterhin den Kooperationspartnern Lorenz Summa (Sandler AG), Harald Boeck (BSH Hausgeräte GmbH), Peter Raich (Rohleder GmbH) für die fruchtende Zusammenarbeit in zahlreichen spannenden Projekten.

Nicht zuletzt danke ich insbesondere den Korrekturlesern Stefanie Schieweck, Dave Fales, Patrick Piedad, Nathaniel Eckert und Nigel Downes für Ihre Bemühungen und der sprachlichen Unterstützung. Abschließend möchte ich mich im besonderen Maße bei meiner Familie und meinen engen Freunden bedanken, die immer ein offenes Ohr hatten, mich stets unterstützten und auch in schwierigen Phasen dieser Arbeit ermutigt und positiv angetrieben haben.

# Lebenslauf

## Persönliche Daten

Name: Stephan Jokisch  
 Geburtsdatum: 04.12.1985  
 Geburtsort: Hoyerswerda  
 Staatsangehörigkeit: deutsch



## Schulbildung

08/2002 - 06/2005 **Erwin-Strittmatter Gymnasium, Spremberg**  
 Abschluss: Allgemeine Hochschulreife

08/1998 - 06/2002 **Gymnasium, Welzow**  
 Abschluss: Mittlere Reife

08/1992 - 06/1998 **Johan-Wolfgang von Goethe Grundschule, Welzow**

## Akademischer Werdegang

10//2018 - 10/2019 **Universität Jena**  
 Fernstudiengang Gewerblicher Rechtsschutz  
 Abschluss: Patent-Ingenieur

seit 11/2011 **Universität Bayreuth, Lehrstuhl Biomaterialien**  
 Wissenschaftlicher Mitarbeiter zur Promotion (Dr.-Ing.) in der  
 Arbeitsgruppe von Prof. Dr. Thomas Scheibel  
 Dissertation zum Thema:  
*„Novel Processing Methods for Artificial Spider Silk Proteins“*

10/2009 - 10/2011 **Universität Bayreuth**  
 Masterstudiengang Biotechnology and Process Engineering  
 Masterarbeit zum Thema:  
*„Technische Anwendungen elektro-gesponnener Spinnenseide“*

10/2006 - 09/2009 **Staatliche Studienakademie Riesa**  
 Dualer Bachelorstudiengang Labor- und Verfahrenstechnik /  
 Biotechnologie  
 Bachelorarbeit bei Dr. Lutz Kröhne, Capsulation Pharma AG,  
 Berlin zum Thema:  
*„Entwicklung einer Antikörper-Drug Delivery Formulierung  
 auf der Basis der LbL/PEC-Technologie“*

### Beruflicher Werdegang/ Praktika

---

- seit 04/2017 **Zimmermann&Partner Patentanwälte mbB**  
Projektmanager, Patent-Ingenieur
- 10/2009 - 09/2011 **Lehrstühle Bioprozesstechnik und Werkstoffverarbeitung, Universität Bayreuth**  
Tätigkeiten als studentische Hilfskraft
- 10/2006 - 09/2009 **Capsulation Pharma AG, Berlin**  
Studienbegleitende Ausbildung im Umfang von 18 Monaten
- 09/2005 - 09/2006 **Mechanisch-Biologische Abfallbehandlungsanlage des Abfallentsorgungsverbands „Schwarze Elster“, Lauchhammer**  
Freiwilliges Ökologisches Jahr

### Veröffentlichungen

---

- 09/2019 **Silk-Based Fine Dust Filters for Air Filtration**  
Jokisch, S., Neuenfeldt, M., H. & Scheibel, T.  
In: *Advanced Sustainable Systems* 10 (1), 2017
- 09/2017 **Spider Silk Foam Coating of Fabric**  
Jokisch, S., Scheibel, T.  
In: *Pure and Applied Chemistry* 89 (12), 2017
- 05/2017 **Einsatz von Biomaterialien in Filtersystemen**  
Jokisch, S., Bargel, H. & Scheibel, T.  
In: *Prototype Nature*, 2017
- 05/2013 **Air filter devices including nonwoven meshes of electrospun recombinant spider silk proteins.**  
Lang, G., Jokisch, S. & Scheibel, T.:  
In: *Journal of Visualized Experiments* 75(e50492), 2013
- 04/2013 **Staubbeutel**  
Amsilk GmbH, Sandler AG, BSH Hausgeräte GmbH  
Patent: *DE202013003445U1*
-

## **Erklärung**

(§7 Abs.3 PromO Fakultät ING, Universität Bayreuth vom 15. September 2017 und Art. 64 Abs. 1 Satz 6 BayHSchG)

Hiermit erkläre ich, dass die beigefügte Dissertation selbständig verfasst und keine anderen als die angegebenen Hilfsmittel genutzt habe. Alle wörtlichen oder inhaltlich übernommenen Stellen habe ich als solche gekennzeichnet.

(§7 Abs.3 PromO Fakultät ING)

Ferner erkläre ich, dass diese Dissertation nicht bereits an anderer Stelle eingereicht wurde oder von anderer Stelle endgültig abgelehnt wurde. Ich versichere, dass ich weder diese noch eine gleichartige Promotionsprüfung endgültig nicht bestanden habe.

(§7 Abs.6 PromO Fakultät ING)

Zudem erkläre ich, dass ich weder in der Vergangenheit Hilfe von einem gewerblichen Promotionsberater bzw. -vermittler in Anspruch genommen habe, noch künftig in Anspruch nehmen werde.

Stephan Jokisch, Bayreuth, 30. Januar 2020

